TABLE OF CONTENTS

Page

LIST OF TABLES

LIST OF FIGURES

LIST OF ABREVIATIONS

BHE	Borehole Heat Exchanger
BTES	Borehole Thermal Energy Storage
COP	Coefficient Of Performance
CPU	Central Processing Unit
CV	Control Volume
CVFDM	Control Volume Finite Difference Method
CVFEM	Control Volume Finite Element Method
DST	Duct Storage System
ÉTS	École de technologie supérieure
EWT	Heat Pump Entering Water Temperature
GCHP	Ground Coupled Heat Pump
GHC	Grant-Harvey Center
GSHP	Ground Source Heat Pump
HVAC	Heating, Venting and Air-Conditioning
IPCC	Intergovernmental Panel on Climate Changes
MLAA	Multiple Load Aggregation Algorithm
RMS	Root-Mean-Square
SBM	Superposition Borehole Method
TDMA	Tri-Diagonal Matrix Algorithm
TRT	Thermal Response Test
UTES	Underground Thermal Energy Storage

LIST OF SYMBOLS AND UNITS OF MEASUREMENTS

Chapter 1

Kusuda model

A	annual average earth temperature	[°F]
BO	projected earth surface temperature amplitude (B at x=0)	[°F]
D	thermal diffusivity	[ft^2/hr]
PO	projected phase angle at the earth's surface (x=0)	[rad]
T	period of the temperature cycle (8766 hrs)	[hr]
x	downward distance coordinate from the earth's surface depth	[ft]
Θ	elapsed time from January 1^{st}, 1^{st} hour	[hr]

Chapter 2

c	Specific heat (J kg^{-1} K^{-1})
D	Borehole diameter used in shape factor definition (m)
dx	Control volume dimension in the x-direction (m)
dy	Control volume dimension in the y-direction (m)
Fo	Fourier number
Fr	Fraction of propylene-glycol in water
inter	Between boreholes (m)
L	Length (m)
k	Thermal conductivity (W m-1 K-1)
$\dot{m}$	Mass flow rate (kg m-3)
q	Heat extraction/injection rate (W)
R	Thermal resistance (m K W-1)
r	Radius (m)
R_c	Shape factor equivalent thermal resistance (m K W-1)
S	Shape factor between borehole and control volume boundaries
S_T	Source term
T	Temperature (°C)

undist Undisturbed

V Volume (m^3)

W Control volume width used in shape factor definition (m)

z Non-dimensional thermal resistance factor

Greek letters

λ Ground thermal conductivity (Eskilson)

ρ Density or specific weight

Subscripts

1 Refers to the branch of the fluid flowing downward in the borehole

2 Refers to the branch of the fluid flowing upward in the borehole

a Average

a related to the thermal resistance between the two pipes of the borehole

b Borehole

c related to the thermal resistance between the borehole and its control-volume

f Fluid

g Grout

s Ground

tot Total

in inlet

out outlet

n,s,e,w North, South, East, West neighbors of node i,j

ne, se, nw, sw North-east, South-east, North-west, South-west

Superscripts

‘ Per unit length

* Effective

Chapter 3

k thermal conductivity ($W\ m^{-1}K^{-1}$)

c_p Fluid specific heat ($J\ kg^{-1}\ K^{-1}$)

$\dot{m}$ mass flow rate (kg s^{-1})

q' heat flux per unit length (W m^{-1})

r radius (m)

xc half shank spacing (m)

T temperature (°C)

x,y,z spatial Cartesian coordinates (m)

x_o,y_o,z_o coordinates of the entrance of the borehole (m)

d diameter (m)

Di Pipe inner diameter (m)

Do Pipe outer diameter (m)

G

h heat transfer coefficient, (W $m^{-2}K^{-1}$)

T_{fi1} Fluid inlet temperature, circuit 1 (°C)

T_{fi2} Fluid inlet temperature, circuit 2 (°C)

L Borehole depth (m)

R Borehole thermal resistance (W m^{-1} K^{-1})

S modified thermal resistances

Z dimensionless depth

Greek letters

α_s soil thermal diffusivity (m^2 s^{-1})

α mass flow ratio

β angle of rotation (deg)

ε efficiency

χ twice the dimensionless borehole depth (Eq. 23)

θ non-dimensional temperature

Subscripts

b borehole

f mean fluid

f_o fluid outlet

g	grout
hp	heat pump
o	far-field
p	pipe
s	soil
i	image
in	inlet

Superscripts

R	with respect to the reference frame (Fig. 1)
b	with respect to the borehole frame
o	new resistances
’	per unit length
~	dimensionless variable
^	dimensionless variable
‾	mean value
Δ	delta circuit

INTRODUCTION

0.1 Context

Ground source heat pumps or low temperature geothermal systems, are used in heating and cooling applications; mainly buildings. Boreholes are drilled into the ground to depths that can reach 600 m and in closed-loop systems, U-tubes are inserted in them. Thus, a heat transfer fluid exchanges heat between heat pumps and the surrounding ground. Low temperature geothermal systems are known for their great efficiency provided by the interesting coefficient of performance (COP) of their heat pumps, but also for their high capital investment mainly caused by drilling depth costs. The Intergovernmental Panel on Climate Changes (IPCC) projects that the heat energy produced by ground source heat pumps will evolve from 0.4 EJ/year in 2010 to 7.2 EJ/year in 2050 (Goldstein and al., 2011).

In many parts if the globe, buildings annual thermal loads are unbalanced between heating and cooling. In cold climates, more heat is extracted from the ground during heating period than injected during its cooling counterpart. This is prone to make the ground colder every year and after a certain period of time, could make the geothermal system unusable. Moreover, if the ground freezes, the boreholes could be permanently damaged. Hybrid systems are then a prospective solution for such an issue.

It is becoming more common to see shared and hybrid geothermal borefields. Many buildings and processes with different heating and cooling loads profiles can share the same geothermal loop. It is possible, sometimes even mostly desirable, to couple complementary load profiles. An example of hybrid geothermal system would be to couple solar thermal collectors with heat pumps to the geothermal loop. Geothermal systems can also be coupled to cooling towers and waste heat from industrial processes. The University of Wisconsin found economic and environmental advantages to hybrid geothermal systems compared to classic by reducing the rate of return on investment and the CO2 emissions (Hackel and Pertzborn, 2011c).

Existing installations of hybrid geothermal systems can be found in Canada. The Drake Landing Solar Community, in Alberta, is composed of 56 residential buildings and a solar collectors loop sharing the same geothermal borefield. The University of Ontario Institute of Technology installed a 384 boreholes borefield to heat and cool 8 of the campus buildings.

In the United States of America, the Ball State University is coupling 47 buildings through a 3 600 boreholes borefield. In 2005, there were about 600 000 ground source heat pumps installed in the USA and 200 000 in Sweden, which is more than 1% of the buildings in the latter case (Curtis and al., 2005).

0.2 Objectives and methodology

Nearly all available geothermal mathematical models consider only one inlet condition for all of the U-tubes and boreholes of a borefield, limiting the amount of possible configurations and control strategies to be simulated and then evaluated.

The objective of this research is to improve the efficiency of shared and hybrid geothermal systems by segregating heat transfer sources. This will be achieved by:

- developing a semi-analytical model that considers independent inlet conditions for each borehole of a borefield in the first part;
- developing a model that considers independent circuits of double U-tubes in each borehole in the second part.

The ground is modeled as a 2D control volume finite difference method (CVFDM). The 3D effect is found after long periods of time with largely imbalanced loads and one objective of this work is to balance the loads, so a 2D model is deemed acceptable for now. Only diffusion of heat is considered for now. Since the boreholes are circular and the control volumes regular and uniform (square), an analytical shape factor is used at the source term control volumes. This part of the model describes the heat transferred between the external

ground and the borehole wall. An analytical model based on thermal resistances is used to describe the heat transferred between the internal fluid and the borehole wall.

A second model is developed to describe the behavior of a double U-tube borehole where the two legs of the U-tubes are coupled to different sources. It is a complement of an existing model (Eslami-Nejad and Bernier, 2011b), in addition of having different capacitances in each leg. This model uses the above-mentioned ground-to-borehole wall model.

0.3 Thesis content

This thesis is divided into four chapters:

1. The first chapter presents a general literature review on low temperature geothermal systems. Main subjects studied were ground source heat pumps, ground models, borehole thermal resistance, configurations, control strategies and sizing of ground source heat pump systems.

2. The second chapter is a paper published in Geothermics on a semi-analytical model that can describe the behavior of geothermal borefields with independent inlet conditions in each borehole. The ground is modeled as a 2D control volume finite difference method. An analytical model is used to describe the heat transfer between the borehole wall and the heat transfer fluid. A shape factor is used to couple the circular borehole to a square control volume. An application of residential/solar hybrid ground source heat pump system is presented where boreholes in the center of a borefield are coupled to solar collectors and the outer boreholes to residential heat pumps.

3. The third chapter is a paper published in Applied Thermal Engineering describing a model where legs of double U-tubes can have different inlet conditions. The model is based on a previous paper (Eslami-Nejad and Bernier, 2011b), that allows to model

double U-tubes with different angles between the legs, but the proposed model also allows the flowrate and the capacitance of the fluid to be different in each leg. Application examples include two heat pumps coupled to different circuits and a residential/solar application, coupling solar collectors to one circuit and residential heat pumps to the other.

4. The fourth chapter is a paper yet to be accepted in Renewable Energy. It presents residential heat pumps and solar applications simulations using the previous models. The objective is to compare the performances of different configurations of hybrid ground source heat pump systems. A base case without solar collectors is compared to a classical mitigated loop configuration. Using the both previously developed models, independent boreholes and independent circuits configurations are also simulated.

This thesis ends with a general conclusion on the three papers, highlighting the advantages and inconvenient of each configuration and recommending further work that could be done.

CHAPTER 1

LITTERATURE REVIEW

Energy can be found in numerous states such as mechanical, electrical, chemical and thermal. Thermal energy can be stored with different methods which can be divided in two main categories: sensible and latent heat storage. Sensible heat storage uses a material's temperature difference to store energy while latent heat storage uses the energy required to change the phase of a material. Even though latent heat storage is usually more compact than sensible heat storage for the same amount of energy stored, there are technical difficulties to implement it such as supercooling, the fact that a heat exchanger that can deal with two phases is hard to build and there is irreversibility in the process (Dinçer and Rosen, 2011).

Generally, thermal storage is divided in three processes: recharge, storage and discharge, as shown in Figure 1-1.

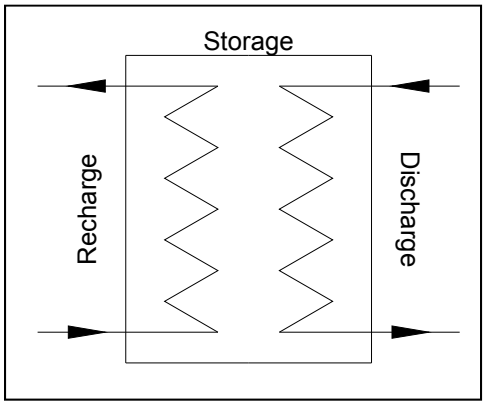

Figure 1-1 Thermal storage processes

The ground can be used as a sensible heat storage medium. Ground heat storage, also known as underground thermal energy storage (UTES), is divided in four main categories (Pahud, 2002):

- Ground diffusive storage, which uses the ground as storage medium and is normally a vertical heat exchanger. Borehole thermal energy storage (BTES) is one type of exchanger;
- Earth storage, which also uses the ground as a storage medium, but is normally horizontal, such as an excavated volume. The top surface can be insulated;
- Aquifer storage that uses underground water and its surrounding ground as storage medium;
- Water storage that can be underground or above ground tanks, insulated or not.

This research deals with shared geothermal fields between different sources. It is divided in major themes: Ground-source heat pump, ground temperature, ground heat exchange, sizing geothermal loops and software.

1.1 Ground-source heat pump

The main utilization of geothermal boreholes and borefields is the coupling with a heat pump, called ground source heat pump or ground coupled heat pump. Heat pumps require low-temperature heat sources, such as ambient air, groundwater and ground. In some locations, air temperature can be too low to extract any heat from it. Groundwater, in sufficient quantities, is an interesting alternative, but is not available everywhere. The ground however, does not involve these limitations.

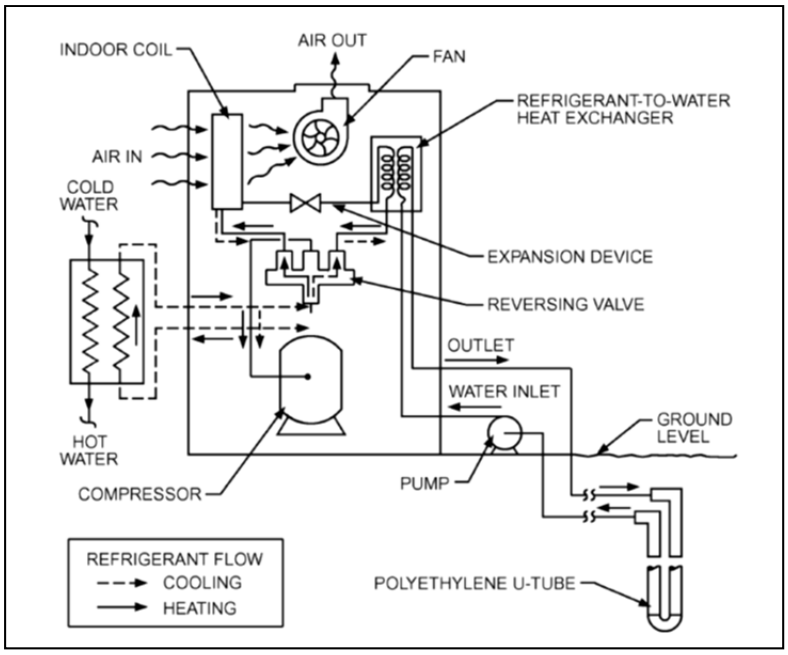

Figure 1-2 Ground-source heat pump (Kavanaugh, 1985)

Ground-source heat pumps (GSHP) or ground-coupled heat pumps (GCHP) shown in Figure 1-2 are systems that circulate water, or a mixture of water and anti-freeze, in a closed-loop circuit. They can be horizontal or vertical. The coupling to a heat pump permits using the ground as a heat sink (condenser) or a heat source (evaporator) for cooling or heating purpose, respectively. In heating mode, the efficiency of the system increases as the entering water temperature (EWT) rises. The efficiency reduces with time if the annual balance is towards heat extraction from the ground. The same efficiency reduction can be observed in cooling mode when the EWT rises. The COP is the ratio of supplied heat to the supplied work consumed by the heat pump. Figure 1-3 represents an example of coefficient of performance (COP) as a function of EWT.

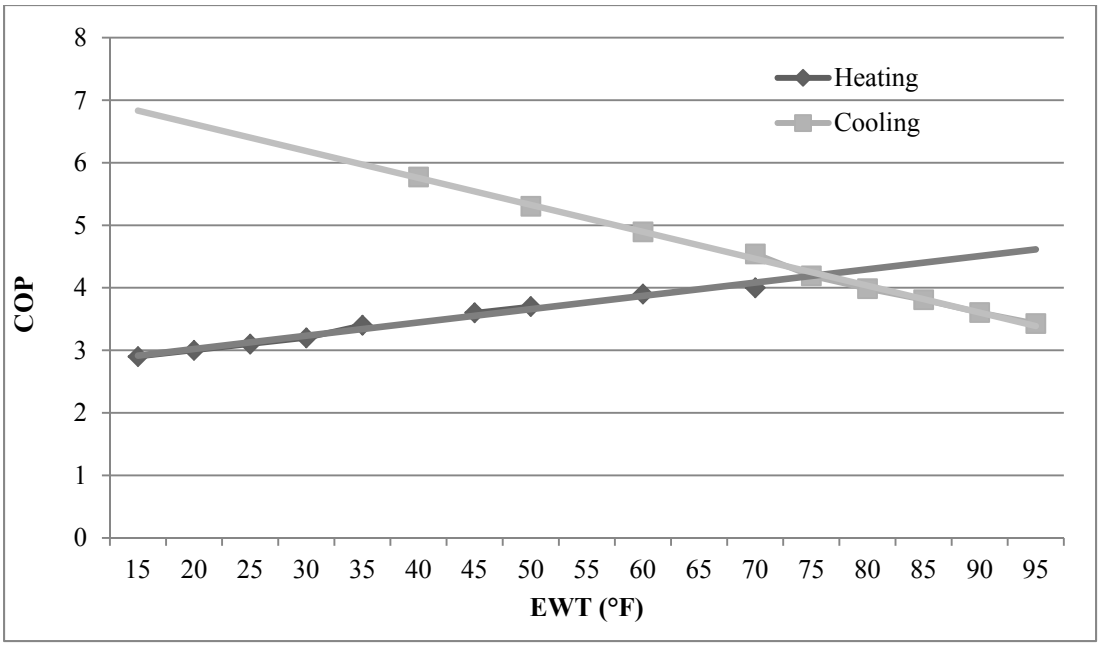

Figure 1-3 Heat pump COP vs. EWT

Each heat pump has its own specifications for minimum and maximum EWT. AHRI/ASHRAE/ISO 13256-1 code (ANSI/ARI/ASHRAE/ISO, 2005) tests heat pumps performances with heating EWT at 0°C (32°F) and cooling EWT at 25°C (77°F), but some can operate between -6°C (21°F) and 48°C (118°F). This heat pump EWT is in fact the leaving water temperature from the borehole, so the design of the BTES should be within the heat pump boundaries.

The other side of the heat pump is the heating and cooling demand, usually from a building. The heat pump can exchange heat with the air, radiant floor water or even domestic hot water. To achieve this, some components are required such as circulation pumps, heat exchangers, compressor, expansion valve and/or a fan. The building heating, ventilation and air-conditioning (HVAC) demand will size the heat pump capacity.

The impact of the on/off cycle of ground-source heat pumps using steady-state models leads to overestimation of energy use and to a different design that would have been done with

dynamic models (Kummert and Bernier, 2008). Therefore, the dimensions of the borefields depend greatly on the assumptions made during the design.

1.2 Ground temperature

Kusuda provides surface temperature profiles as simple harmonic presentation, which are considered by the authors as a "fair approximation of monthly average earth temperature except near the surface, provided the annual average temperature, the annual amplitude and phase angle of the surface temperature, and the thermal diffusivity are known." (Kusuda and al., 1965). Kusuda model is used in TRNSYS® and TESS® components. The model is presented in equation 1.1.

$$T = A - BO \exp^{-\sqrt{\left(\frac{\pi}{DT}\right)}x} \cos\left(\frac{2\pi\theta}{T} - \sqrt{\frac{\pi}{DT}}x - PO\right) \tag{1.1}$$

Figure 1-4 shows ground temperature profile using Kusuda supplied parameters for Ottawa, Ont. (Canada): A = 47.0°F, B0 = 21.0°F, P0 = 0.64, D = 0.025.

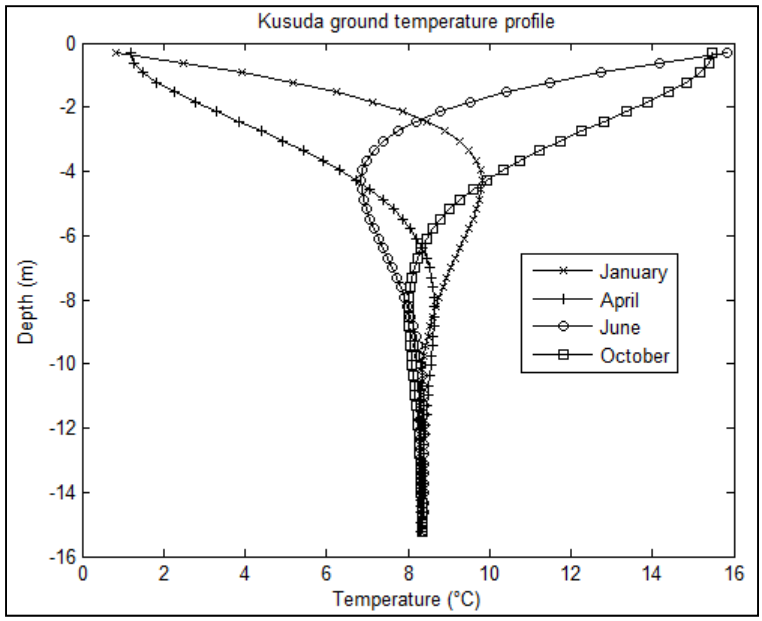

Figure 1-4 Ottawa ground temperature profile

This model shows that seasonal weather impacts are limited in depth in the ground. Temperature stabilizes around 15 m deep to 8.3°C (47°F). Mihalakakou developed a surface ground temperature model based on many factors such as convective energy exchange between air and soil, solar radiation absorbed, evaporation and long-wave radiations emission (Mihalakakou and al., 1997). Figure 1-5 represents these factors.

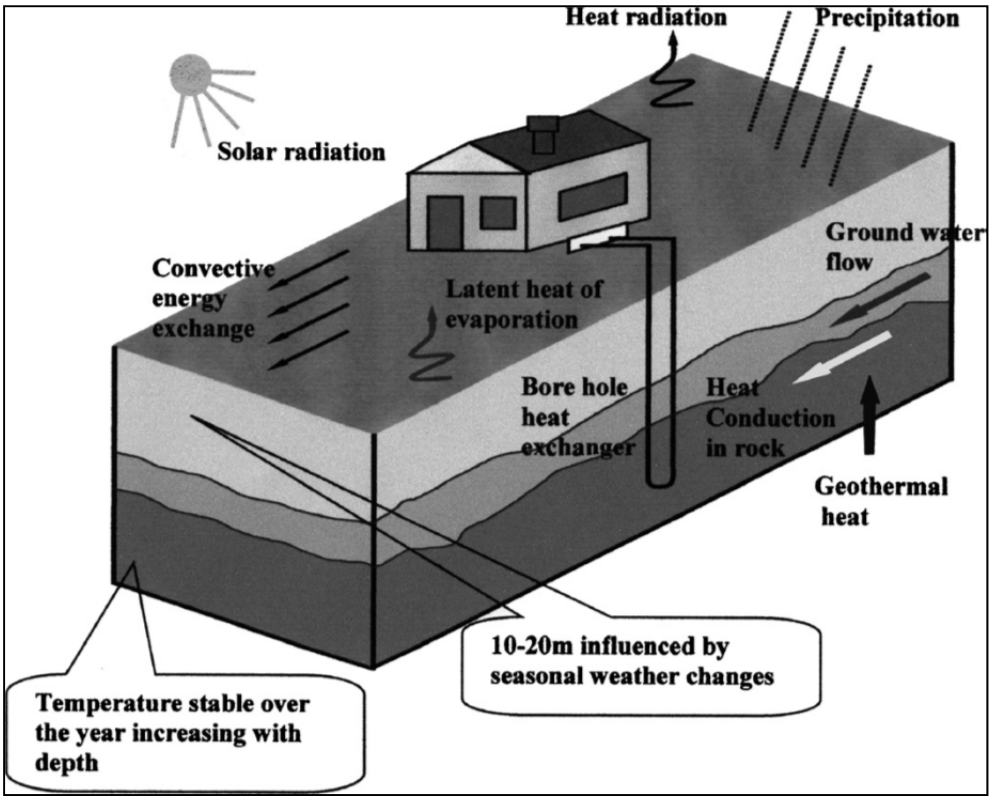

Figure 1-5 Energy balance on ground (Florides and Kalogirou, 2007)

Near the surface (0 - 10 m), heat is exchanged with the environment (sun, evaporation, ambient air, etc.). At mid-distance, fewer variations can be observed (10 m - 20 m). Deeper than 20 m, very low variations are observed. Energy transferred from the Earth's core gives a geothermal gradient of about 15 to 35 °C/km in the United States (Nathenson and Guffanti, 1988). Depending on the depth considered for thermal storage, the weather conditions might not always have a significant impact on it; such could be the case for BTES.

A more recent study based on energy balance of the ground surface takes into consideration convection from the wind, solar energy, sky temperature and water evaporation factors has shown good agreement with experimental results (Badache and al., 2016).

1.3 Ground Heat Exchange

The BTES method is normally found in the form of a vertical U-tube heat exchanger buried in the soil. It is composed of a plastic pipe, inserted in a vertically drilled borehole which is can be filled with grout as schematically shown in Figure 1-6.

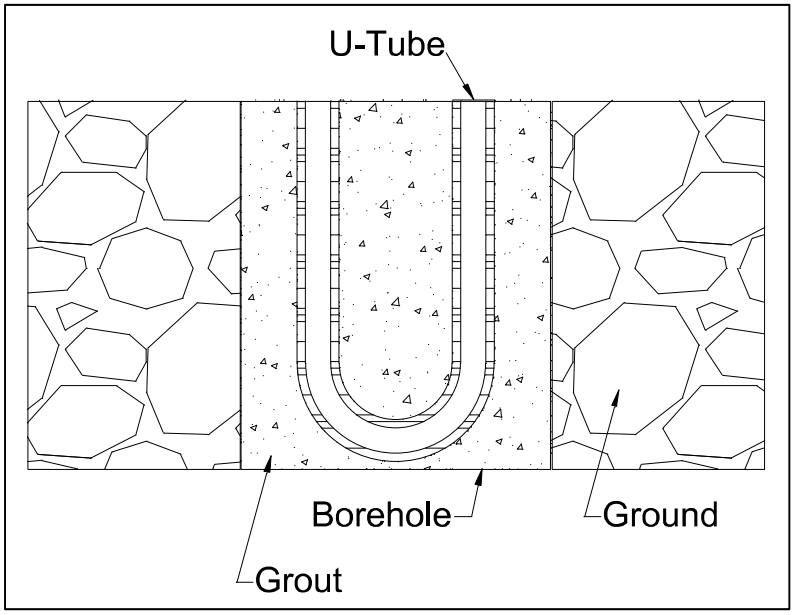

Figure 1-6 Schematic of a section of a vertical borehole

To ensure heat transfer to and/or from the ground, a heat transfer fluid is circulated through the plastic tube. Convective heat transfer occurs between the fluid and the inner surface of the plastic tube and conductive heat transfer occurs through the plastic pipe from the inner to the outer surface. There is a contact resistance between the tube and the grout. Then, heat is diffusing across this resistance and the grout. This whole portion of heat transfer is modeled herein as an equivalent borehole thermal resistance that accounts for the four phenomena. However, the contact resistance is found to be negligible and is not considered herein. The

outer part, composed of conductive heat transfer from the borehole to the ground and convective heat transfer from groundwater to the borehole, is called ground heat exchanger.

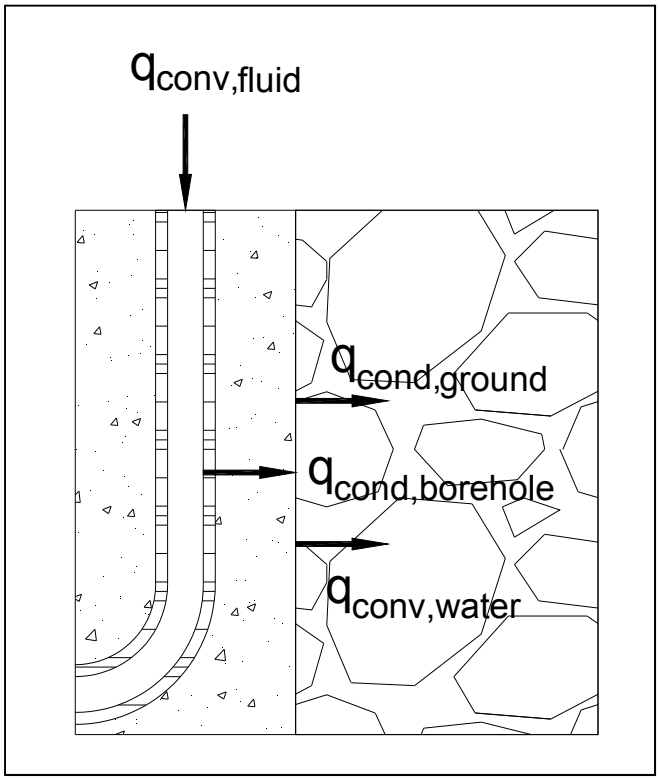

Figure 1-7 Heat transfer of BTES

The impact of groundwater flow on geothermal borefields has been studied and models are available (Bauer and al., 2009; Chiasson, 1999; Lee and Lam, 2007; Molina-Giraldo and al., 2011; Niibori and al., 2005; Sutton and al., 2003; Wang and al., 2009). The axial effect and groundwater flow is recommended to be taken into considerations with Peclet numbers between 1.2 and 10 (Molina-Giraldo and al., 2011). Nevertheless, the present research will not take groundwater flow into consideration.

For most of the available studies, the approach to model a BTES system considers heat transferred between:

- the fluid and the inside of the pipe;

- the inside of the pipe and the outside of the borehole;
- the outside of the borehole and the ground;

This framework will be adopted in this study.

1.3.1 Boreholes thermal resistance

In order to evaluate the heat transferred from the borehole surface to the fluid, the thermal resistance approach can be used. The heat transfer per unit length, subject to the above-mentioned assumptions, through all components (q'_b) is represented in eq. (1.2). It can be modeled as thermal resistances as shown in eq. (1.3) (Incropera and DeWitt, 2007) and represented in Figure 1-8.

$$T_b - T_f = q'_b R'_b \tag{1.2}$$

$$R'_b = R'_{conv,f} + R'_{cond,p} + R'_g \tag{1.3}$$

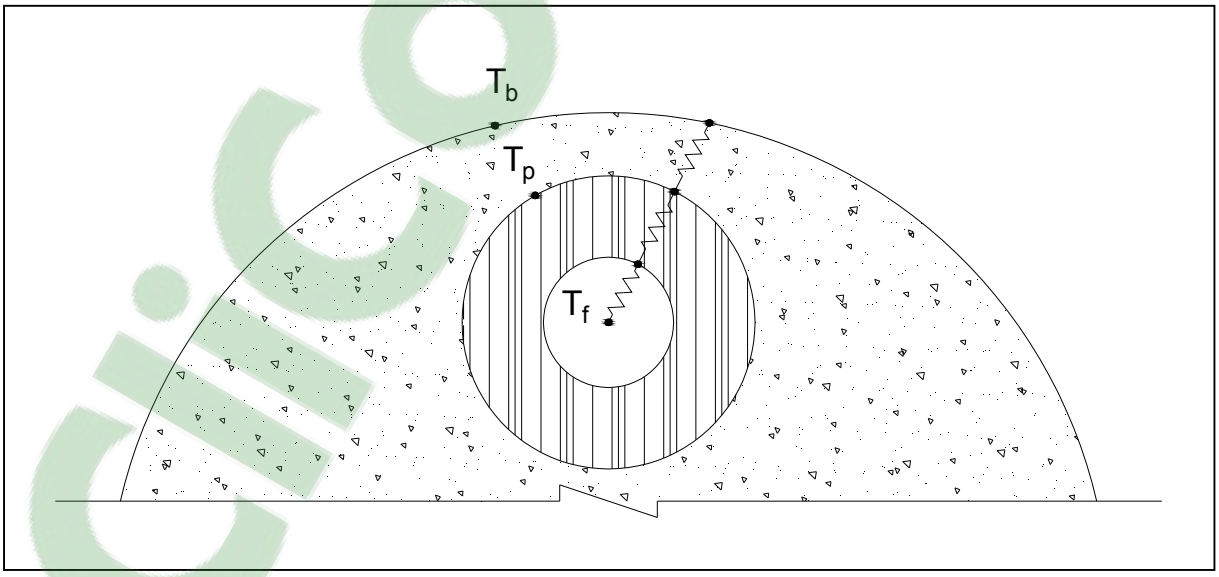

Figure 1-8 Thermal resistance of a borehole heat exchanger

The heat from the source is exchanged with the fluid. This source can be steady or unsteady. The heat is then transferred to the surface of the U-tube based on eqs. (1.4) and (1.5) (Incropera and DeWitt, 2007).

$$q_{conv,f} = hA_p\Delta T \tag{1.4}$$

Here, ΔT is the temperature difference between surfaces and h is the convection heat transfer coefficient. Since there are two pipe sections per U-tube, the convection resistance per unit length can be divided by 2,

$$R'_{conv,f} = \frac{1}{4\pi r_{pi} h} \tag{1.5}$$

where r_{pi} is the internal radius of the pipe. The second resistance is between the inside of the pipe and the grout ($R'_{cond,p}$),

$$R'_{cond,p} = \frac{\ln\left(r_{po} / r_{pi}\right)}{4\pi k_p} \tag{1.6}$$

where k_p is the thermal conductivity of the pipe.

Many models are available to evaluate the borehole thermal resistance (R'_g) :

- Paul (Paul, 1996);
- Sharqawy (Sharqawy, 2008);
- Line-source (Hellström, 1991);
- Multipole (Bennet and al., 1987; Claesson and Hellström, 2011).

These models have been compared with a 2D and 3D finite element analysis with COMSOL® (Lamarche and al., 2010). The 2D models gave better results for the Multipole model, except for the cases where the temperature was constant all around the borehole, such as when steel casing is used.

The 3D approach, based on borehole resistance and internal resistance, showed that the Zeng contribution resembles to COMSOL® results. The COMSOL® analysis was also compared with DST model results. Both methods gave comparable results on long term simulations, but since the capacitance of the borehole is not taken into account in DST, the short term simulations results were incoherent. The 2D models (except Hellström) are analytical, thus does not need to be computed unlike the 3D models numerical analysis.

In most of the models, the fluid is considered to be at uniform temperature (T_b) at the pipe interface, but having different temperatures at the inner and outer part of the U-tube could be more accurate (Lamarche and al., 2010).

Other models are quasi 3D models to take into account the axial heat transfer: Zeng (Zeng and al., 2003), P-linear (Marcotte and Pasquier, 2008) and Spectral (Al-Khoury, 2011).

Models also take thermal capacities into account to improve short time simulation results. (Bauer and al., 2011; De Carli and al., 2010; Pasquier and Marcotte, 2012; Zarrella and al., 2011), which is an important factor for short-term simulations precision.

From this borehole resistance model, the temperature at the outer surface of the borehole (T_b) is calculated and then transferred to the ground models.

1.3.2 Ground models

Ground models can be organized in two categories: analytical and numerical models. Classical analytical models are: Infinite line source model (Ingersoll and Plass, 1948),

infinite cylindrical source and finite line source (Claesson and Javed, 2011; Lamarche and Beauchamp, 2007a; Zeng and al., 2002). These models have been reviewed and their validity ranges have been compared (Philippe and al., 2009) as well as their short step-time validity (Lamarche, 2013). Most of the analytical models evaluate the mean borehole surface temperature assuming a uniform heat flow along the borehole, some others evaluate the mean heat flux assuming a uniform borehole temperature (Cimmino and Bernier, 2014). In all cases, the solutions are given for a constant heat pulse, and temporal superposition is used to evaluate the effect of the variation of the heat load into the ground.

Geothermal models have been reviewed by others (Ruan and Horton, 2010; Yang and al., 2010). In these models, the heat transfer is purely conductive, no groundwater convection is considered. The analytical models studied by Philippe et al. (Philippe and al., 2009) are:

- Infinite line source model (Ingersoll and Plass, 1948);
- Infinite cylindrical source (Ingersoll, 1954);
- Finite line source (Eskilson, 1987).

For longer periods (months), the finite line source is more accurate since the effects at the ends of the borehole are taken into account. Most of the analytical models neglect the axial heat transfer, giving more accurate estimations to numerical models.

Some numerical and hybrid analytical/numerical models are reviewed by Yang et al. (Yang and al., 2010) are:

- Duct Storage System (DST) (Hellström, 1989);
- Rottmayer (Rottmayer, 1997);
- Li (Li and Zheng, 2009);
- Superposition Borehole method (SBM) (Eskilson and Claesson, 1988);
- Koohi-Fayegh et Rosen's (Koohi-Fayegh and Rosen, 2014).

The DST simulation model (Hellström, 1989; Pahud and al., 1996), available on TRNSYS (TRNSYS, 2011a) as a component. It is divided in local and global processes and uses cylindrical coordinates and the storage volume is considered cylindrical. Using the finite difference method and an analytical model, the DST model predicts the behavior of a geothermal borefield through time. The method is described in a manual supplied with TRNSYS (Hellström, 1989) and in a thesis (Chapuis, 2008). The DST borefield can only simulate one inlet temperature and flow rate in borefields and the boreholes are considered as uniformly distributed in the borefield.

Rottmayer (Rottmayer, 1997) developed a vertical U-tube heat exchanger model based on Euler's finite difference numerical technique. The storage volume is divided axially into two-dimensional cylindrical mesh sections. The model is also used in TRNSYS software and returned comparable results to Hellström's model.

Li (Li and Zheng, 2009) developed a 3D unstructured finite volume model using Delaunay triangulation mesh method. The model divides the ground in layers to take fluid temperature variation into account. It also takes the interaction between the legs of the U-tube into account. It showed good agreement with experimental values.

Eskilson (Eskilson and Claesson, 1988) uses finite difference method, with radial-axial coordinates, to evaluate the impact of time-dependent step heat extraction or injection, and superposes them. The model computes non-dimensional temperature response factors (g-functions). The axial conductive heat transfer is incorporated in the numerical model by an analytical solution. The time-step is, however, accurate for long time-step (from a few hours to months). Equation (1.7) shows the g-function used to find borehole temperature T_b. T_m is the average fluid temperature entering and leaving the borehole, q' is the heat extraction/injection rate per length unit, λ the mean ground conductivity, Es is the Eskilson number, r_b the borehole radius, H the borehole length.

$$T_b(t) = T_m - \frac{q'}{2\pi\lambda} g\left(Es, r_b / H\right) \tag{1.7}$$

$$Es = \frac{t}{t_s} \tag{1.8}$$

Where,

$$t_s = \frac{H^2}{9\alpha_s}$$

t_s is the steady-state time, t the simulation time step and α the thermal ground conductivity. The validity limit of t is within

$$\frac{5r_b^2}{\alpha_s} < t < \frac{t_s}{10} \tag{1.9}$$

which stands between a few hours and a few years (Eskilson, 1987).

Yavusturk developed a short time-step (one hour or less) model for vertical boreholes models (Yavuzturk and Spitler, 1999). It is a transient two-dimensional finite volume model and is implemented in a component of TRNSYS software (TRNSYS, 2011a). Its model also returns temperature response in non-dimensional values (g-functions). The grout resistance (R'_b) is based on Paul's model. A load aggregation algorithm is used to reduce computation time and the aggregated loads are superimposed.

A spectral model has been developed for shallow geothermal systems (Al-Khoury, 2011). The resolution of the problem is done with discrete Fourier transform and takes into account axial temperature variations.

Degradation of performances occurs due to interference between the legs of the U-tube whilst the downward and upward fluid flow temperature differs. The number of U-tubes per bore also interferes. Kavanaugh and Eskilson take these factors into consideration in their models. There is also interference between multiple boreholes.

When several boreholes heat exchangers are close to each other, the heat transferred to the ground by each of them can affect the others. Usually coupled in parallel, the fluid enters in each borehole at the same temperature, but goes out at a different one. The temperature distribution can be as shown in Figure 1-9.

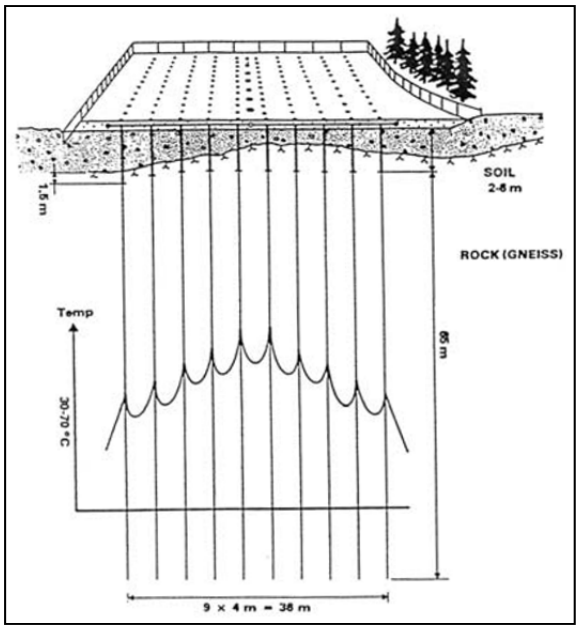

Figure 1-9 Schematic representation of interference between boreholes (Hellström, 1991)

In this case, heat in injected in the borefield. Since the ground temperature around the borefield is colder than the injected fluid, the temperature surrounding peripheral boreholes is lower than the center ones. Factors that influence this interaction are evaluated as "temperature penalty" (ASHRAE, 2007), g-functions (Eskilson, 1987) and have been studied in a 2D finite element model (Koohi-Fayegh and Rosen, 2012). They are: distance between boreholes, heat flux from the borehole wall and time of system operation.

Work has been done for faster computation of the solution:

- Multiple Load Aggregation (MLAA) (ASHRAE, 2008) (Bernier and al., 2004);
- Finite line source new contribution (Lamarche and Beauchamp, 2007a);
- g-functions, faster computation (Lamarche, 2009).

1.3.3 Configurations

An approach to evaluate the impact of each borehole temperature on others in a borefield has been developed for the ASHRAE method (Kavanaugh and al., 1997). A penalty temperature is imposed on borehole surface temperature. This method has been modified to take into account location of the boreholes in a borefield (Fossa, 2011). The shapes evaluated for the borefield are in-line, rectangular, L-shaped and square.

These shapes also have been evaluated by Eskilson (Eskilson, 1987). Long-term influence of each borehole on another can be evaluated from g-functions. Claesson states that the influence between boreholes can be neglected for the first year of operation, if the distance separating the boreholes exceeds 10 m (Claesson and Eskilson, 1988). The g-functions are given for more than 200 configurations taking into consideration boreholes number, spacing, depth, as well as borefield shape: In-line, triangle, square, rectangle, U-shape, L-shape, circle, fan-shaped, for vertical and inclined boreholes.

More than one U-tube can be inserted in a borehole. A model of a double U-tube with two independent circuits (Eslami-Nejad and Bernier, 2011a) has been developed. It takes into account different inlet conditions such as fluid temperature and flowrate.

A network-based model allowing the simulation of different inlet conditions in boreholes of a borefield has recently been proposed by Lazzarotto (Lazzarotto, 2014).

1.3.4 Control strategy

Even if some models take a continuous heat injection control into account, the operation of a heat pump is intermittent and most of the numerical models are able to handle short-step simulations. A study concerning shallow geothermal boreholes (20 m deep) concluded that by injecting a constant temperature fluid in discontinuous operation mode, the heat transfer rate was increased as shown in (Miyara, 2011).

Table 1-1 Discontinuous operation heat transfer rate increase

Pulse (hours On/Off)	Single U-tube	Double U-tube	Multi U-tube
2	17.1 %	22.6 %	16.3 %
6	32.6 %	39.8 %	32.1 %
12	14.0 %	15.1 %	13.9 %

Hybrid systems can reduce the size of the borefield by supplying extra heating or cooling to buildings during peak demand from conventional HVAC equipment (Gentry and al., 2006; Hackel and Pertzborn, 2011a; Hern, 2004; Yavuzturk and Spitler, 2000). A thermodynamic analysis proved that this approach is more efficient than air-source heat pump (Lubis and al., 2011).

It can also be useful to balance loads on the borefield. An example would be in cold climates where more heat is extracted from the ground for heating than injected back for cooling of buildings. A study also couples a borefield to solar panels for heating dominated climates (Chiasson and Yavuzturk, 2003).

Figure 1-10 shows an example of a hybrid system with a cooling tower.

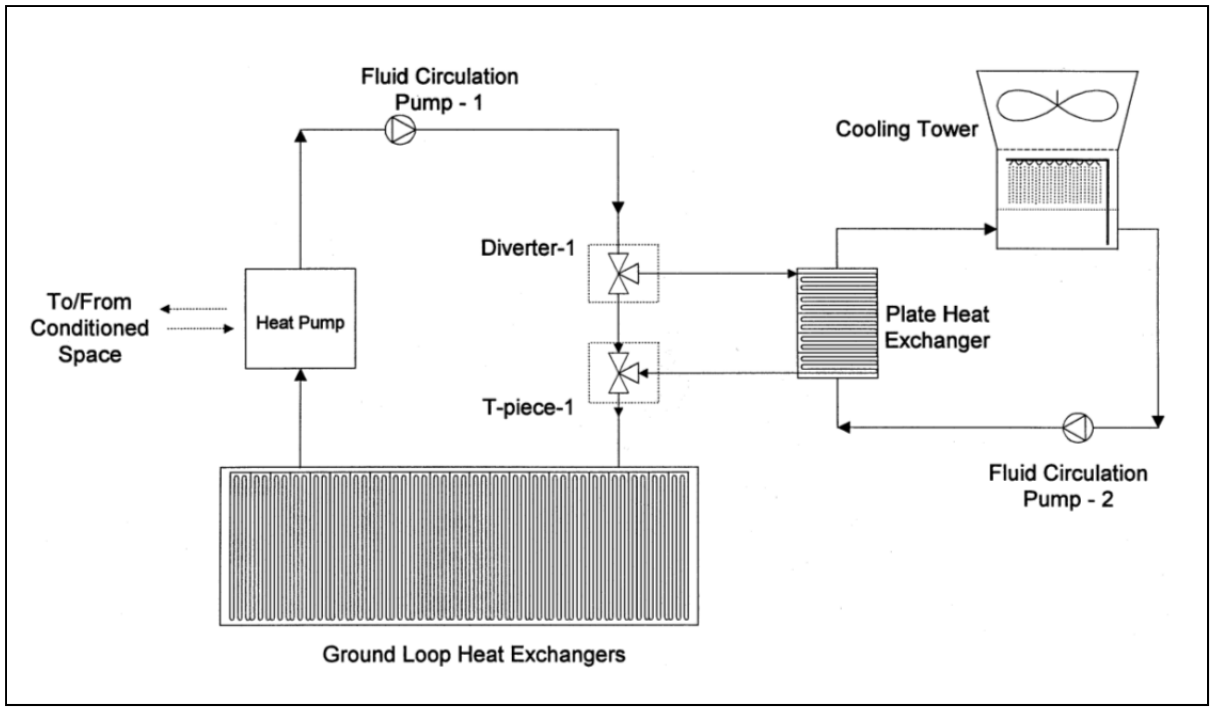

Figure 1-10 Hybrid system (Yavuzturk and Spitler, 2000)

Other options can be evaluated such as complementary loads from buildings and waste heat from an industrial process but it becomes difficult to simulate such systems with monthly loads approach used by most current methods and software.

1.4 Sizing geothermal loops

Thermal energy can be stored in the ground, but the performances of such a medium depends on several factors, such as the ground composition, the location of the storage, water content, temperature of the storage, etc.

Dimensioning geothermal boreholes and borefield is done by:

- Evaluating the heating and refrigeration loads by rules of thumb (Bell, 2007), energy simulation software such as DOE2 (EnerLogic and James J. Hirsch & Associates, 2009), Simeb® (Simeb, 2011) or TRNBUILD (TRNSYS, 2011a);
- Choosing HVAC equipment from manufacturer's catalogues, such as the heat pump, which will define the loads to be exchanged to the ground;

- Determining ground properties with a thermal response test (TRT) or geotechnical investigation (Hwang and al., 2010);
- Choosing refrigerant to be circulated through the BHE, as well as the fluid flow rate, constant or variable flow rate. The flow would have to be turbulent to increase heat transfer rate, considering that the pumping power increases with the flow;
- Design the piping loop, including pipe size, header connection, reverse or direct return piping, system flushing and the mechanical room layout;
- Specifying borefield configuration, including its shape and distance between boreholes, one or more U-tubes per bore;
- Elaborating a control strategy, including the fraction of the peak load to be covered by the BHE, the auxiliary heaters operation, hybrid systems and algorithms;
- Calculating preliminary boreholes length with one or more of the different methods;
- Fine tuning the design by evaluating different variations of each of these steps.

Kavanaugh et al. developed a method that uses cyclic blocks (annual, monthly and 4 hours) for the cylindrical source model (Kavanaugh and al., 1997). This method is recommended by ASHRAE. It has been modified for hourly loads (Bernier and al., 2004). It is also called Multiple Load Aggregation Algorithm and uses, like Yavusturk, load aggregation. The model has been compared with Hellstrom's DST for single borehole and a borefield. The RMS value of the difference between models is below 1 K over a 10 years simulation period on both arrangements.

Long-term simulation of a borefield (Rybach, 2001; Signorelli and al., 2005) showed that the time for the ground to recover its initial conditions roughly equals the operation time (ex.: 30 years of operation, 30 years of recovery). Another factor that impacts the performances of borefields is its configuration.

1.5 Software

Many computer programs are available to evaluate the dimensions of geothermal boreholes and borefields. Here is a non-extensive list:

- Lund Programs;
- Earth Energy Designer (EED) (Blomberg and al., 2008; Hellström and al., 1997);
- GshpCalc (Kavanaugh, 2010);
- GS2000 (Morrison, 2000);
- TRNSYS with DST module (Pahud and al., 1996; TRNSYS, 2011a);
- PILESIM (Pahud, 1999);
- Ground Loop Design (Thermal Dynamics Inc., 2012);
- EWS (Wetter and Huber, 1997).

Figure 1-11 shows different simulation results comparison by Shonder et al.

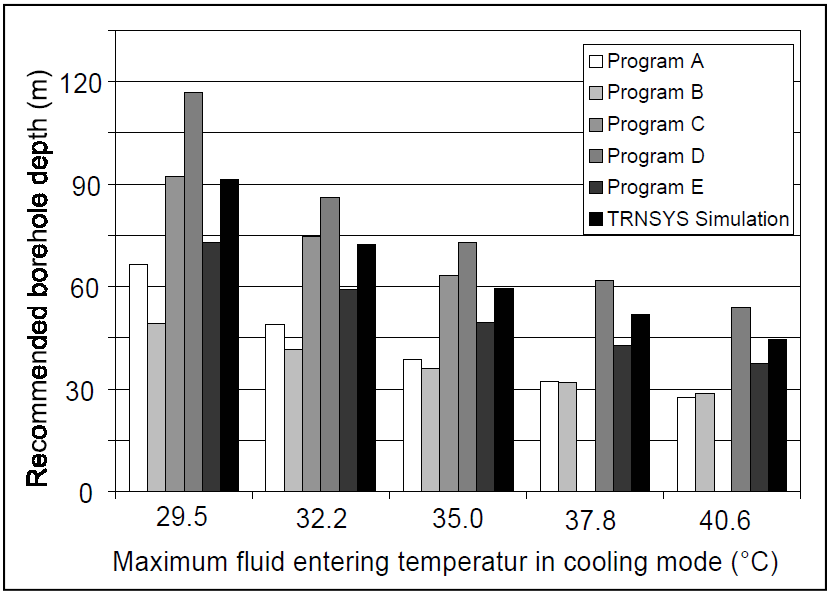

Figure 1-11 Simulation programs comparison (Shonder and Hughes, 1998)

In their paper, the authors do not state the name pf the programs used, but the differences in length from the software in 1998 were disturbing. In 1999, the same authors compared a new version of the software and the results were more consistent. The lengths of boreholes varied from 7% for cooling dominated simulations to 16% for heating dominated simulations. These differences are mainly due to the assumptions made from the software (Hellström and Sanner, 2001; Shonder and al., 1999).

CHAPTER 2

SEMI-ANALYTICAL MODEL FOR GEOTHERMAL BOREFIELDS WITH INDEPENDENT INLET CONDITIONS

Patrick BELZILE, Louis LAMARCHE, Daniel R. ROUSSE

Département de génie mécanique, École de technologie supérieure,
1100, rue Notre-Dame Ouest, Montréal (Québec), Canada, H3C 1K3

Article published in "Geothermics" journal in January 2016

2.1 Abstract

A model has been developed to simulate a geothermal borefield for which borehole inlet conditions can be defined independently. The borefield is modeled with a control-volume finite difference method while boreholes are modeled as analytical thermal resistances. An analytical shape factor is used to link the borehole models to the surrounding ground models. The main advantages of the proposed model are its versatility with respect to the specification of different inlet conditions and that the temperature of the disturbed ground can be known at any point of the borefield. Application examples, coupling solar collectors and heat pumps, showed that segregating the components into two loops requires 4.3% more energy from the heat pumps than a single loop arrangement for the first five years, but will require less energy after. The examples demonstrate the interest of the proposed method.

2.2 Introduction

Geothermal heat pump systems have been in use for years in building heating, ventilation and air conditioning (HVAC) applications. District heating and cooling applications could provide an economy of scale in energy consumption for larger construction projects.

Nevertheless, when a geothermal borefield must be shared, the calculation is done in a classical manner such that each borehole in the borefield has the same inlet temperature and flow rate.

The objective of this paper is to present a geothermal model that allows independent inlet conditions for each borehole in a borefield. The interest of the method is shown by comparing the energy required from heat pumps to supply the residential heating and cooling loads in different geothermal heat pump and solar collector configurations.

In this paper, a short literature survey is presented, followed by a description of the new model for shared geothermal borefields and a comparison of different configurations of geothermal heat pump systems coupled with solar collectors.

2.3 Brief literature review

Geothermal borefield models can be organized in two categories: analytical and numerical models. The classical analytical models are: the infinite line source model (Ingersoll and Plass, 1948), infinite cylindrical source model (Ingersoll, 1954) and finite line source model (Zeng and al., 2002), including a contribution to the finite line source model (Lamarche and Beauchamp, 2007a). These models have been reviewed and their validity ranges have been compared (Philippe and al., 2009) as well as their short step-time validity (Lamarche, 2013). Most of the analytical models evaluate the mean borehole surface temperature assuming a uniform heat flow along the borehole, others evaluate the mean heat flux assuming a uniform borehole temperature (Cimmino and Bernier, 2014). In all cases, the solutions are given for a constant heat pulse, and temporal superposition is used to evaluate the effect of the variation of the heat load into the ground. Models also take thermal capacities into account to improve short time simulation results (Bauer and al., 2011; Pasquier and Marcotte, 2012).

Numerical and hybrid analytical/numerical models have been proposed: Duct Storage System (DST) (Hellström, 1991), Rottmayer's (Rottmayer, 1997), Li's (Li and Zheng, 2009),

Superposition Borehole method (SBM) (Eskilson and Claesson, 1988) and Koohi-Fayegh and Rosen's (Koohi-Fayegh and Rosen, 2014).

Among these, Eskilson and Claesson use a finite difference method, with 2-D axisymmetric coordinates, to evaluate the impact of time-dependent step heat extraction or injection, and superpose them. The authors compute dimensionless temperature response factors (g-functions). The axial conductive heat transfer is incorporated in the numerical model by an analytical solution.

When more than one borehole heat exchangers are close to another, the heat transferred to the ground by each of them can influence the behaviour of the others. The boreholes are usually coupled in parallel and the temperature at which the fluid enters each borehole is the same, but different when it exists. Factors that influence this interaction are evaluated as "temperature penalty" (ASHRAE, 2007), g-functions (Eskilson, 1987) and have been studied in a 2D finite element model (Koohi-Fayegh and Rosen, 2012). These factors include the distance between the boreholes, the heat flux from the borehole wall, the time of system operation and ground properties.

Using the finite difference method and an analytical model, the DST model estimates the behavior of a geothermal borefield through time. The method is described in a manual supplied with the TRNSYS® software (TRNSYS, 2011b) (Hellström, 1989) and in Chapuis' thesis (Chapuis, 2008). The DST model is divided into three parts: local process, global process, and steady flux. The borehole resistance (R'_b) is based on the Hellström line-source model (Hellström, 1991). The DST simulation model (Hellström, 1989; Pahud and al., 1996) can only simulate one inlet temperature and flow rate in borefields and the boreholes are considered as uniformly distributed in the borefield. All of these models are valid for a minimum period of a few hours.

Work has been done to shorten the time-step of different methods: Yavusturk (Yavuzturk and Spitler, 1999) developed a short time-step (one hour or less) model for vertical boreholes. Li

developed a 3D unstructured finite volume model using Delaunay's triangulation mesh method (Li and Zheng, 2009). The model divides the ground into layers to take fluid temperature variation into account. It also considers the interaction between the legs of the U-tube. More recently, a study modeled the two legs of a U-tube as a single equivalent pipe in an analytical model (Claesson and Javed, 2011).

A spectral model has been developed for shallow geothermal systems (Al-Khoury, 2011). The problem is solved using the discrete Fourier transform and takes into account axial temperature variations.

Many models exist to evaluate a borehole's thermal resistance (R'_b). Some are 2D models: Paul (Paul, 1996), Sharqawy (Sharqawy, 2008), Line-source (Hellström, 1991), and Multipole (Bennet and al., 1987). Others are quasi 3D models to take into account the axial heat transfer: Zeng (Zeng and al., 2003), P-linear (Marcotte and Pasquier, 2008) and Spectral (Al-Khoury, 2011).

These models were compared in a 2D and 3D finite element analysis using COMSOL® (Lamarche and al., 2010). Generally, the 2D models gave better results for the Multipole model, except in cases for which the temperature was constant all around the borehole, such as when steel casings are used. The 3D approach, based on borehole resistance and internal resistance, showed that the Zeng contribution provides results comparable to COMSOL® results. The COMSOL® analysis was also compared with DST model results.

Finally, a network-based model allowing the simulation of different inlet conditions in boreholes of a borefield has recently been proposed by Lazzarotto (Lazzarotto, 2014).

2.4 Description of the proposed model

The proposed model is a semi-analytical model that evaluates temperature exchange between a fluid and the ground through geothermal boreholes.

For now, the numerical part uses a 2-D control volume finite difference method (CVFDM) to solve the conduction problem in the ground. As a result, the problem is assumed to be independent of depth, L_p. A point-by-point Gauss-Seidel iterative method is used to evaluate the temperature field caused by diffusion in the surrounding ground. A tri-diagonal matrix algorithm (TDMA) method was tried, but did not yield any advantage in the computational time. On structured grids, a TDMA usually decreases the CPU time as the information from the boundaries is distributed much faster within the domain. Here, the boreholes drive the problem and information comes from within the domain. This may explain the results obtained with a TDMA.

The analytical part of the model is composed of a multipole borehole thermal resistance (Claesson and Hellström, 2011). The link between the analytical and numerical parts is done with a shape factor, under a quasi-steady-state assumption.

2.4.1 Numerical part

For a ground assumed to involve constant thermophysical properties, the two-dimensional Cartesian heat conduction governing equation in a horizontal plane is based on Fourier's law:

$$\rho c_s \frac{\partial T}{\partial t} = k_s \left[\frac{\partial}{\partial x}\left(\frac{\partial T}{\partial x} \right) + \frac{\partial}{\partial y}\left(\frac{\partial T}{\partial y} \right) \right] + S_T \tag{2.1}$$

In eq. (2.1), the source term S_T is defined by analytical models in the relevant areas of the domain.

The control volume finite difference method (CVFDM) is used to discretize the space-time domain problem in *x, y, t*. as most borehole arrangements have a structured pattern.

Discretization is done through a structured regular mesh. A "Type A" grid is used, which involves half-control volumes at the boundaries (Patankar, 1980). Dirichlet boundary conditions are imposed on the four boundaries considering the ground temperature is undisturbed at a certain distance from the boreholes. Standard interpolation functions for properties and dependent variables are implemented, but not used as the properties are assumed to be constant (Patankar, 1980) in this first work on the subject.

2.4.2 Analytical part

The heat rate between the borehole heat exchanger and the surrounding ground is calculated from the convective heat transfer of the fluid passing through the U-tubes of the boreholes.

$$q = \dot{m}_f c_f \left(T_{f,in} - T_{f,out} \right) \tag{2.2}$$

As the problem is considered independent of depth L_b, from eq. (2.2), the source term in eq. (2.1) can be determined such that:

$$S_T = \frac{q}{dV} = \frac{q}{dx \cdot dy \cdot L_b} \tag{2.3}$$

But the outlet temperature, $T_{f,out}$ must be determined to calculate this source term. And this is the subject matter of this section.

First, the ground surrounding a borehole is modeled as a square control volume for which the thermal properties are uniform and constant and for which the boundary temperature is uniform at $T = T_a$. The inner borehole is then assumed to be at a fixed and uniform temperature $T = T_b$. Figure 2-1 depicts the relationship between the CV boundary and the borehole located at its geometric center.

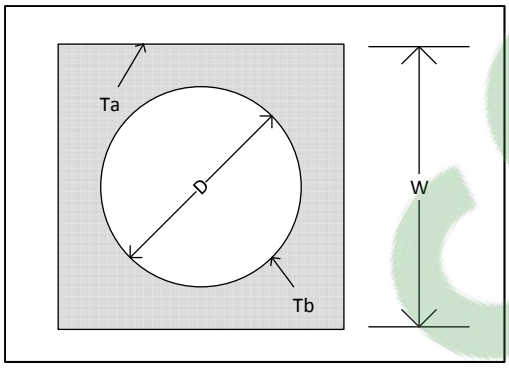

Figure 2-1 Shape factor

The heat flux equation per unit depth between the borehole (surface b) and the control-volume (surface a) is then given by:

$$q' = \frac{S \times k_s}{L_b}\left(T_b - T_a\right) = \frac{\left(T_b - T_a\right)}{R_c'} \tag{2.4}$$

For the above-prescribed assumptions, the shape factor S is readily given by (Incropera and DeWitt, 2007):

$$S = \frac{2\pi L_b}{\ln\left(1.8\left(\frac{W}{D}\right)\right)} \tag{2.5}$$

The unit length resistance R_c' can be introduced such that:

$$R_c' = \frac{L_b}{S \times k_s} \tag{2.6}$$

which represents the resistance to the conductive heat transfer between surface *a* and surface *b*.

But still the borehole temperature, T_b, is unknown. Then, the Multipole borehole thermal model proposed by Claesson and Hellström (2011) is employed. This model evaluates thermal interaction between pipes inserted in a cylinder. The resulting borehole thermal resistances, R_a', R_b', R_1', R_2', R_{12}', are functions of geometrical parameters, such as the radii

of the borehole and the pipes and distance between the pipes, as well as thermal properties of the pipe, grout, and the surrounding ground.

Hence, the heat flux between the fluid circulating in the pipe and the surrounding control volumes can be represented by the thermal resistance analogy, as shown in Figure 2-2.

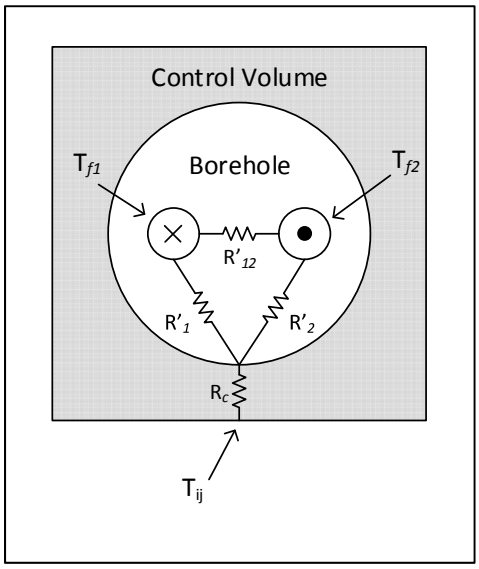

Figure 2-2 Combined borehole and shape factor thermal resistance analogy

The outlet fluid temperature $T_{f,out}$ is a function of the average ground temperature T_a. This temperature is evaluated from a weighted average of the nine ground control volume temperatures adjacent and contiguous for which the central control volume embeds a borehole, as depicted in Figure 2-3.

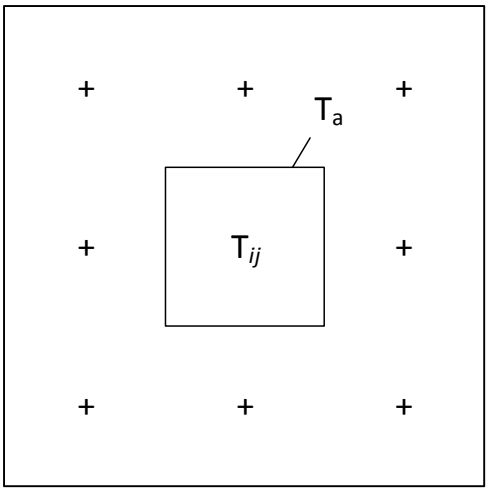

Figure 2-3 Ground temperature surrounding a source term

Hence, T_a is defined such that:

$$T_a = \left(\frac{T_n + T_e + T_s + T_w}{16} \right) + \left(\frac{T_{ne} + T_{se} + T_{sw} + T_{nw}}{16} \right) + \left(\frac{T_{i,j}}{2} \right) \tag{2.7}$$

This equation represents the link between the CVFDM and the analytical model that can determine the source term in the energy conservation equation.

The outlet fluid temperature can be determined from the known inlet temperature. As the z-axial variations are neglected, an average fluid temperature, T_f, can be defined as the arithmetic mean of the inlet and outlet temperature such that:

$$T_f = \frac{T_{f,in} + T_{f,out}}{2} \tag{2.8}$$

$T_{f,out}$ can be explicitly expressed, see eq.(2.2), such that:

$$T_{f,out} = T_{f,in} - \frac{q' L_b}{\dot{m}_f c_f} \tag{2.9}$$

The resistance between the fluid temperature, T_f, and the borehole wall temperature, T_b, then consists of two parallel and coupled resistances, R_1',and R_2'.

$$R_b' = \frac{R_1' \times R_2'}{R_1' + R_2'} \tag{2.10}$$

Then, a heat balance will require that the heat rate per unit depth between the fluid and the control volume surface a is equal to the heat rate per unit depth transferred to (or from) the ground to the fluid. This yields:

$$q' = \frac{T_f - T_a}{R_b' + R_c'} = \frac{\dot{m}_f c_f}{L_b}\left(T_{f,in} - T_{f,out}\right) \tag{2.11}$$

Substituting eqs. (2.8) and (2.9) into eq. (2.11) and combining both thermal resistances into a total resistance, $R_b' + R_c' = R_{tot}'$, the heat rate per unit length transferred from the fluid to the control volume surface (or conversely) can be expressed as a function of the inlet fluid temperature such that:

$$q' = \frac{\left[\frac{\left(T_{f,in} + T_{f,\text{out}}\right)}{2}\right] - T_a}{R_{tot}'} = \frac{\left[\frac{T_{f,in}}{2} + \frac{T_{f,in}}{2} - \frac{q'L_b}{2\dot{m}_f c_f}\right] - T_a}{R_{tot}'} = \frac{T_{f,in} - T_a - \frac{q'L_b}{2\dot{m}_f c_f}}{R_{tot}'} \tag{2.12}$$

Rearranging eq. (2.12) yields:

$$q' + \frac{q'L_b}{2\dot{m}_f c_f R_{tot}'} = q'\left[1 + \frac{L_b}{2\dot{m}_f c_f R_{tot}'}\right] = \frac{T_{f,in} - T_a}{R_{tot}'} \tag{2.13}$$

Or,

$$q' = \frac{T_{f,in} - T_a}{R_{tot}'}\frac{z}{z+1} \tag{2.14}$$

Where dimensionless constant z is conveniently defined so that:

$$z = \frac{2\dot{m}_f c_f R'_{tot}}{L_b} \tag{2.15}$$

Substituting (2.14) into (2.9), we obtain:

$$T_{f,out} = \frac{\left[(z-1)T_{f,in} + 2T_a\right]}{(1+z)} \tag{2.16}$$

Eq. (2.16) enables the connection between the proposed analytical solution for the borefield and the numerical solution for 2D heat conduction in the surrounding ground. The point of interest here is that for each borehole a different inlet temperature can be prescribed.

Once the heat transfer is computed through an iterative process, T_f, and ultimately $T_{f,out}$ can readily be determined from eqs. (2.9) and (2.8), respectively.

A more precise approach would be to take into account the thermal interference between both paths, T_{f1} and T_{f2} in Figure 2-2. Hellström shows that the new mean fluid temperature can be expressed in the same way by changing the borehole resistance by a modified and hence effective resistance:

$$R_b'^{*} = R'_b \eta \operatorname{cotanh}(\eta) \tag{2.17}$$

With

$$\eta = \frac{L_b}{m_p c_f}\sqrt{\frac{1}{R'_b R'_a}} \tag{2.18}$$

and considering R_1' = R_2', the internal resistance of the borehole, R_a', becomes:

$$\frac{1}{R'_a} = \frac{1}{2R'_1} + \frac{1}{R'_{12}} \tag{2.19}$$

With the proposed approach, one must modify this last expression to take into account the shape factor resistance. In the usual Hellström approach, the following heat balance is used:

$$q_1' = \frac{T_{f1} - T_b}{R_1'} + \frac{T_{f1} - T_{f2}}{R_{12}'} \quad \text{and} \quad q_2' = \frac{T_{f2} - T_b}{R_1'} + \frac{T_{f2} - T_{f1}}{R_{12}'} \tag{2.20}$$

Since:

$$T_b = \frac{T_f R_c' + T_a R_c'}{R_b' + R_c'} \tag{2.21}$$

$$q_1' = \frac{T_{f1} - T_a}{R_1' + 2R_c'} + \left(T_{f1} - T_{f2}\right)\left(\frac{1}{R_{12}'} + \frac{R_c'}{R_1'(R_1' + 2R')}\right) \tag{2.22}$$

comparing (2.20) to (2.22), the Hellström formalism can be used to substitute the resistances by:

$$R_1' \rightarrow R_{1n}' = R_1' + 2R_c' = 2R_{tot}' \tag{2.23}$$

$$R_{12}' \rightarrow R_{12n}' = \left(\frac{1}{R_{12}'} + \frac{R_c'}{R_1' R_{1n}'}\right)^{-1} \tag{2.24}$$

Hence, the new internal resistance is now:

$$\frac{1}{R_{at}} = \frac{1}{2R_{1n}'} + \frac{1}{R_{12n}'} \tag{2.25}$$

Another approach, which is equivalent, has been proposed by Zeng et al. (Zeng and al., 2003). For the single U-tube, these authors found that the non-dimensional exit temperature can be expressed by:

$$\eta_t = \frac{L_b}{mC}\sqrt{\frac{1}{R_{tot} + R_{at}}} \tag{2.26}$$

$$\theta'' = \frac{T_{f,out} - T_b}{T_{f,in} - T_b} = \frac{\eta_t S_1 \cosh(\eta_t) - \sinh(\eta_t)}{\eta_t S_1 \cosh(\eta_t) + \sinh(\eta_t)} \tag{2.27}$$

$$R_{tot}^* = R_{tot}' \eta_t \operatorname{cotanh}(\eta_t) \tag{2.28}$$

Where:

$$S_1 = \frac{2m_f c_f R_b'}{L_b} \tag{2.29}$$

The outlet temperature is then:

$$T_{f,out} = T_{f,in}\,\theta'' + T_b\left(1-\theta''\right) \tag{2.30}$$

In the case of the current study, we replaced the borehole resistances by their equivalent expressions (2.24), thus modifying eq. (2.29) and found:

$$T_{f,out} = T_{f,in}\Theta'' + T_a(1-\Theta'') \tag{2.31}$$

Equation (2.31) is equivalent to (2.16) but it has the advantage of being more easily generalized to offer configurations where only the expression of Θ" will change.

2.4.3 Potential of the proposed model

The main advantages of the proposed model are that it enables one to define independent inlet conditions for each borehole and evaluate the ground temperature at any point of the discretized domain.

To illustrate this assertion, this subsection presents a simulation that shows the possibilities of the proposed model. The demonstration parameters are: one year hourly simulations of a 4x4 borefield, with 6 m between each borehole and 20 m around the borefield. The depth of each borehole is L = 200 m, with a diameter of 6" (150 mm). The mass flow rate in each U-tube of 25 mm sdr-11 is 0.5 kg/s. Ground conductivity is 2.2 W/m-K, grout conductivity is 1.0 W/m-K and pipe conductivity is 0.4 W/m-K. The ground density is 2500 kg/m^3, with a specific heat of 500 J/kg-K. The fluid is a 20% propylene-glycol mixture. The undisturbed ground temperature (or boundary condition) is 10°C and the inlet fluid temperature for the 12 peripheral boreholes is -5°C while for the four central boreholes the inlet temperature is 30°C. Figure 2-4 shows the ground temperature profile.

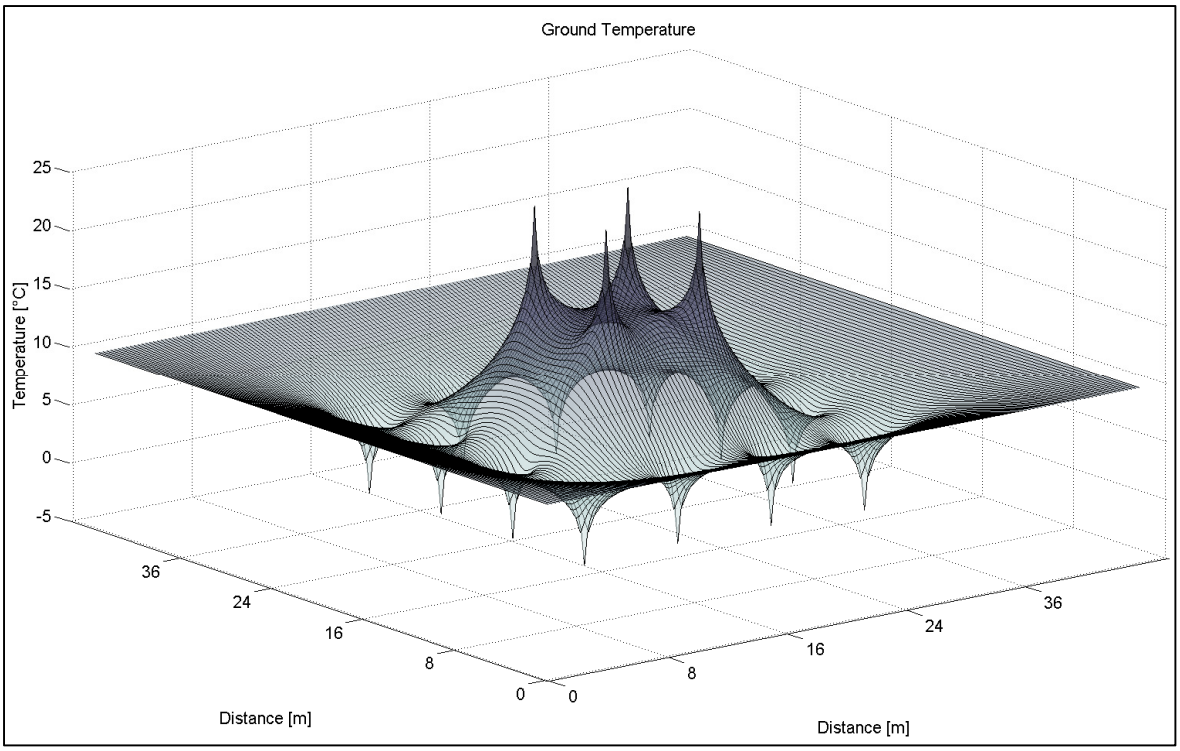

Figure 2-4 Proposed model ground temperature, 4x4 borefield, 1 year simulation

When the discretization is implemented, care must be taken to avoid a computational domain that could involve important gradients at the boundaries. In such a case, a Dirichlet condition imposed on the outer limits of the domain would provide a false representation of the physics of the problem and hence a false solution. Increasing the size of the domain until nearly adiabatic conditions are obtained could solve this problem, but computational time would increase significantly. Hence, a compromise is required between ground domain size and acceptable heat rates at the boundary. An adaptive or variable size mesh could solve this issue, but this is beyond the scope of this study.

Hence, the solution neglects the axial (vertical) effect and it is then limited to moderate Fourier numbers (Fo < 400) or less than several years for a typical borehole (Philippe and al., 2009). Another study showed that the lesser the distance between boreholes, *S*, to borehole length ratio, *L* (*S/L* ratio) is, the less important the axial effect over time (Marcotte and al., 2010). In their paper, the authors showed that 15% less boreholes are required with 50 m length boreholes distanced by 6 m and 7% for 100 m length distanced by 6 m. This paper

hence uses small *S/L* ratios and thus, axial effects can indeed be neglected and the model will be limited to 2-D.

A last drawback of the method could be the computational time. The model is highly non-linear, which requires an iterative solution procedure. Here, it is solved point by point and this could potentially lead to relatively long CPU times. The following section addresses this particular issue.

2.5 Validation

Two variables of interest are investigated with the proposed model: the ground temperature distribution and the fluid outlet temperature of each borehole. In this section, the ground temperature 2D diffusion solver is validated by use of an analytical solution to a well-known problem. The outlet fluid temperature of a single borehole and multiple boreholes obtained from predictions based on the proposed model are then compared to those obtained with the DST model, with constant and time dependent inlet fluid temperatures.

2.5.1 A first validation of the 2D solver

To validate the formulation and implementation of the 2D diffusion solver, it was compared to the known solution of steady homogeneous heat conduction without heat generation in a rectangular domain of *W x L.* The boundary conditions are $T=T_2$ on the upper boundary and $T= T_1$ elsewhere. The analytical dimensionless solution $\theta=(T-T_1) / (T_2-T_1)$ for this problem can be obtained in several textbooks (Incropera and DeWitt, 2007).

$$\theta(x,y)=\frac{2}{\pi}\sum_{n=1}^{\infty}\frac{(-1)^{n+1}+1}{n}\sin\frac{n\pi x}{L}\frac{\sinh(n\pi y/L)}{\sinh(n\pi W/L)} \tag{2.32}$$

The results for $\theta(x,y)$ are shown in Figure 2-5.

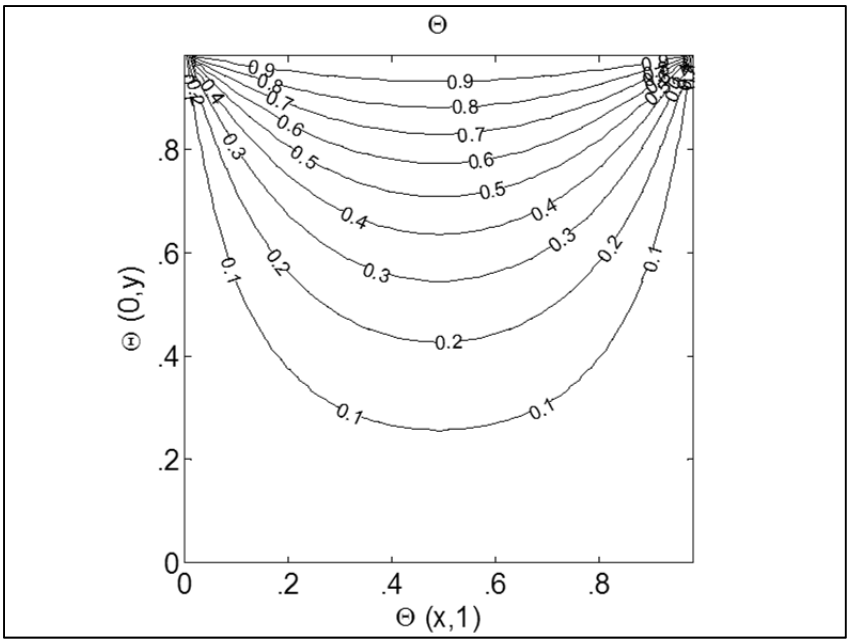

Figure 2-5 Analytical solution of 2-D steady homogeneous heat conduction without source, θ(x,1)=1, θ =0, elsewhere

To obtain a dimensionless solution, the ground conductivity, density and specific heat have been set to unitary value, as well as the lengths of the domain, $W = L = 1$. In the first discretization of the domain, 51 control volumes were used, which creates a centro-symmetric discretization. The second grid used involved 101 grid nodes in each direction. The difference, abs(Θ_{num}-Θ_{ana}), between the numerical (proposed) model and the analytical model is shown in Figure 2-6 for two grid sizes.

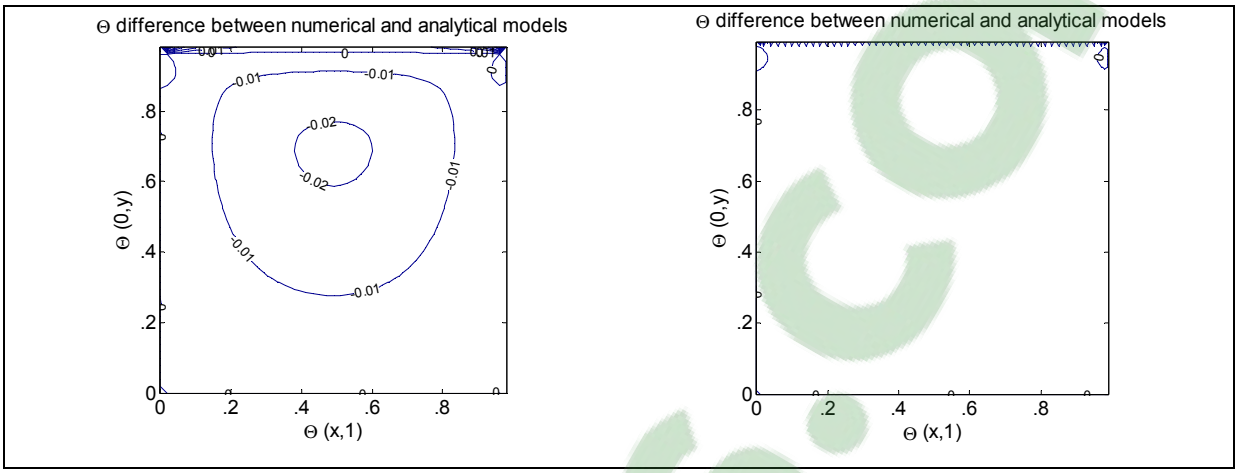

Figure 2-6 Discrepancy between the numerical and analytical solutions: Control-volumes (CV) per axis: left-51 ; and right-101.

The difference lies between 0.02 at the center and 0.08 near the corners of the calculation domain for the 51 CVs per axis and it drops to zero with 101 CVs in each direction. The non-null boundary condition was moved systematically on the four boundaries to ensure grid independence and correct implementation of the 2D formulation.

2.5.2 The determination of the appropriate grid size

To determine to what extent shape has as an impact on the numerical solution, a single borehole at the center of a domain has been used to compare the evolution of the outlet fluid temperature with time for different grid sizes. The simulated parameters for this problem are akin to those described in the illustrative example. The sole difference is that 10 m of ground are considered on each side of the borehole. The simulation is carried out over 1000 hours, with a 1 hour step time. The inlet fluid temperature is constant at 10°C and the undisturbed ground temperature at the boundaries is 5°C.

Figure 2-7 shows the variation of the outlet fluid temperature with time for selected values of the grid-size

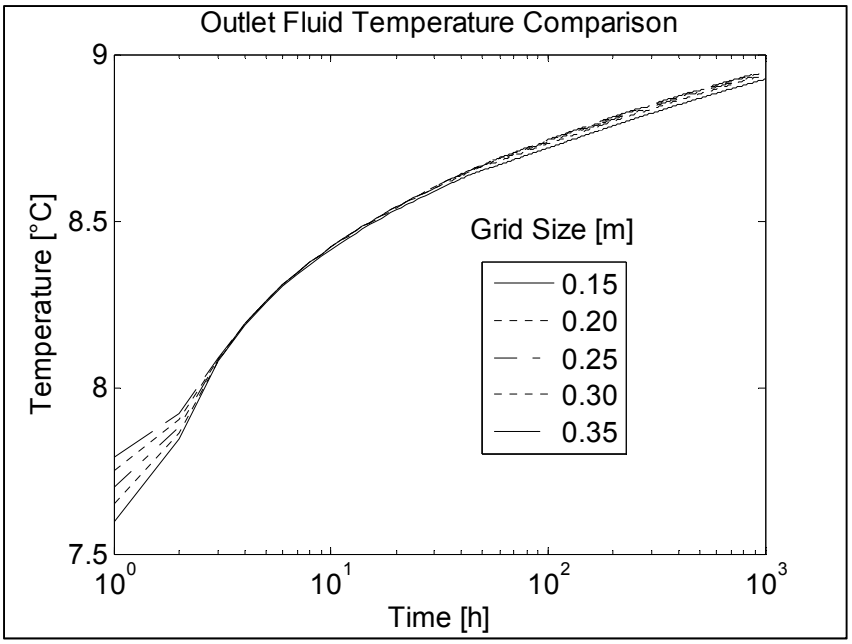

Figure 2-7 Variation of the outlet fluid temperature with time for selected values of the grid size

Figure 2-7 indicates that the shape factor has an important influence for the first few hours of the simulation, which implies that variable inlet conditions over short periods of time – less than 2-3 hours – could influence the outlet temperature more than constant inlet conditions. The steady-state assumption might be involved in this case.

Figure 2-8 shows the inlet temperature and the outlet temperature difference between grid sizes.

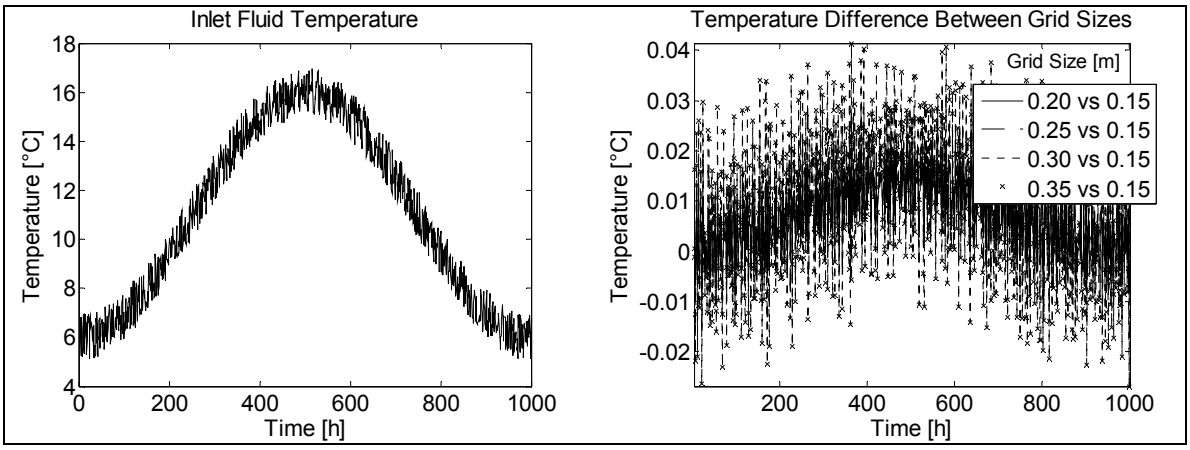

Figure 2-8 Effect of grid size on outlet fluid temperature

The maximum temperature difference between grid sizes is 0.15°C for the first four hours of simulation, but peaks at 0.04°C for the rest of the time. The first four hours have been truncated in Figure 2-8 to emphasise the differences for the remaining simulations.

Richardson's extrapolation enables one to evaluate the grid sensitivity of a numerical model. The results of the extrapolation of the final outlet fluid temperature of the previous case control volume sizes are shown in Table 2-1.

Table 2-1 Richardson's Extrapolation

Grid Size (m)	$T_{f,out}$ (°C) Model	$T_{f,out}$ (°C) Rich.	Difference (°C)
0.15	8.9245	-	-
0.20	8.9369	8.9369	0
0.25	8.9422	8.9440	-0.0017
0.30	8.9463	8.9496	-0.0032
0.35	8.9489	8.9522	-0.0033

The Richardson's extrapolated value indicated that a grid size of 0.2 m should be used. However, a 0,003°C difference at a grid size of 0.35 m is non-significant. Hence, because of

the relative invariance of the solution with the variation of grid size for long simulations, the solution for 0.35 m has been retained for the following comparisons.

2.5.3 Comparison with the DST method for steady inlet temperature

The very same problem has been solved using the proposed model and the DST model (Type 557a) in TRNSYS®, calculating the resistance of the borehole. Figure 2-9 compares the prediction of the outlet fluid temperature as calculated by the DST and by the proposed model for a single borehole with constant inlet fluid temperature.

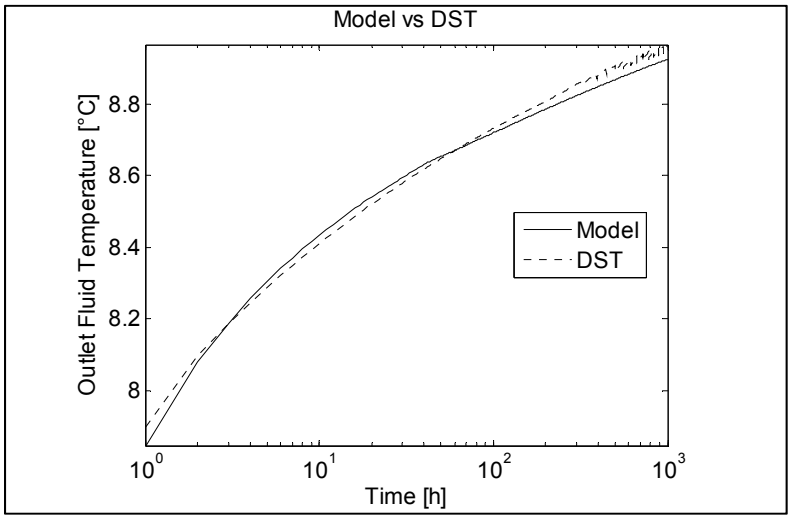

Figure 2-9 Comparison of the DST and proposed model for the predictions of the outlet fluid temperature with time: one borehole, steady inlet temperature

The difference between both temperatures is at most 0.03°C, with an average of 0.009°C. The proposed method produces results in excellent agreement with the standard DST method. One should note that the outlet fluid temperature oscillates after 200 hours for the DST, which corresponds to exchange periods between local and global processes (Chapuis, 2008).

2.5.4 Comparison with the DST method for unsteady inlet temperature

Another problem has been used to assess the validity of the proposed model. For this problem, a 3 by 3 symmetric borefield is investigated. All other parameters are set to values that were used in the former problems. However, in this problem, each borehole has a variable but similar inlet temperature with respect to time. A comparison of the DST and proposed model for the predictions of the outlet fluid temperature with time is shown in Figure 2-10.

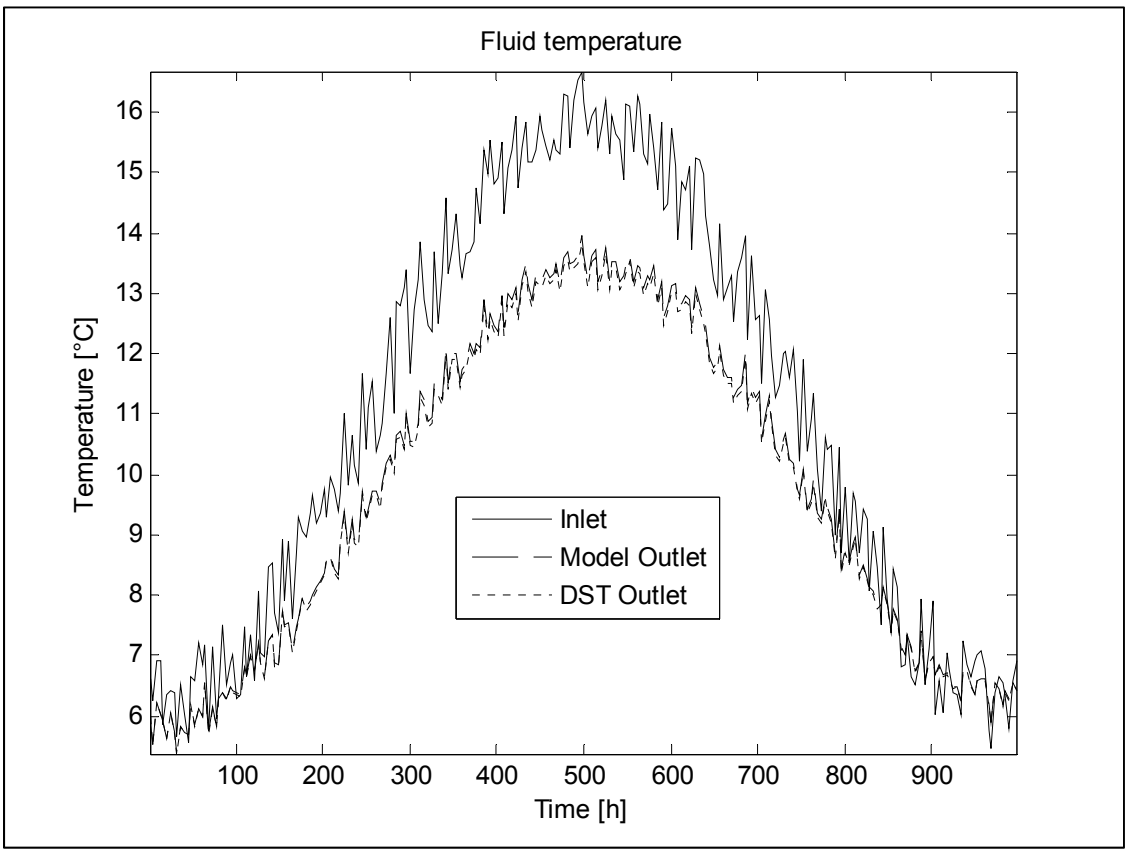

Figure 2-10 Comparison of the DST and proposed model for the predictions of the outlet fluid temperature with time: 3x3 borehole, unsteady inlet temperature

The absolute difference between both models outlet temperature peaked at 0.15°C, with an average of 0.07°C on a global basis. Figure 2-10 shows that both models gave comparable results to the same inlet conditions for each borehole in a borefield. After a series of

validations, the main objective is to evaluate the impact of having spatially different inlet conditions for boreholes, which cannot be achieved with the DST model.

2.6 Application example with variable inlet temperatures

Coupling a geothermal borefield with solar collectors is a common way to balance a geothermal system where heating loads predominate. The purpose here is not to optimize the design of such a system, but rather to show the possibilities and usefulness of the proposed method to evaluate several possibilities for an implementation.

A TRNSYS® simulation couples 12 residential buildings, with 24 m^2 of solar collectors (Type 1) for each building, to a geothermal borefield. The proposed model is used under a Matlab component (Type 155). The simulation uses weather data for Montreal, Canada. The simulation time step is 15 minutes to resemble the cycle periods of heat pumps.

The residential buildings are modeled with a Type 759 component and the weather file (TMY2) used is for Montreal, Canada. Figure 2-11 presents the residential building loads and the heat pump power.

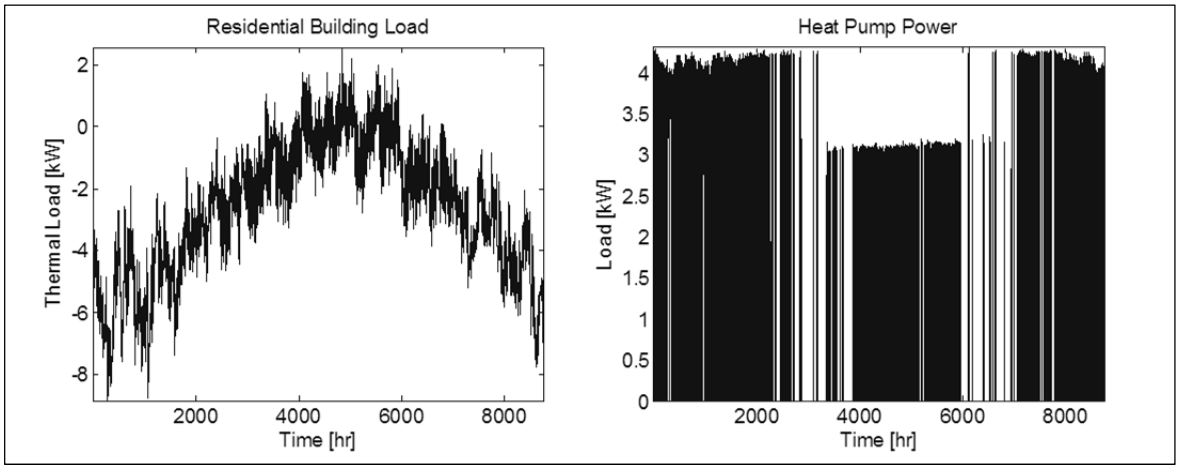

Figure 2-11 Residential loads (left) and heat pump power (right)

The building loads include sensible and latent loads, which peak at 9 kW during the heating period and 2 kW during cooling. The heat pump electrical heating loads peaks at 4.4 kW and the cooling loads peaks are at 3.1 kW. The heat pump has been sized to supply the total thermal sensible and latent loads of the building, without auxiliary heaters.

The selected heat pump capacity is 21.4 kW (about 6 Tons) modeled with a Type 919 component. There is an imbalanced load to the borefield. The heat extracted to heat the building is 16 000 kWh and only 3 000 kWh is injected back to the borefield. Without external heat inputs, this would result in a reduction of the ground temperature up to a point where it could freeze and then damage the buried pipes. It is estimated that this freezing point will be reached within a 15-year period.

The parameters used to size the geothermal borefield are described in Table 2-2.

Table 2-2 Typical geothermal parameters

Parameter	Value	Units	Description
L_{undist}	30	m	Undisturbed ground distance
L_{inter}	6	m	Distance between boreholes
T_{undist}	10	°C	Undisturbed ground temperature
L_b	300	m	Geothermal boreholes length
k_s	2.2	W/m-K	Conductivity of the ground
k_g	1	W/m-K	Conductivity of the grout
k_p	0.4	W/m-K	Conductivity of the pipe
ρ_s	2500	kg/m3	Density of the ground
c_s	500	J/kg-K	Specific heat of the ground
Fr	0.3		Fraction of propylene glycol in water
pipe	33.4	mm	Outside pipe diameter
r_b	0.075	m	Borehole radius

The single-loop configuration is schematically represented in Figure 2-12.

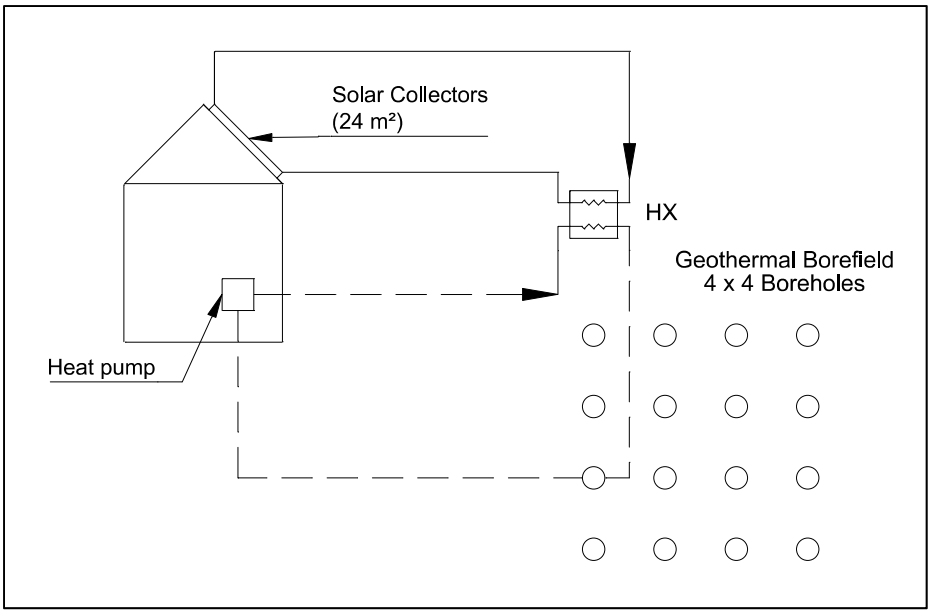

Figure 2-12 Schematic of a single-loop geothermal borefield with inline collectors and a 4x4 borehole arrangement

In this configuration, the solar collectors' circuit is coupled to the geothermal heat pump circuit through a heat exchanger. The solar collectors' circuit is controlled by a differential controller, which operates if the fluid temperature of the solar collector circuit is higher by 10°C than the geothermal heat pump circuit. It stops if this temperature difference is lower than 2°C. The solar collectors' circuit does not operate from May to September.

The second configuration segregates the heat pump and solar collector loops in the borefield, as shown in Figure 2-13.

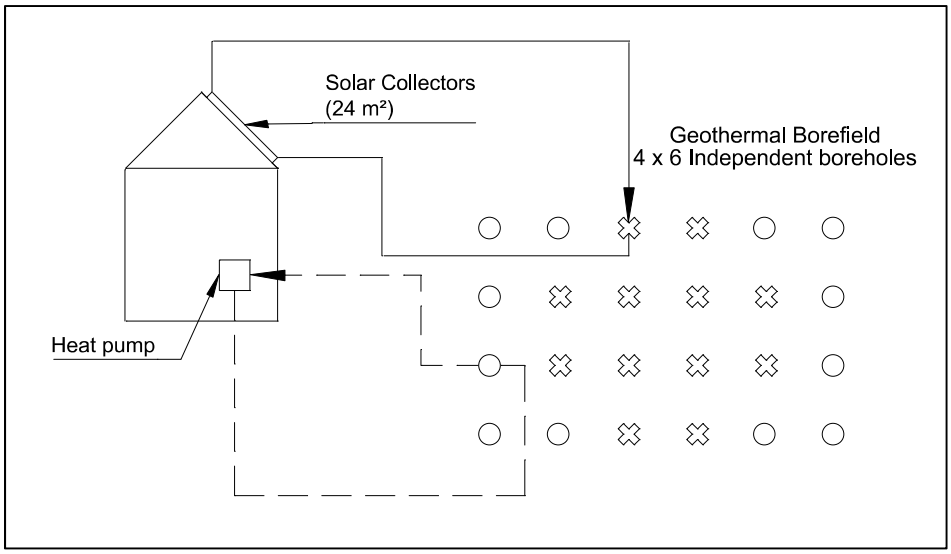

Figure 2-13 Schematic of an independent borehole geothermalborefield with central connected solar collectors and a 4 x 6 borehole arrangement

In the investigated 4 by 6 borefield, the 12 boreholes in the center (denoted as Xs in Figure 5-2) are only connected to the solar collector loop. The 12 peripheral boreholes (illustrated by circles) are used by the heat pump loop. The control strategy of the solar collectors is defined in such a manner that the pump operates if the fluid temperature is higher than 20°C and stops if less than 12°C.

The first configuration can be modeled by available geothermal models. The second configuration highlights the interest of the proposed model.

2.7 Results

The single-loop configuration outlet fluid temperature of the geothermal heat pump circuit is represented in Figure 2-14 for the first and fifth year of simulation.

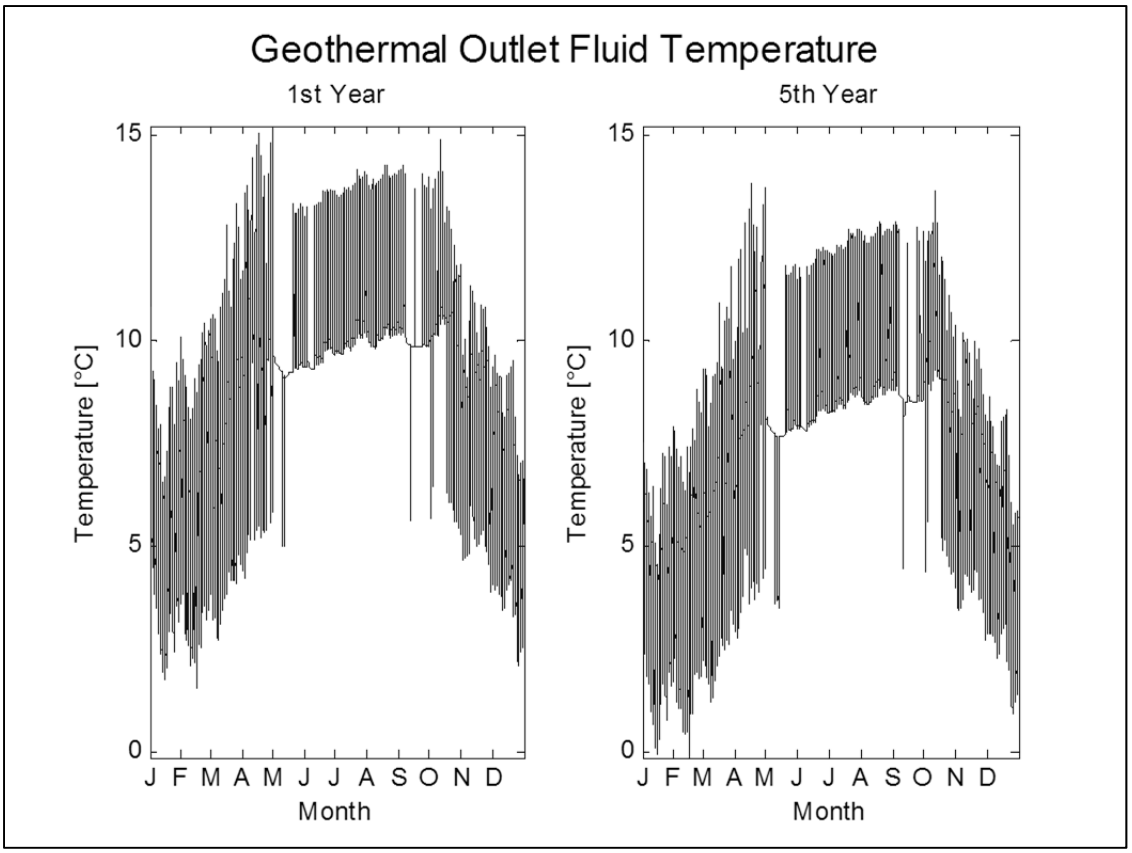

Figure 2-14 Single-loop 4x 4 configuration outlet fluid temperature predictions of the geothermal heat pump: (left) after one year; (right) after 5 years of operation

The lowest fluid outlet temperature predicted is -0.1°C. This low temperature occurs at the fifth year and lowers every year. This tendency would increase the risk of damaging the geothermal boreholes by freezing its surrounding ground. The energy used by the residential heat pump is 27 482 kWh and the solar collectors supply 31 016 kWh to the circulation loop. The ground temperature drops to 5.2°C at the end of the fifth year of simulation.

For the independent boreholes configuration, the outlet fluid temperature of the boreholes in the heat pump circuit for the first and fifth years is presented in Figure 2-15.

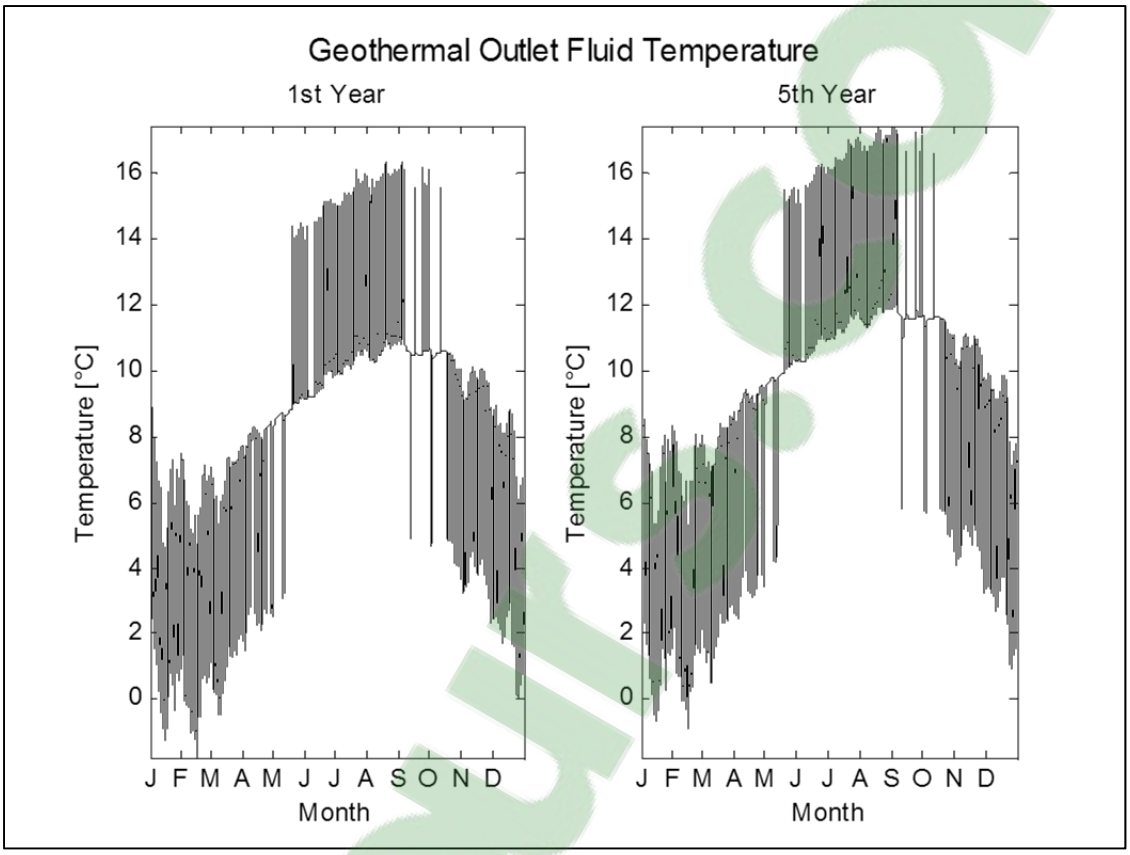

Figure 2-15 Independent borehole central 4 x 6 configuration outlet fluid temperature predictions for the geothermal heat pump: (left) after one year; (right) after 5 years of operation

The 12 boreholes for the heat pump circuit resulted in outlet fluid temperatures below freezing point, as low as -1.8°C, during a few hours in the year. The highest outlet fluid temperature is 17.5°C, with an average of 8.0°C the first year and 9.0°C the fifth.

In this configuration, the energy consumption of each residential heat pump reaches 28 740 kWh over five years of simulation. The solar collectors inject 91 616 kWh of energy in the borefield, 80 148 kWh are extracted by the heat pump to heat the building and 14 758 kWh are injected back to cool it down, resulting in a heat balance of 31 933 kWh in the borefield. The ground temperature profile at the end of the fifth year is shown in Figure 2-16.

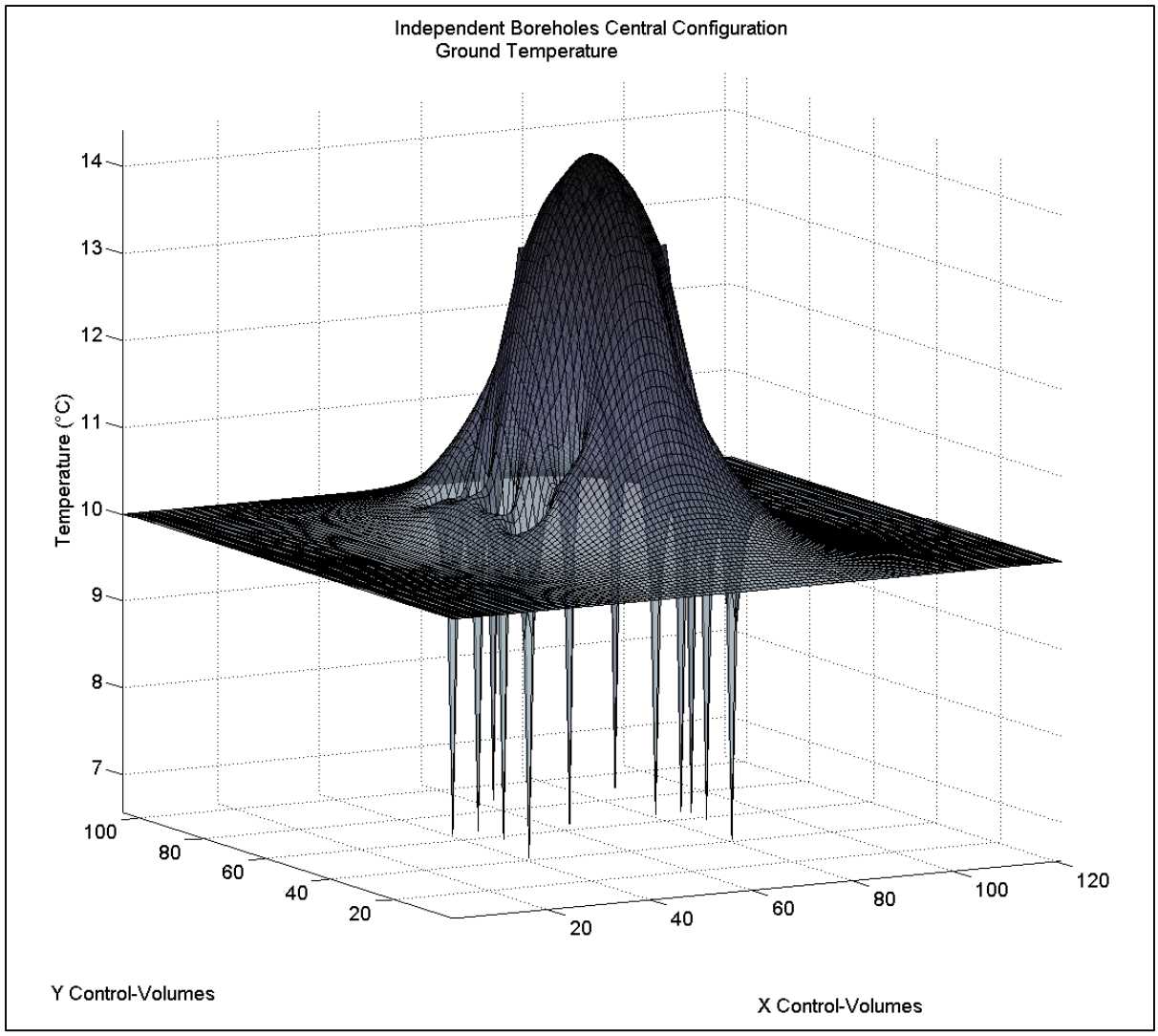

Figure 2-16 Independent boreholes central configuration ground temperature profile

Coupling the solar collectors' circuit at the center of the borefield allowed the storage of a considerable amount of energy. The lowest temperature is 6.6°C around the boreholes and the highest is 14.4°C at the center.

Table 2-3 summarises the energy balance for the entire borefield.

Table 2-3 Simulation results comparison [kWh]

	HP heat extracted	HP heat injected	Solar collectors	Energy balance
Single-loop	-80 449	14 583	31 016	-34 850
Independent boreholes	-80 763	14 693	91 616	25 546

The heat balance over the geothermal borefield is negative for the single-loop and positive for the independent boreholes. The independent borehole configuration enables year round ground storage of a large quantity of solar energy. This stored energy interacts with the heat pump circuit fluid. Table 2-4 shows the comparison of the borefield outlet fluid temperature simulation.

Table 2-4 Geothermal outlet fluid temperature comparison

	Min fluid T°	Max fluid T°	Mean fluid T° Year 1	Mean fluid T° Year 5
Single-loop	-0.1	15.2	8.9	7.4
Independent boreholes	-1.8	17.5	8.0	9.0

The main difference can be found at the end of the fifth year of simulation, the ground energy being extracted on a yearly basis for the single-loop. The temperature of the fluid will have an effect on the performances of the heat pumps. Table 2-5 shows the energy consumption of the residential heat pumps.

Table 2-5 Energy consumption comparison [kWh]

	HP Energy consumption
Single-loop	27 482
Independent boreholes	28 740

The difference of energy consumption of the heat pump over the five year simulation is 4.3%. The annual evolution of both systems is shown in Figure 2-17.

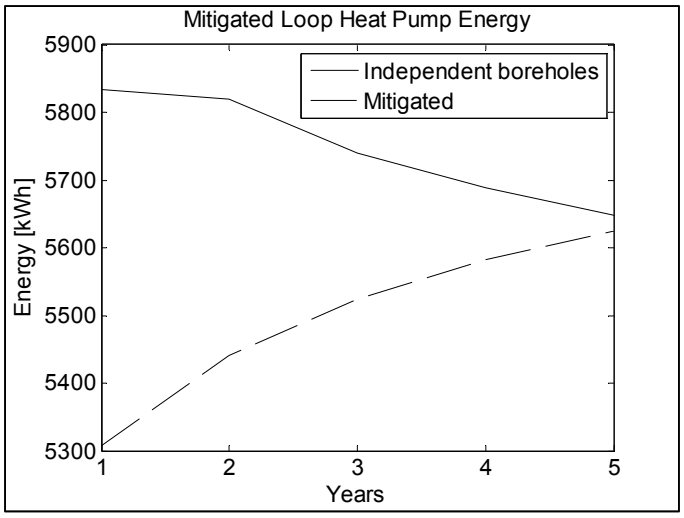

Figure 2-17 Heat pump energy consumption

The energy consumption of the two configurations will intersect at the beginning of the 6th year of simulation. The single loop configuration used 16 geothermal boreholes and the heat exchanged by the 24 m^2 solar collectors' circuit to the heat pumps' circuit did not succeed in balancing the thermal loads on the borefield. The independent borehole configuration used 12 geothermal boreholes for the heat pumps circuit and 12 boreholes for the solar collectors' circuit. This configuration allowed a greater amount of heat to be supplied by the solar collectors and stored in the borefield. The long term results are more interesting for this last configuration at the cost of more boreholes.

2.8 Conclusion

Most of the available geothermal borehole models only take into account one inlet fluid condition for each borehole in a borefield. A model has been developed using a 2D control volume finite difference method for the ground and an analytical thermal resistance model for the boreholes.

The proposed model has been validated against acknowledged problems and solution methods: it showed agreement. The main advantage of the proposed model is its versatility:

the inlet fluid conditions of each borehole can be defined independently and the outlet fluid and the ground temperatures can be analysed in a more precise manner.

Application examples showed that segregating the loops for solar collectors and residential heat pumps resulted in more energy consumption by the heat pumps for the first five years, but will be lower from the sixth year. The objective of showing the capabilities of the proposed model has been achieved.

Different configurations will be presented in future works to share borefields with different sources more efficiently. Future works will involve the development of a 3D model and analysis of different borefield configurations to suit different load profiles.

CHAPTER 3

GEOTHERMAL HEAT EXCHANGE IN BOREHOLES WITH INDEPENDENT SOURCES

Patrick BELZILE, Louis LAMARCHE, Daniel R. ROUSSE

Département de génie mécanique, École de technologie supérieure,
1100, rue Notre-Dame Ouest, Montréal (Québec), Canada, H3C 1K3

Article published in "Applied Thermal Engineering" journal in January 2016

3.1 Abstract

Geothermal boreholes have been used for many years to extract and store thermal energy. For a long time, the behavior of such systems was studied using analytical and numerical models, but the configurations were mostly limited to one inlet and one outlet per bore field. In recent years, some interest has been given to more complex bore field systems, in which heat can be shared between suppliers and customers. This paper is concerned with a system that shares energy through two independent loops within the same borehole. In the literature, a model was recently found to study the heat transfer in this type of arrangement, but it is limited to a symmetric configuration. This paper broadens the method to non-symmetric borehole configurations. A comparison is made between the performance of an optimum configuration and a symmetric one. In one application, where two heat pumps, one in cooling mode and one in heating mode, as much as 3.5% improvement was observed between both configurations. However in our second application, where a detailed hourly simulation coupling residential heat pumps and solar collectors to the same bore field is presented, the non-symmetric configuration energy consumption of the heat pumps gave comparable results to the symmetric configuration. Further analysis would be needed to evaluate the full impact of all the parameters on the final performance of independent loops.

Keywords: Geothermal, Ground-source heat pump, Ground loop heat exchanger, Borehole heat transfer

3.2 Introduction

In the past few years, analytical and numerical models for the heat transfer in single U-tube boreholes have been suggested. A clever solution has been proposed by Young (Young, 2004), based on a formal solution found by Carslaw and Jaeger (Carslaw and Jaeger, 1959) for the short response-time of boreholes. More recently, Lamarche and Beauchamp (Lamarche and Beauchamp, 2007b) approximated this short response-time using a formal solution to the unsteady heat conduction solution for the problem of concentric cylinders (Carslaw and Jaeger, 1959). Fifteen years ago, Remund (Remund, 1999) calculated the steady-state borehole thermal resistances based on conduction shape factors. An analytical model accounting for the heat capacity of boreholes was also proposed by Man et al. (Man and al., 2010). They assumed a homogenous medium for the entire calculation domain including the ground surrounding the borehole.

A 3-D numerical simulation to evaluate the borehole thermal resistance from experimental data was formulated, implemented and validated by Marcotte and Pasquier (Marcotte and Pasquier, 2008). In this work, the authors proposed a “p-linear” average temperature to estimate the thermal resistance in a borehole thermal conductivity test. A 3-D Finite Volume Method (FVM) was also proposed by He et al. (He and al., 2009) to simulate the dynamic response of the circulating fluid and unsteady heat transfer within and around the boreholes.

Classical ground source heat pumps (GSHP) extract heat in the ground during winter and reject heat during summer. Ideally, the ground loads are balanced and the ground temperature remains constant throughout the year. However, in many cases, in very cold or very hot climates, the seasonal loads will be highly unbalanced and the borefield design will need to be very large to overcome eventual long term deterioration (Bernier and al., 2008). A

practical way to avoid this is to use hybrid systems, which use in the case of heating dominated loads for instance, a secondary heat source such as solar collectors or industrial heat rejection (Hackel and Pertzborn, 2011b). Thus, the heating source can share the thermal energy through a common mixed secondary loop. Hybrid geothermal-solar systems have been studied for some time in heating and cooling for residential building applications. Trillat-Berdal et al. (Trillat-Berdal and al., 2007) conducted simulations and experiments on such systems. Toshkov et al. (Toshkov, 2013; Toshkov and al., 2014) studied hybrid heating and cooling systems for residential buildings. Kim et al. (Kim and al., 2013) coupled solar collectors to a CO_2 heat pump. Eslami-Nejad et al. (Eslami-Nejad and Bernier, 2011b) developed a model for such applications with independent inlet conditions in a symmetric configuration. Chiasson et al. (Chiasson and al., 2004) proposed a replacement hybrid geothermal-solar system for a school.

Another possibility would be to share the heat through the ground using independent boreholes for heat pumping and heat supplying. Recently, Belzile et al. (Belzile and al., 2016b) proposed a model that can simulate this type of arrangement. In their paper, the authors provided an example simulating the bore field, schematically shown in Figure 3-1, where heat is supplied to the internal boreholes by solar collectors while heat is extracted from the peripheral boreholes.

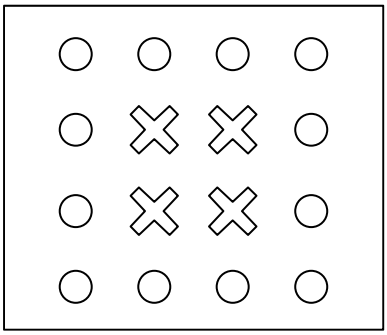

Figure 3-1 Independent borehole arrangement: X, solar supplied heat; O, extracted heat

Lazzarotto (Lazzarotto, 2014) developed a network-based method to achieve the same objective. A novel approach has recently been proposed for which two independent U-tubes exchange heat within a common borehole (Eslami-Nejad and Bernier, 2011a). The adjacent ground can store excess energy or mitigate a shortage of energy. Since it is common in ground heat exchanger simulations to decouple the ground from the borehole heat transfer, classical methods can be used to analyse such a scheme as long as a model for the new borehole is known. Eslami-Nejad and Bernier (Eslami-Nejad and Bernier, 2011a; Eslami-Nejad and Bernier, 2011b) propose two interesting contributions to treat this problem for a special configuration. The purpose of this paper is to expand their results to more general configurations and to show how this can improve the overall thermal performance.

3.3 Original symmetric double U-tube configuration

Eslami-Nejad and Bernier (Eslami-Nejad and Bernier, 2011a; Eslami-Nejad and Bernier, 2011b) were the first to model the thermal behavior of a borehole with two independent circuits. Their approach is a generalization of the Zeng et al. (Zeng and al., 2003) method that was used to simulate a double U-tube configuration in parallel or in series. The idea is to find the expression of the temperature profile for two independent fluid circuits that are within a single borehole. The physical problem is represented in Figure 3-2.

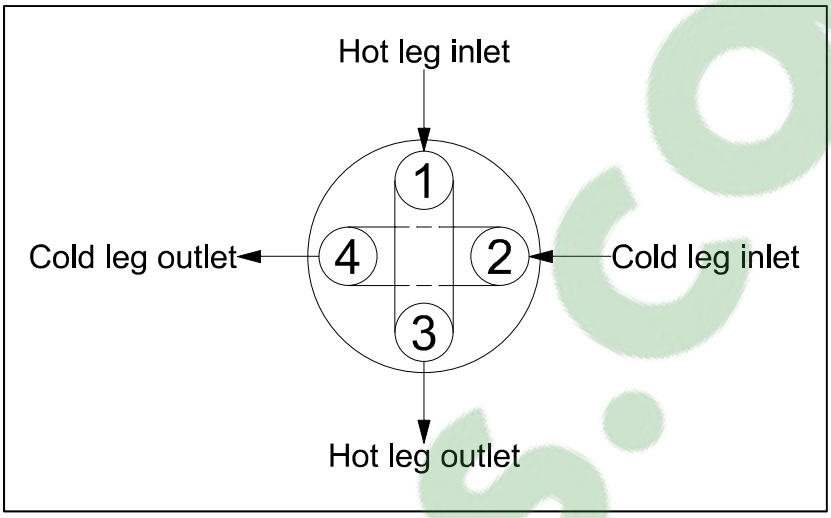

Figure 3-2 Double U-tube geothermal system

A hot fluid arrives in the heat source leg and exchanges heat with a colder fluid travelling through the second circuit. Both legs can also exchange heat with the ground. Three different configurations were analysed by Eslami-Nejad and Bernier (Figure 3-3). One of their conclusions, as might easily have been expected, is that configuration 1-3, 2-4 is the best, since the distance between hot and cold fluid is smaller and the short-circuit between the heat source circuit is less important. Based on this fact, this paper will be solely concerned with this configuration. To analyse the phenomenon, an energy balance in the four tubes is needed.

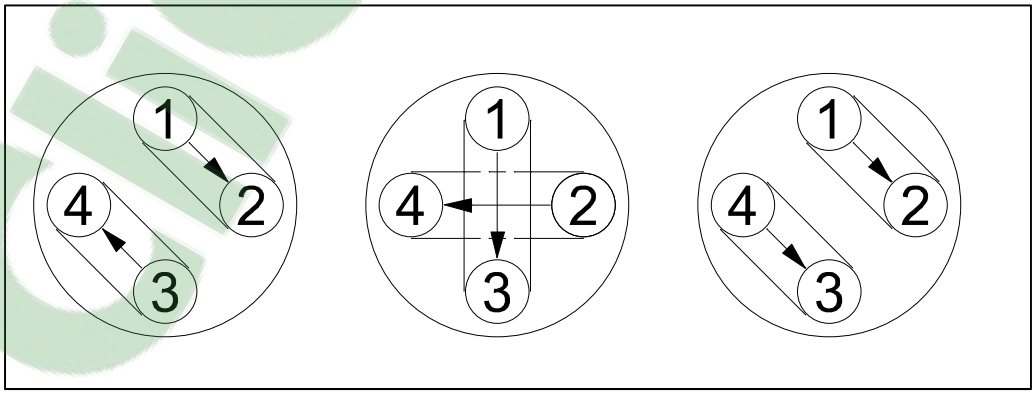

Figure 3-3 Heat flow patterns of two U-tubes in a borehole: 1-2, 3-4; 1-3, 2-4; 1-2, 4-3.

In their first paper (Eslami-Nejad and Bernier, 2011a), they restrict their analysis to the case where both fluids have the same capacitance ($\dot{m}C_p$) and deduced the following energy balance for the four tubes:

$$\begin{aligned}
-\frac{d\theta_1}{dZ} &= a\,\theta_1 + b\,\theta_2 + c\,\theta_3 + b\,\theta_4 + d \\
-\frac{d\theta_2}{dZ} &= b\,\theta_1 + a\,\theta_2 + b\,\theta_3 + c\,\theta_4 + d \\
\frac{d\theta_3}{dZ} &= c\,\theta_1 + b\,\theta_2 + a\,\theta_3 + b\,\theta_4 + d \\
\frac{d\theta_4}{dZ} &= b\,\theta_1 + c\,\theta_2 + b\,\theta_3 + a\,\theta_4 + d
\end{aligned} \tag{3.1}$$

where

$$\theta_i = \frac{(T_{f,i} - T_{f1,in}) + (T_{f,i} - T_{f2,in})}{T_{f1,in} - T_{f2,in}} \quad , \quad T_{f1,in} \neq T_{f2,in} \quad i = 1,2,3,4 \tag{3.2}$$

is the dimensionless temperature introduced by Eslami-Nejad and Bernier (Eslami-Nejad and Bernier, 2011a; Eslami-Nejad and Bernier, 2011b). The coefficients are related to the internal resistances:

$$a = \frac{1}{S_1} + \frac{1}{S_{12}} + \frac{1}{2S_{13}} \quad , \quad b = -\frac{1}{2S_{12}} \quad , \quad c = -\frac{1}{2S_{13}} \quad , \quad d = -\frac{\theta_b}{S_1} \tag{3.3}$$

$$S_1 = C\,R_1'^{\Delta} \quad , \quad S_{12} = \frac{C\,R_{12}'^{\Delta}}{2} \quad , \quad S_{13} = \frac{C\,R_{13}'^{\Delta}}{2} \quad , \quad C = \frac{\dot{m}c_p}{H} \tag{3.4}$$

The internal resistances can be calculated by different methods. Eslami-Nejad and Bernier (Eslami-Nejad and Bernier, 2011a; Eslami-Nejad and Bernier, 2011b) followed the same steps as Zeng (Zeng and al., 2003) and used the line-source method introduced by Hellström (Hellström, 1991). Without going into all the details, the final results for the symmetric can be resumed as:

$$
\begin{aligned}
R_1'^{\Delta} &= R_{11}'^{o} + R_{13}'^{o} + 2R_{12}'^{o} \\
R_{12}'^{\Delta} &= \frac{R_{11}'^{o,2} + R_{13}'^{o,2} + 2R_{11}'^{o} R_{13}'^{o} - 4R_{12}'^{o,2}}{R_{12}'^{o}} = R_{14}'^{\Delta} = R_{23}'^{\Delta} = R_{34}'^{\Delta} \\
R_{13}'^{\Delta} &= \frac{(R_{11}'^{o} - R_{13}'^{o})(R_{11}'^{o,2} + R_{13}'^{o,2} + 2R_{11}'^{o} R_{13}'^{o} - 4R_{12}'^{o,2}}{R_{13}'^{o,2} + R_{11}'^{o} R_{13}'^{o} - 2R_{12}'^{o,2}} = R_{24}'^{\Delta}
\end{aligned}
\tag{3.5}
$$

where the thermal resistances R^o given by the line-source method are given by:

$$
R_{ii}'^{o} = \frac{1}{2\pi k_b}\left[\log\left(\frac{r_b}{r_p}\right) - \sigma\log\left(\frac{r_b^2 - x_c^2}{r_b^2}\right)\right] + R_p' \tag{3.6}
$$

$$
\begin{aligned}
R_{ij}'^{o} &= \frac{1}{2\pi k_b}\left[\log\left(\frac{r_b}{z_{ij}}\right) - \frac{\sigma}{2}\log\left(\frac{{r_b}^4 + x_c^4 + {z_{ij}}^2 - 2x_c^2}{{r_b}^4}\right)\right], i \neq j \\
z_{ij} &= \sqrt{(x_i - x_j)^2 + (y_i - y_j)^2}
\end{aligned}
\tag{3.7}
$$

R_p' is the usual « pipe resistance » (Lamarche and al., 2010) taking into account the convection resistance as well as the conduction resistance of the plastic pipe.

For the 1-3,2-4 case, (Fig 3-3b), the last system of differential equations, eqs.(3.1), can be solved with the following boundary conditions:

$$
\theta_1(0) = 1\ ,\ \theta_2(0) = -1\ ,\ \theta_1(1) = \theta_3(1)\ ,\ \theta_2(1) = \theta_4(1) \tag{3.8}
$$

This yields the following results for dimensionless temperature:

$$
\theta_1(Z) = \theta_b - \theta_b\cosh(\gamma Z) + P_1\sinh(\gamma Z) + \cosh(\eta Z) - P_2\sinh(\eta Z) \tag{3.9}
$$

$$
\theta_2(Z) = \theta_b - \theta_b\cosh(\gamma Z) + P_1\sinh(\gamma Z) - \cosh(\eta Z) + P_2\sinh(\eta Z) \tag{3.10}
$$

$$
\begin{aligned}
\theta_3(Z) = \theta_b + \left(\frac{\theta_3(0) + \theta_4(0)}{2} - \theta_b\right)\cosh(\gamma Z) + \\
P_3\sinh(\gamma Z) + \frac{\theta_3(0) - \theta_4(0)}{2}\cosh(\eta Z) + P_4\sinh(\eta Z)
\end{aligned}
\tag{3.11}
$$

$$\theta_4(Z) = \theta_b + \left(\frac{\theta_3(0)+\theta_4(0)}{2} - \theta_b \right) \cosh(\gamma Z) + P_3 \sinh(\gamma Z) - \frac{\theta_3(0)-\theta_4(0)}{2} \cosh(\eta Z) - P_4 \sinh(\eta Z) \tag{3.12}$$

with P factors combining several modified S resistances such that:

$$P_1 = \frac{2S_{12}S_{13}\theta_b + S_1/2\,(S_{12}+S_{13})(\theta_3(0)+\theta_4(0))}{2S_1S_{12}S_{13}\gamma} \tag{3.13}$$

$$P_2 = \frac{(2S_{12}S_{13}+3S_1S_{13}+S_{12}S_1) + S_1/2\,(S_{13}-S_{12})(\theta_3(0)-\theta_4(0))}{2S_1S_{12}S_{13}\eta} \tag{3.14}$$

$$P_3 = \frac{(S_{12}S_{13}+\frac{1}{2}S_1S_{13}+\frac{1}{2}S_1S_{12})(\theta_3(0)+\theta_4(0)) - 2S_{12}S_{13}\theta_b}{2S_1S_{12}S_{13}\gamma} \tag{3.15}$$

$$P_4 = \frac{(S_{12}S_{13}+\frac{3}{2}S_1S_{13}+\frac{1}{2}S_{12}S_1)(\theta_3(0)-\theta_4(0)) + S_1(S_{13}-S_{12})}{2S_1S_{12}S_{13}\eta} \tag{3.16}$$

which yields the following expressions for the inlet dimensionless temperature θ_3 (0)and $\theta_4(0)$ and heat fluxes :

$$\theta_3(0) = Q_1 + Q_2 \quad , \quad \theta_4(0) = Q_1 - Q_2$$
$$Q_1 = \frac{2\theta_b \sinh(\gamma)}{S_1\gamma\cosh(\gamma)+\sinh(\gamma)} \quad , \quad Q_2 = \frac{S_1S_{12}\eta\cosh(\eta)-(2S_1+S_{12})\sinh(\eta)}{S_1S_{12}\eta\cosh(\eta)+(2S_1+S_{12})\sinh(\eta)} \tag{3.17}$$

where γ and η are given by:

$$\gamma = \sqrt{\frac{1}{S_1^2}+\frac{1}{S_1S_{12}}+\frac{1}{S_1S_{13}}} \ , \ \eta = \sqrt{\frac{1}{S_1^2}+\frac{3}{S_1S_{12}}+\frac{2}{S_{12}^2}+\frac{1}{S_1S_{13}}+\frac{2}{S_{12}S_{13}}} \tag{3.18}$$

Eslami-Nejad and Bernier (Eslami-Nejad and Bernier, 2011a) also analysed the others configurations depicted in Figure 3-3 but this is not taken into account in the current analysis.

3.4 New non-symmetric double U-tube configuration

As previously mentioned, Eslami-Nejad and Bernier (Eslami-Nejad and Bernier, 2011a) showed that the above described configuration 1-3, 2-4 is the best for two reasons: heat

transfer between the hot and cold fluid is better and the thermal short-circuit is reduced. One cannot argue with the second reason, since the distance between each leg of a circuit must be as far as possible. However, better heat transfer could be achieved if the pipes of the two independent circuits are closer, β≠o (Figure 3-4). For this, the equations of the last section must be modified.

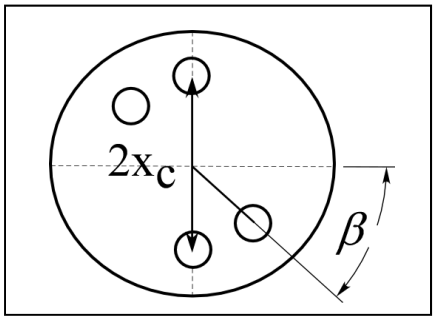

Figure 3-4 Non-symmetric configuration

It cannot be assumed that $R'^{\Delta}_{12} = R'^{\Delta}_{23}$ and $R'^{\Delta}_{34} = R'^{\Delta}_{14}$. However, this study will restrict its scope to the case where $R'^{\Delta}_{12} = R'^{\Delta}_{34}$, $R'^{\Delta}_{23} = R'^{\Delta}_{14}$. This is not mandatory, but will probably be the case in most practical applications. In this case, it can be shown that the new resistance's expressions are given such that:

$$
\begin{aligned}
R'^{o}_{11} &= \frac{1}{2\pi k_b}\left[\log\left(\frac{r_b}{r_p}\right) - \sigma\log\left(\frac{r_b^2 - x_c^2}{r_b^2}\right)\right] + R'_p \\
R'^{o}_{13} &= \frac{1}{2\pi k_b}\left[\log\left(\frac{r_b}{2x_c}\right) - \sigma\log\left(\frac{r_b^2 + x_c^2}{r_b^2}\right)\right] \\
R'^{o}_{12} &= \frac{1}{2\pi k_b}\left[\log\left(\frac{r_b}{z_{12}}\right) - \frac{\sigma}{2}\log\left(\frac{r_b{}^4 + x_c^4 + z_{12}{}^2 - 2x_c^2}{r_b{}^2}\right)\right] \\
R'^{o}_{14} &= \frac{1}{2\pi k_b}\left[\log\left(\frac{r_b}{z_{14}}\right) - \frac{\sigma}{2}\log\left(\frac{r_b{}^4 + x_c^4 + z_{14}{}^2 - 2x_c^2}{r_b{}^2}\right)\right]
\end{aligned}
\qquad (3.19)
$$

where

$$\sigma = \frac{k_b - k}{k_b + k}$$

$$
\begin{aligned}
R'^{\Delta}_{12} &= \frac{X}{R'^{o2}_{11}R'^{o}_{12} - 2R'^{o}_{11}R'^{o}_{13}R'^{o}_{14} - R'^{o3}_{12} + R'^{o}_{12}R'^{o2}_{13} + R'^{o}_{12}R'^{o2}_{14}} \\
R'^{\Delta}_{13} &= \frac{X}{R'^{o2}_{11}R'^{o}_{13} - 2R'^{o}_{11}R'^{o}_{12}R_{14} - R'^{o3}_{13} + R'^{o}_{13}R'^{o2}_{12} + R'^{o}_{13}R'^{o2}_{14}} \\
R'^{\Delta}_{14} &= \frac{X}{R'^{o2}_{11}R'^{o}_{14} - 2R'^{o}_{11}R'^{o}_{12}R'^{o}_{13} - R'^{o3}_{14} + R'^{o}_{14}R'^{o2}_{12} + R'^{o}_{14}R'^{o2}_{13}} \\
X &= (R'^{o}_{11} + R'^{o}_{12} - R'^{o}_{13} - R'^{o}_{14})(R'^{o}_{11} - R'^{o}_{12} + R'^{o}_{13} - R'^{o}_{14}) \\
&\quad (R'^{o}_{11} - R'^{o}_{12} - R'^{o}_{13} + R'^{o}_{14})(R'^{o}_{11} + R'^{o}_{12} + R'^{o}_{13} + R'^{o}_{14})
\end{aligned}
\tag{3.20}
$$

The energy balance also needs to be modified such that:

$$
\begin{aligned}
-\frac{d\theta_1}{dZ} &= a\theta_1 + b\theta_2 + c\theta_3 + d\theta_4 + e \\
-\frac{d\theta_2}{dZ} &= b\theta_1 + a\theta_2 + d\theta_3 + c\theta_4 + e \\
\frac{d\theta_3}{dZ} &= c\theta_1 + d\theta_2 + a\theta_3 + b\theta_4 + e \\
\frac{d\theta_4}{dZ} &= d\theta_1 + c\theta_2 + b\theta_3 + a\theta_4 + e
\end{aligned}
\tag{3.21}
$$

where the constants are:

$$
a = \frac{1}{S_1} + \frac{1}{2S_{12}} + \frac{1}{2S_{13}} + \frac{1}{2S_{14}} \;,\; b = -\frac{1}{2S_{12}} \;,\; c = -\frac{1}{2S_{13}},\; d = -\frac{1}{2S_{14}} \;,\; e = -\frac{\theta_b}{S_1} \tag{3.22}
$$

The solution for the temperature profiles will have the same form as before (Eqs. 3.9-12), but with new P parameters:

$$
P_1 = \frac{2S_{14}S_{13}\theta_b + S_1/2\,(S_{14} + S_{13})(\theta_3(0) + \theta_4(0))}{2S_1S_{14}S_{13}\gamma} \tag{3.23}
$$

$$
P_2 = \frac{(2S_{12}S_{13}S_{14} + 2S_1S_{13}S_{14} + S_{12}S_1(S_{13} + S_{14})) + S_1/2\,S_{12}(S_{13} - S_{14})(\theta_3(0) - \theta_4(0))}{2S_1S_{12}S_{13}S_{14}\eta} \tag{3.24}
$$

$$P_3 = \frac{(S_{14}S_{13} + \frac{1}{2}S_1S_{13} + \frac{1}{2}S_1S_{14})(\theta_3(0) + \theta_4(0)) - 2S_{14}S_{13}\theta_b}{2S_1S_{14}S_{13}\gamma} \tag{3.25}$$

$$P_4 = \frac{(S_{12}S_{13}S_{14} + S_1S_{13}S_4 + \frac{1}{2}S_{12}S_1(S_{13} + S_{14}))(\theta_3(0) - \theta_4(0)) + S_1S_{12}(S_{13} - S_{14})}{2S_1S_{12}S_{13}S_{14}\eta} \tag{3.26}$$

with

$$\theta_3(0) = Q_1 + Q_2 \quad , \quad \theta_4(0) = Q_1 - Q_2 \tag{3.27}$$

$$\begin{aligned} Q_1 &= \frac{2\theta_b \sinh(\gamma)}{S_1\gamma\cosh(\gamma) + \sinh(\gamma)} \quad , \\ Q_2 &= \frac{S_1S_{12}S_{14}\eta\cosh(\eta) - (S_{12}S_{14} + S_1(S_{12} + S_{14}))\sinh(\eta)}{S_1S_{12}S_{14}\eta\cosh(\eta) + (S_{12}S_{14} + S_1(S_{12} + S_{14}))\sinh(\eta)} \end{aligned} \tag{3.28}$$

$$\begin{aligned} \gamma &= \sqrt{\frac{1}{S_1^2} + \frac{1}{S_1S_{14}} + \frac{1}{S_1S_{13}}} \quad , \\ \eta &= \sqrt{\frac{1}{S_1^2} + \frac{2}{S_1S_{12}} + \frac{1}{S_{12}^2} + \frac{1}{S_1S_{13}} + \frac{1}{S_1S_{14}} + \frac{1}{S_{12}S_{13}} + \frac{1}{S_{12}S_{14}} + \frac{1}{S_{13}S_{14}}} \end{aligned} \tag{3.29}$$

It is possible to compare the exit temperatures obtained introducing the asymmetry angle β with those produced by the symmetric configuration (β=0) to evaluate the effect of the variation of the borehole's position. To compare this, the same parameters as those proposed by Eslami-Nejad and Bernier (Table 1 in reference (Eslami-Nejad and Bernier, 2011b)) are used. The only difference for the non-symmetric case is that β=25.5°. Figure 3-5 presents the cold and hot leg temperature profiles with respect to the dimensionless depth Z for different angles. In this figure, results for βavg correspond to the average angle between symmetric and βmax cases, where βmax refers to the case in which the two tubes are in contact.

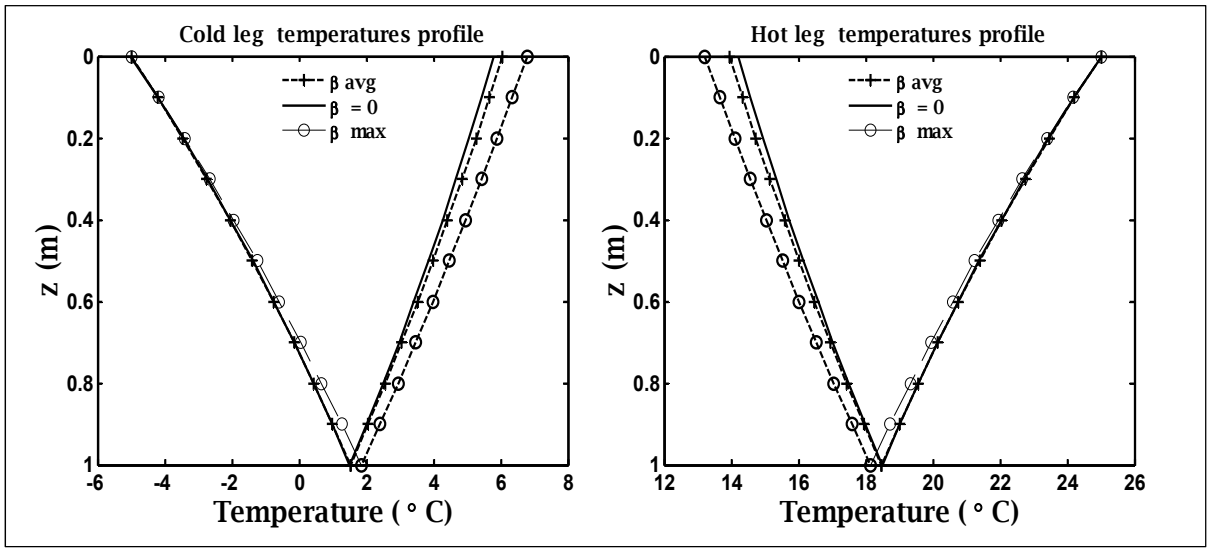

Figure 3-5 Temperature profiles, cold leg left, hot leg right

As shown in Figure 3-5, the cold leg exit temperature increases as the distance between the boreholes decreases.

In the special case treated by Eslami-Nejad and Bernier, $\theta_b = 0$. In that case, the borehole can be seen as a typical heat exchanger and thus, the efficiency of this exchanger is given by:

$$\varepsilon = \frac{\theta_4(0)+1}{2} \tag{3.30}$$

For the special configuration described by Eslami-Nejad and Bernier (Eslami-Nejad and Bernier, 2011a; Eslami-Nejad and Bernier, 2011b), the efficiency of the heat exchanger increases from 36% to 38%, a 5.5% improvement. In other configurations (not reported herein), the increase can be up to 15%.

3.5 Effect of flow rate variation

The set of equations described in the last two sections are limited to a case in which the same fluid travels at the same flow rate in both paths of the borehole. This constraint limits its use for practical applications. Using different flow rates in the non-symmetric case, the new energy balance, Eq.3.21, becomes:

$$
\begin{aligned}
-\frac{d\theta_1}{dZ} &= a\,\theta_1 + b\,\theta_2 + c\,\theta_3 + d\,\theta_4 + e \\
-\frac{d\theta_2}{dZ} &= \alpha(b\,\theta_1 + a\,\theta_2 + d\,\theta_3 + c\,\theta_4 + e) \\
\frac{d\theta_3}{dZ} &= c\,\theta_1 + d\,\theta_2 + a\,\theta_3 + b\,\theta_4 + e \\
\frac{d\theta_4}{dZ} &= \alpha(d\theta_1 + c\,\theta_2 + b\,\theta_3 + a\,\theta_4 + e)
\end{aligned}
\tag{3.31}
$$

where

$$
\alpha = \frac{\left(\dot{m}\,c_p\right)_{1-3}}{\left(\dot{m}\,c_p\right)_{2-4}} \tag{3.32}
$$

Although the new equation system may not be very different, its solution becomes much more cumbersome. In their second paper, Eslami-Nejad and Bernier (Eslami-Nejad and Bernier, 2011b) solved the problem for the symmetric case ($b = d$). The solution will not be given here for the sake of brevity. In this paper, the non-symmetric case was solved. Its solution is given by the following relations:

$$
\theta_i(Z) = \theta_b + P_{i2}\cosh(\gamma Z) + \frac{P_{i3}}{\gamma}\sinh(\gamma Z) + P_{i4}\cosh(\eta Z) + \frac{P_{i5}}{\eta}\sinh(\eta Z) \qquad i = 1,2,3,4 \tag{3.33}
$$

where

$$
P_{ij} = \frac{G_{ij} + G_{ij}'\,\theta_3(0) + G_{ij}''\,\theta_4(0)}{\gamma^2 - \eta^2} \tag{3.34}
$$

The final expressions for all the new coefficients are provided in the Appendix I. It can be verified that the general expressions reduce to the same expressions as those given by Eslami-Nejad and Bernier when $b = d$. The simulation was performed using the same parameters as before (Table 1 in reference [14]), except that $\alpha = 0.5$. To validate the solution,

the analytic solution was compared with the numerical Runge-Kutta solution of Eqs. 24. The comparison is shown in Figure 3-6.

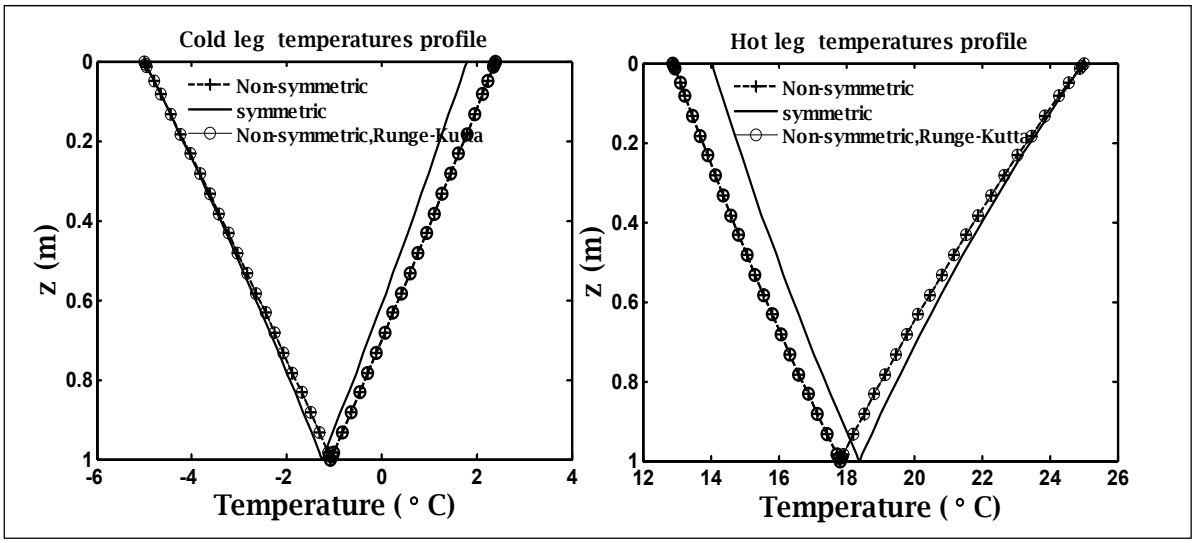

Figure 3-6 Solution comparison, cold leg left, hot leg right

Figure 3-6 illustrates that the results of the non-symmetric analytical solution are in good agreement with the Runge-Kutta solution.

3.6 Applications

As a first example, it is proposed to analyze the effect of the configuration of the borehole on the performance of a two heat pumps system where a heat pump is rejecting heat as the same time where a second one is in heating mode. In our example the first heat pump is pumping 12 kW of heat from the building and the heat rejected in the borehole will depend on its COP. The second heat pump is giving 10 kW of heat in the building. The configuration is shown in Figure 3-7.

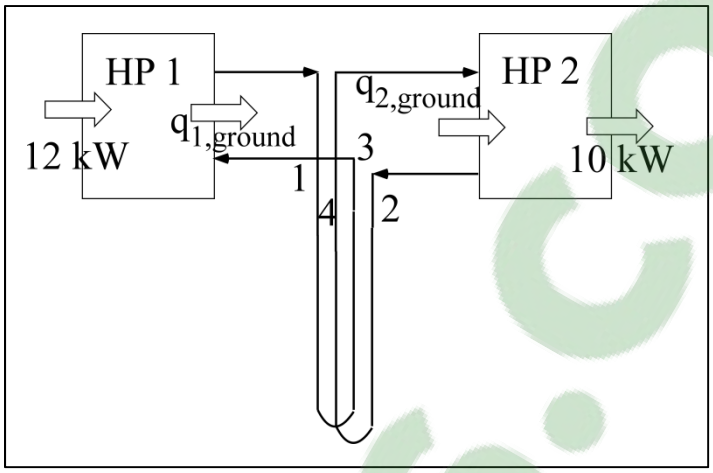

Figure 3-7 Application configuration

Both COP's will depend on the return temperatures which will be affected by the borehole configuration and we are interested in the power consumption defined as:

$$W_{cooling}(kW) = \frac{12}{COP_{cooling}}$$
$$W_{heating}(kW) = \frac{10}{COP_{heating}} \tag{3.35}$$

$$q_{1,ground,des}(kW) = 12\,\frac{COP_{cooling}+1}{COP_{cooling}}$$
$$q_{2,ground,des}(kW) = 10\,\frac{COP_{heating}-1}{COP_{heating}} \tag{3.36}$$

The COP's are evaluated from the following formula:

$$COP_{heating} = 3.06 + 0.075\,EWT - 0.00084\,EWT^2$$
$$COP_{cooling} = 6.90 - 0.145\,EWT + 0.0011\,EWT^2 \tag{3.37}$$

At each time the following iterative procedure is followed:

1) $T_{f1,in}$ and $T_{f2,in}$ are initialized

2) $T_{f3,out}$ and $T_{f4,out}$ are evaluated from our model
3) $COP_{heating}$ and $COP_{cooling}$ are evaluated
4) $q_{1,groud,des}$ and $q_{2,ground,des}$ are evaluated using Eq. 29
5) These values are compares with :

$$q_{2,ground}(kW) = \dot{m}C_p(T_{f,3} - T_{f,1})$$
$$q_{1,ground}(kW) = \dot{m}C_p(T_{f,2} - T_{f,4}) \quad (3.38)$$

New values of inlet temperatures are chosen until convergence

After convergence, the power consumption of the compressors are evaluated and at the end, the total energy consumption is compared. Two simulations are done, one with $\beta = 0$ and the other with $\beta = \beta_{\max}$. The parameters of the borehole are given in Table 3-1.

Table 3-1 Simulation parameters

T_o	r_b	r_{po}	r_{pi}	k_{soil}	k_{grout}
[°C]	[m]	[m]	[m]	[W/m-K]	[W/m-K]
10	0.075	0.017	0.014	3	1
k_{pipe}	Cp_{fluid}	$\dot{m}$	$(\rho Cp)_{soil}$	x_c	L
[W/m-K]	[kJ/kg K]	[kg/s]	[MJ/m^3 K]	[m]	[m]
0.4	3.82	0.52	1.25	0.058	150

The entering fluid temperatures (EWT) for both $\beta = 0$ and $\beta = \beta_{\max}$ are presented in Figure 3-8 and Figure 3-9.

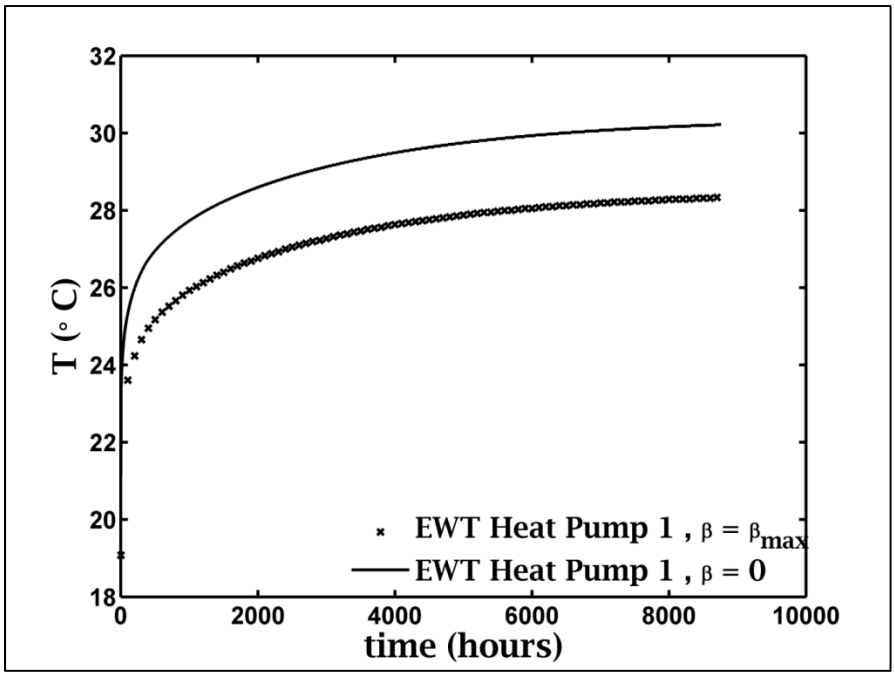

Figure 3-8 EWT of the heat pump 1

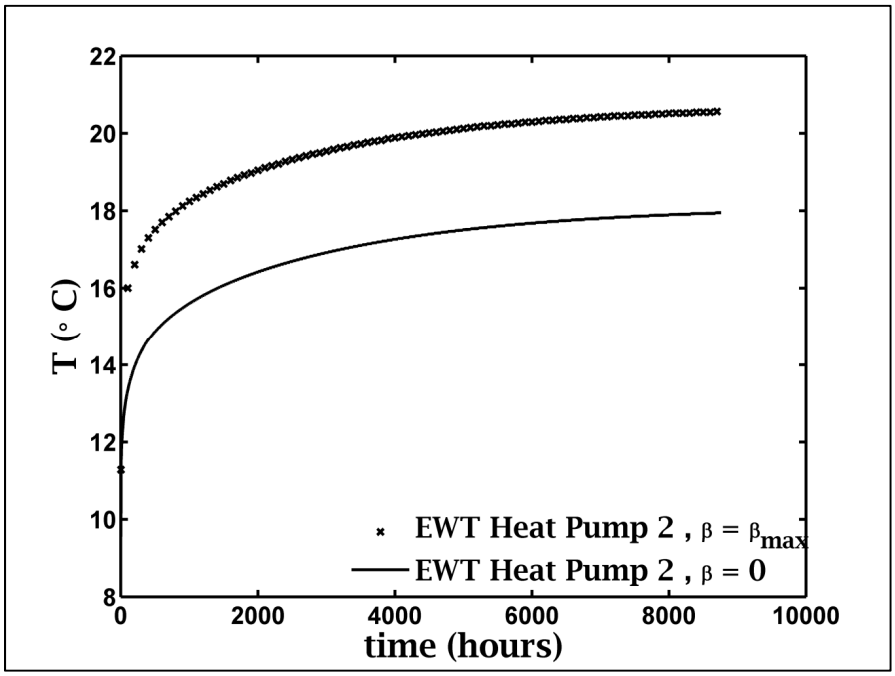

Figure 3-9 EWT of the heat pump 2

The fluid temperature is nearly 2°C lower with the $\beta = \beta_{\max}$ configuration. The results of the simulation done for one year are given in Table 3-2.

Table 3-2 Total energy balance

	$W_{cooling}$ [kWh]	$W_{heating}$ [kWh]	W_{total} [kWh]	Mean COP cooling	Mean COP heating
$\beta = 0$	21425	29151	50776	3.60	4.09
$\beta = \beta_{max}$	20830	27971	48802	3.76	4.21

A 3.5 % total energy consumption difference is evaluated between both configurations. The energy balance of the simulations is shown in Table 3-3.

Table 3-3 Energy balance [MWh]

	β	
	0	max
Heat Pump 1	66.52	67.13
Heat Pump 2	133.88	132.7
Balance (in the ground)	67.36	65.57

The energy balance is lower from the borehole with the $\beta = \beta_{max}$ configuration, showing more energy transferred between the circuits and less through the surrounding ground.

3.7 TRNSYS Model

A TRNSYS simulation is presented for a model that couples 12 residential building heat pumps to a geothermal bore field. For each building, the chosen heat pump capacity is 21.4 kW (about 6 Tons, modeled with a Type 919 component) and the surface area of the solar collectors is 24 m^2 at an inclination of 45°, due south, modeled in TRNSYS with a Type 1 component. The residential buildings are modeled with a Type 759 component and the

weather file (TMY2) used is for Montreal, Canada. Figure 3-10 presents the building thermal and the heat pump four hours blocks average load, for each residence.

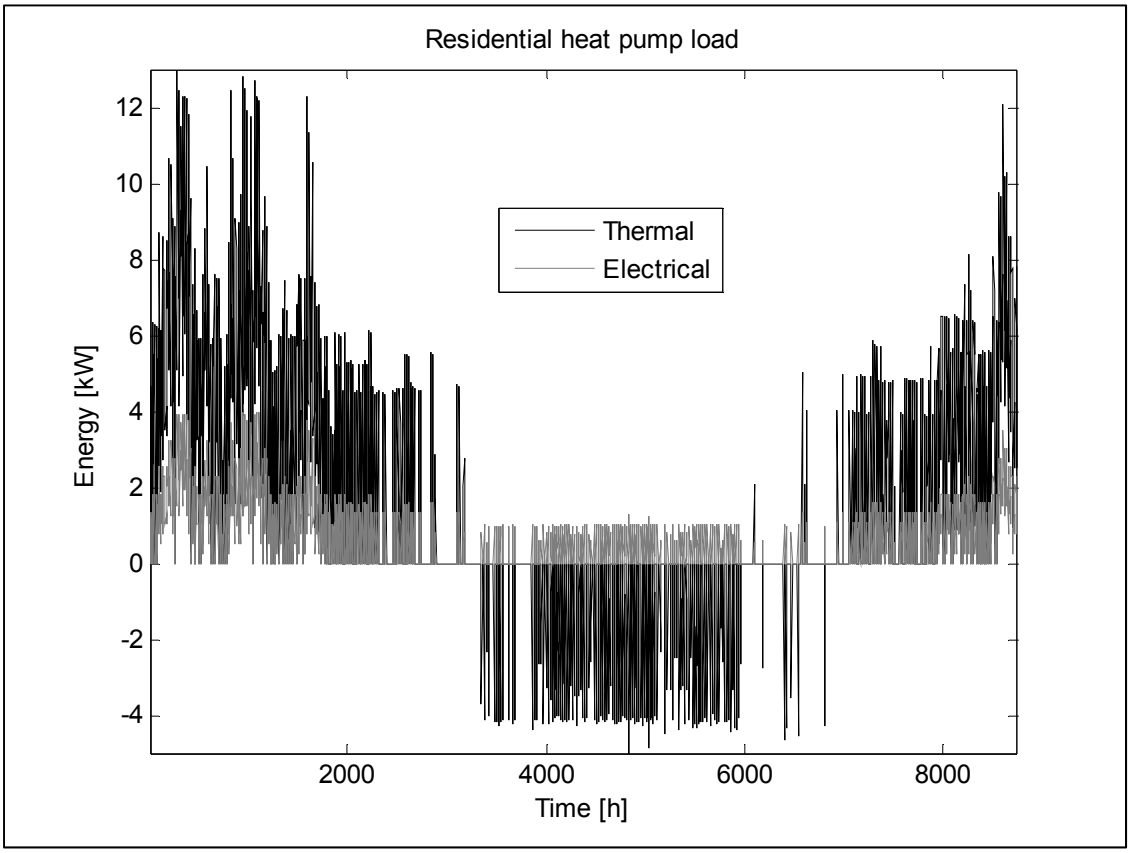

Figure 3-10 Residential thermal and heat pump energy

The building loads include sensible and latent loads, which peak at 21 kW during heating periods and 16 kW during cooling. The peaks of the electrical heat pump are 4.5 kW for the heating loads and 3.3 kW for the cooling loads. The heat pump has been sized to supply the total thermal sensible and latent loads of the building, without auxiliary heaters.

There is an imbalanced load to the borefield. The heat extracted to heat the building is 16 000 kWh and only 3 000 kWh is injected back to the borefield. The parameters used to size the geothermal borefield are provided in Table 3-4.

Table 3-4 Typical geothermal parameters

Parameter	Value	Units	Description
L_{undist}	30	[m]	Undisturbed ground distance
L_{inter}	6	[m]	Distance between boreholes
T_{undist}	10	[°C]	Undisturbed ground temperature
k_s	2.2	[W/m-K]	Conductivity of the ground
k_g	1	[W/m-K]	Conductivity of the grout
k_p	0.4	[W/m-K]	Conductivity of the pipe
ρ_s	2500	[kg/m3]	Density of the ground
c_{ps}	500	[J/kg-K]	Specific heat of the ground
Fr	0.3	-	Fraction of propylene glycol in water
D	33.4	[mm]	Outer pipe diameter
r_b	0.075	[m]	Borehole radius

The simulations were carried out with double U-tube boreholes with two independent circuits: one for the heat pumps and the other for the 24 m^2 of solar collectors for each residential building. The control strategy commands the solar collector loop to operate when the outlet fluid temperature of the solar collectors is higher than 10°C above the heat pump outlet fluid temperature, and stop when this difference is below 2°C.

3.8 Symmetric double U-tubes

For the symmetric case, the legs of each U-tube are equally spaced in the borehole, as shown in Figure 3-11.

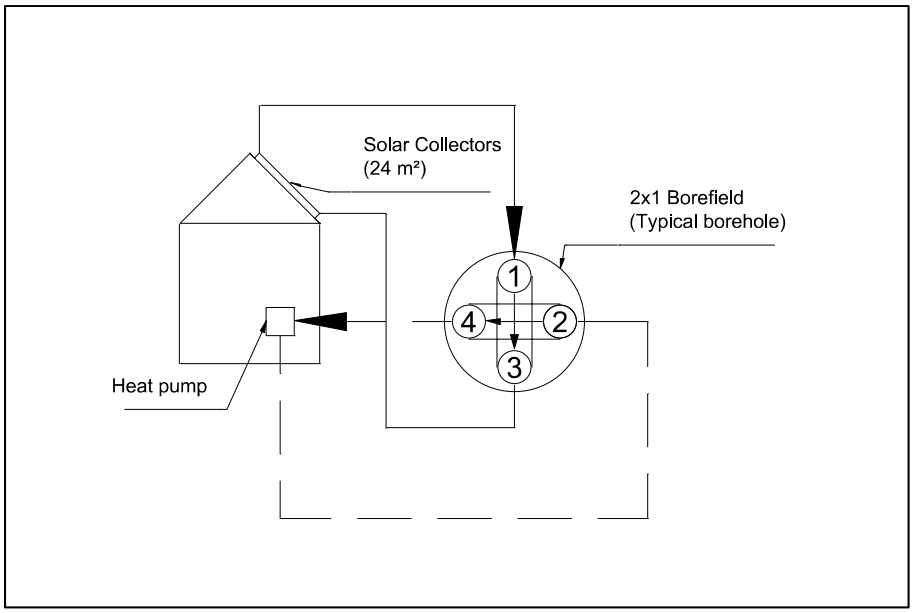

Figure 3-11 Schematic of the system involving one heat pump, one collector area and a symmetric configuration for the borefield

Figure 3-12 shows the heat transferred to the geothermal borefield by the heat pump and solar collectors, in four hour blocks average loads.

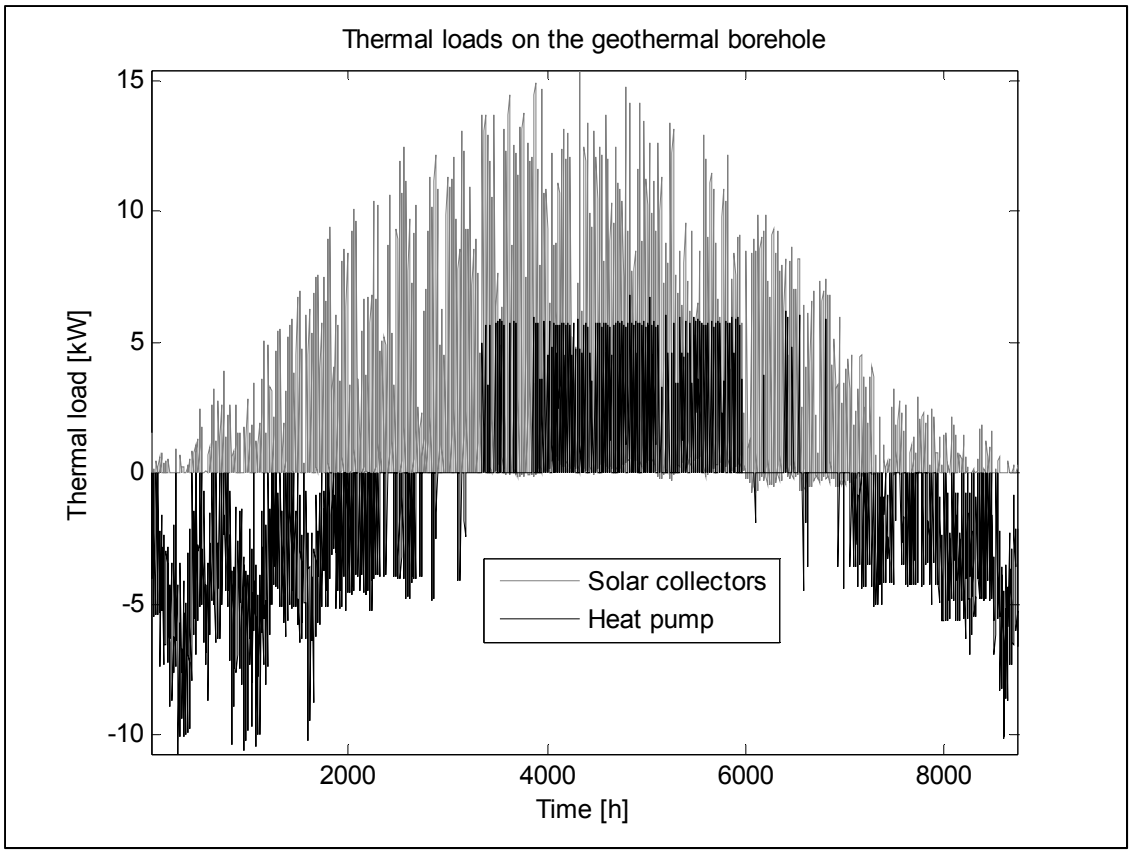

Figure 3-12 Geothermal borehole thermal loads

For the symmetric configuration, the energy consumption of the residential heat pump is 26 412 kWh and the solar collectors supply 94 989 kWh to the borefield. The heat pump extracts 77 667 kWh during the heating period and injects 14 858 kWh during the cooling period. The heat balance over the borefield is 32 180 kWh (injected heat).

The solar collectors operating during summer periods will deteriorate the performances of the heat pump in cooling mode, but the heat stored in the ground compensates in better performances during heating period, which is predominant in this application.

Figure 3-13 shows the outlet fluid temperature of the borefield for the heat pump circuit.

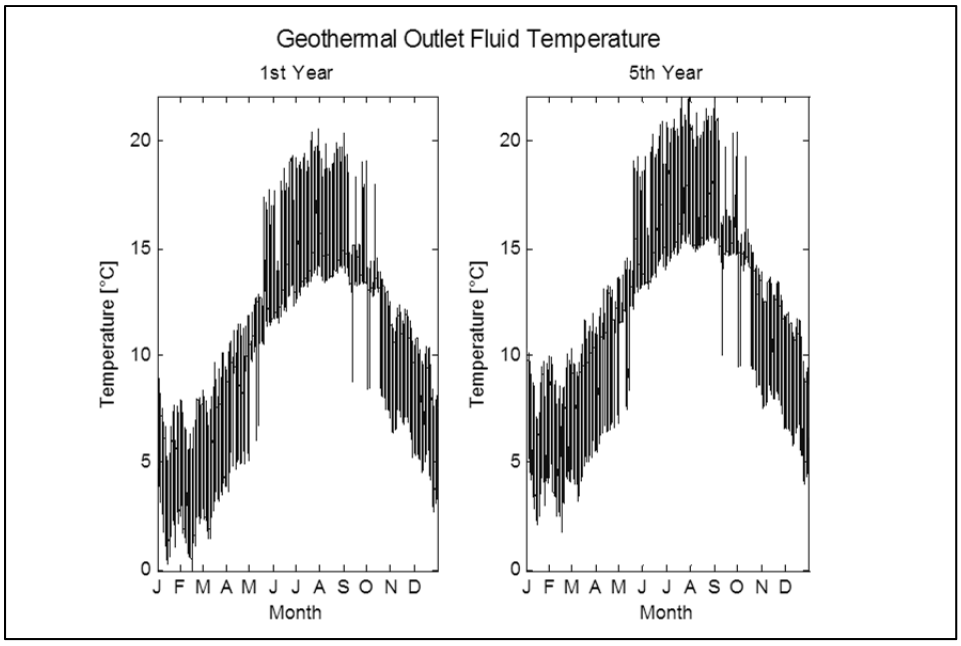

Figure 3-13 Symmetric configuration heat pump circuit borefield outlet fluid temperature with respect to time:
(left) after one year; (right) after 5 years of operation

Figure 13 indicates that the temperature has increased over the first five year simulation, highlighting the overall increase of ground temperature. The lowest outlet fluid temperature is -0.1°C occurring the first year and the highest value reaches 22.1°C occurring the fifth year during a cooling period (summer). The average fluid temperature is 10.5°C the first year and slightly higher at 12.1°C the fifth.

3.9 Non-symmetric double U-tubes

The non-symmetric configuration of double U-tubes consists in bringing the legs of the two U-tubes closer. The inlet legs are in contact with one another, as are the outlet legs as depicted in Figure 3-14.

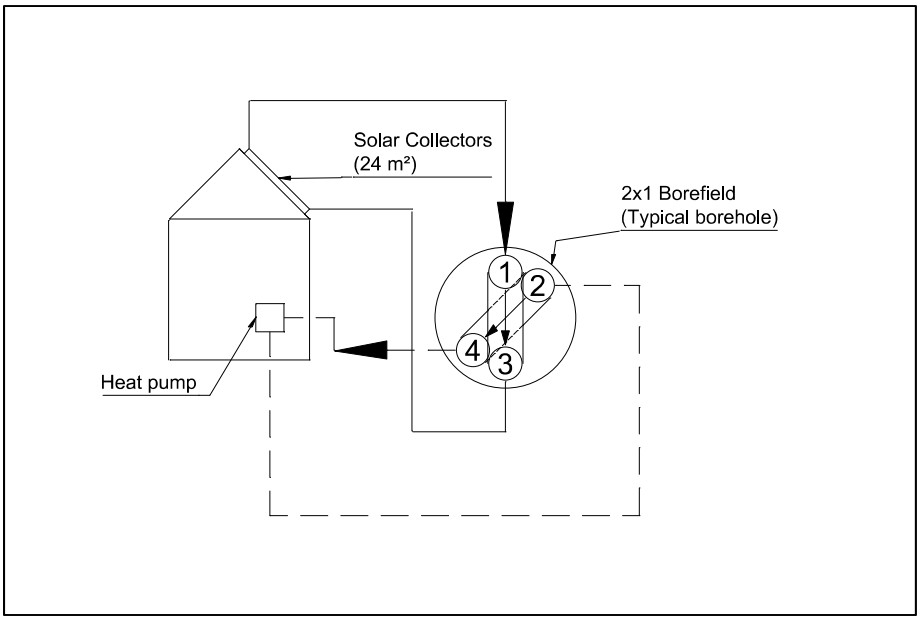

Figure 3-14 Schematic of the system involving one heat pump,one collector area and a non-symmetric configuration for the borefield.

For this configuration, the heat pump energy consumption is now 26 349 kWh and the solar collectors inject 94 761 kWh of heat into the borefield. The heat pump extracts 77 502 kWh during the heating period and injects 14 950 kWh back during cooling.

Figure 3-15 presents the outlet fluid temperature from the borefield profile for the heat pump circuit.

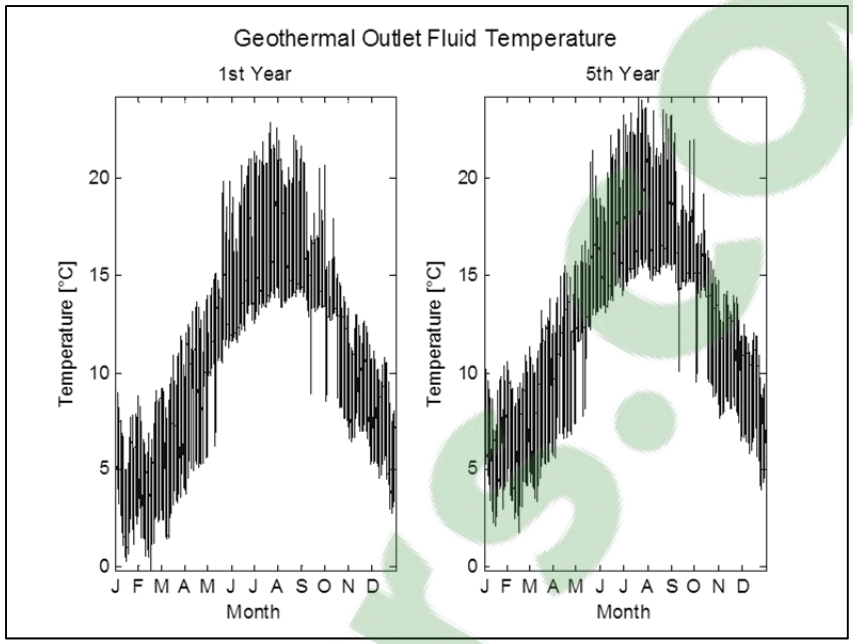

Figure 3-15 Non-symmetric configuration heat pump circuit borefield outlet fluid temperature with respect to time: (left) after one year; (right) after 5 years of operation

In Figure 3-15, one should note that the fluid temperature profile is higher than that of the symmetric configuration. Here, in the first year the minimum temperature reaches -0.2°C during the winter of the first year while the maximum outlet fluid temperature reaches 24.2°C during the summer of the fifth year. The average fluid temperature is 11°C the first year and 12.5°C the fifth.

Table 3-5 summarises the energy balance over the borefield.

Table 3-5 Simulation results for the two configurations: Heat extracted and injected by the heat pump, heat provided by the solar collectors and energy balance [kWh]

	HP Heat Extracted [kWh]	HP Heat Injected [kWh]	Solar Collectors [kWh]	Energy Balance [kWh]
Symmetric	-77 667	14 858	94 989	32 180
Non-symmetric	-77 502	14 950	94 761	32 209

The heat balance of the borefield is comparable in both cases. Table 3-6 shows the energy consumption of the residential heat pumps.

Table 3-6 Energy consumption comparison using simulation results for the two configurations [kWh]

	Energy HP	Savings
Symmetric	26 412	2997
Non-symmetric	26 349	3060

Independent circuits in double U-tubes in a non-symmetric configuration offered comparable results to the symmetric configuration. The differences are insignificant.

3.10 Conclusion

In this paper, a new borehole model to simulate complex geothermal systems is proposed. An analytical solution for double U-tubes with independent inlet conditions in a non-symmetric arrangement is presented. Inlet fluid temperatures, mass flow rates and the angle between the legs of the double U-tubes can be specified. In the validation phase, results produced by the proposed analytical solution for temperature predictions of the two legs of a geothermal borefield showed good agreement with results obtained with a Runge-Kutta method. Results for a detailed hourly simulation coupling residential heat pumps to 24 m^2 of solar collectors

are presented in terms of energy and outlet borefield temperature. The results showed comparable energy consumption of the residential heat pumps with either a symmetric or non-symmetric configuration. However, in the case of two heat pumps working side-by-side, improvement in the order of 3.5 % was observed between both configurations. A parametric study should now be conducted to highlight the effect of different geothermal borefield and borehole parameters on the global energy efficiency of heat pump systems. Design methods based on classical independent boreholes should also be reviewed when shared boreholes are considered.

CHAPTER 4

HYBRID RESIDENTIAL SOLAR GEOTHERMAL BOREFIELD CONFIGURATIONS

Patrick BELZILE, Louis LAMARCHE, Daniel R. ROUSSE

Département de génie mécanique, École de technologie supérieure,
1100, rue Notre-Dame Ouest, Montréal (Québec), Canada, H3C 1K3

Article submitted to "Renewable Energy" journal in March 2016

4.1 Abstract

Hybrid geothermal systems are a solution to decrease the size of geothermal borefields. In classical hybrid configurations, a separated system either provides part of the heat to the building in heating mode, or draws it in cooling mode. In previous papers from the authors, original models that allow the analysis of shared bore fields (where some boreholes receive heat while others provide some) were presented. This allows the analysis of new hybrid configurations where the alternate source is directly coupled with the ground. The objective of this paper is to present different hybrid geothermal borefield configurations where geothermal heat pumps are coupled with solar collectors and to discuss their effect on the energy consumption and fluid temperatures. Different control strategies are also compared. Three main configurations are compared: (1) a mitigated loop which is a classical hybrid configuration; (2) independent boreholes, and (3) independent circuits which could not have been analyzed without shared borefield models. A detailed hourly simulation is executed over three years to compare the solutions. A total of 12 boreholes, 300 m deep, for 12 residential building heat pumps are necessary for a base configuration to keep the fluid temperature above -1°C in the first year. Solar collectors with a surface of 24 m^2 are installed for each residential building. The independent boreholes required 24 boreholes to avoid a

fluid temperature below 0°C in the first year: 12 for the heat pumps and 12 for the solar collectors. A difference of about 9 % of electrical energy consumption was observed between the different configurations and borehole length reduction of 150 meters was achieved when proper design strategies are adopted.

4.2 Introduction

Ground source heat pumps are heat exchangers systems mainly used in building HVAC applications. Heat is transferred to the surrounding ground through vertical boreholes or horizontal loops. Ground source heat pump systems can be sized using different methods (ASHRAE, 2007; Bernier, 2006; Eskilson, 1987; Kavanaugh and al., 1997) and simulated with several strategies (Hellström, 1989; Pahud and al., 1996; TRNSYS, 2011b). Ground models can be analytical (Carslaw and Jaeger, 1959; Cimmino and Bernier, 2014; Ingersoll and Plass, 1948; Lamarche and Beauchamp, 2007a; Zeng and al., 2002) or numerical (Al-Khoury, 2011; Bennet and al., 1987; Hellström, 1991; Pasquier and Marcotte, 2012; Paul, 1996; Sharqawy, 2008; Zeng and al., 2003). There could be advantages to share a geothermal borefield, particularly when loads are complementary. A good example is a ground source heat pump system located in Northern countries that has an unbalanced annual load extracting more heat from the ground to warm up a building in the winter that injecting heat to cool the same building in the summer and solar collectors injecting heat in the ground.

The main point of hybrid systems is to reduce the size of the borefield by supplying extra heating or cooling to buildings during peak demand from conventional HVAC equipment (Gentry and al., 2006; Hackel and Pertzborn, 2011a; Hern, 2004; Yavuzturk and Spitler, 2000). A thermodynamic analysis proved that this approach is more efficient than air-source heat pump (Lubis and al., 2011). A study was also found to couple a borefield to solar panels for heating dominated climates (Chiasson and Yavuzturk, 2003). In another study, three cases are presented showing that hybrid systems can be cost effective (Hackel and Pertzborn, 2011b). Geothermal systems coupled to solar collectors have also been studied in heating for residential building applications (Girard and al., 2015). Trillat-Berdal et al. (Trillat-Berdal and al., 2007) and Toshkov et al. (Toshkov, 2013; Toshkov and al., 2014) simulated and

demonstrated the concept. Kim et al. (Kim and al., 2013) coupled solar collectors to a CO_2 heat pump.

All of these studies are using a mitigated loop, which only has one circuit connected to the geothermal borefield. With reference to the previous work of the authors involved herein, two novel applications can now be simulated: independent boreholes and independent circuits. Belzile et al. (Belzile and al., 2016b) proposed a model that can simulate a geothermal borefield where the boreholes can have independent inlet conditions. The authors developed a semi-analytical model using a control-volume finite difference method for the ground heat transfer and an analytical model for the borehole thermal resistance. Lazzarotto (Lazzarotto, 2014) developed a network-based method that solves a similar problem using an analytical solution. A second approach is to have two double U-tubes in each borehole connected to different circuits. Eslami-Nejad and Bernier (Eslami-Nejad and Bernier, 2011a; Eslami-Nejad and Bernier, 2011b) were the first to model the thermal behavior of a borehole with this configuration. Their approach is a generalization of the Zeng et al. (Zeng and al., 2003) method that was used to simulate a double U-tube configuration in parallel or in series. Belzile et al. (Belzile and al., 2016a) modified and extended the former approach to be able to vary the angle between each U-tube.

The classical approach to simulate geothermal borefields is to set the same inlet conditions for each borehole. This is mainly due to the fact that models to simulate segregated inlet conditions are not available. This paper presents applications involving two models: (1) independent boreholes, where each borehole have independent inlet conditions, and (2) independent circuits. For each model, each leg of a double U-tube can have different inlet conditions. The applications of hybrid geothermal systems are compared with the more classical mitigated loop configuration. Two previous papers focus attention on the development and validation of the models (Belzile and al., 2016a; 2016b). This paper presents the results of simulations of residential/solar hybrid systems and discusses the main advantages of different borefield configurations.

4.3 Base configuration

A TRNSYS simulation model couples 12 residential building heat pumps to a geothermal borefield, as shown in Figure 4-1. For clarity, only one building is depicted in Figure 4-1 and subsequent schematics. .

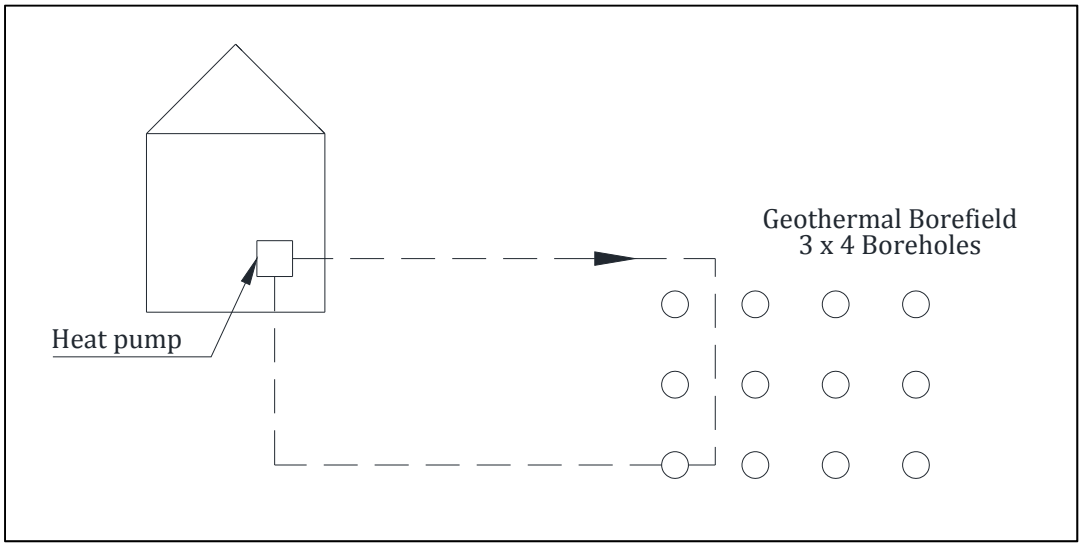

Figure 4-1 Base configuration

The residential buildings are modeled with a Type 759 component and the weather file (TMY2) used is for the city of Montreal, Canada. Figure 4-2 presents the typical residential building thermal loads.

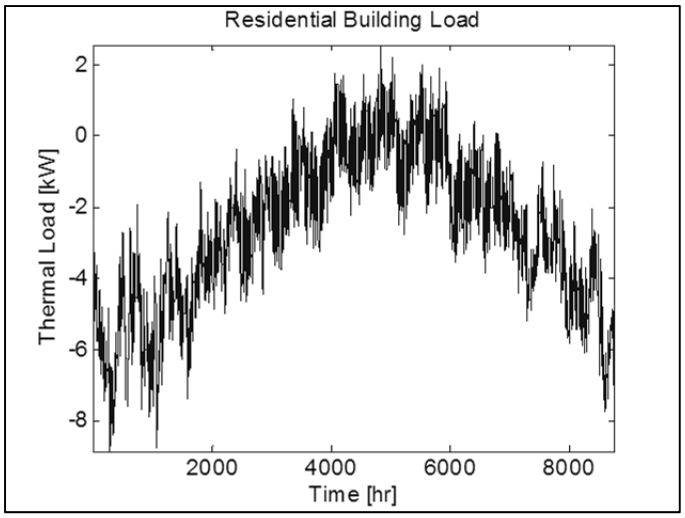

Figure 4-2 Residential thermal loads

These building loads include sensible and latent loads which peak at 9 kW during the heating period (in winter between 0 to 2000 hours) and 2 kW during the cooling period (in summer between 4000 and 6000 hours).

The selected heat pump is modeled with a Type 919 component. In Montreal, there is an unavoidable imbalanced load to the borefield. In the basic configuration, the heat extracted is 12 500 kWh and 4 000 kWh are injected back to the borefield. Without external heat inputs, this would result in a reduction of the ground temperature up to a point where it could freeze and then damage the system.

The parameters used to simulate the geothermal borefields are concisely presented in Table 4-1.

Table 4-1 Typical geothermal parameters

Parameter	Value	Units	Description
L_{undist}	30	m	Undisturbed ground distance
L_{inter}	6	m	Distance between boreholes
T_{undist}	10	°C	Undisturbed ground temperature
L_b	300	m	Geothermal boreholes length
k_s	2.2	W/m-K	Conductivity of the ground
k_g	1	W/m-K	Conductivity of the grout
k_p	0.4	W/m-K	Conductivity of the pipe
ρ_s	2500	kg/m3	Density of the ground
C_s	500	J/kg-K	Specific heat of the ground
Fr	0.3		Fraction of propylene glycol in water
d_p	33.4	mm	Pipe outer diameter
r_b	0.075	m	Borehole radius

Except where indicated in the description of the configurations, these parameters will be used for all simulations.

4.3.1 Base case simulation

A base case scenario simulation using a 3x4 borefield configuration with 300 m boreholes and no solar collectors was carried out using the proposed model. The predicted outlet fluid temperature from the geothermal borefield is shown in Figure 4-3 for year one and year three.

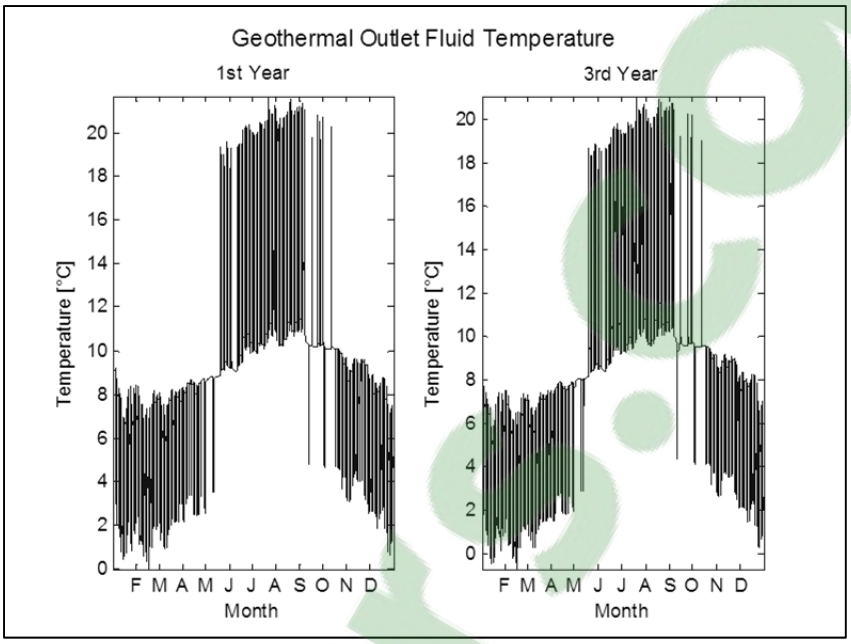

Figure 4-3 Geothermal Outlet Fluid Temperature
Base Case 3x4 Borefield

Figure 4-3 indicates that the geothermal borefield outlet fluid temperature drops to -0.7°C at the beginning of the third year: a fluid temperature below freezing point could be problematic. In this case however, it occurs for short periods, a few hours, so the surrounding ground may not reach freezing point. For longer periods, freezing the water contained in the ground could collapse the boreholes and make them unusable (Nordell and Ahlström, 2007).

The electrical energy consumed by each residential heat pump over the three years simulation is 10 884 kWh.

In order to try to balance the loads and to reduce the size of the borefield, hybrid geothermal systems could be considered. In this case, solar collectors are coupled to the geothermal heat pump system. In the following section, three main classes of configurations are compared:

1. The first is called **mitigated loop** where the solar collectors loop warms up the geothermal loop during heating season through a heat exchanger;
2. A second class of configurations is called **independent boreholes** which segregates the residential heat pumps and the solar collector loops in different boreholes (Belzile

and al., 2016b). In this case, there are 12 boreholes used by the heat pumps and 12 other boreholes used by the solar collectors.

3. A third class is called **independent circuits** (Belzile and al., 2016a). The 12 heat pumps and the solar collectors loops are coupled to two independent circuits of double U-tube in each boreholes.

The base and the mitigated loop configurations could be modeled with conventional geothermal models such as the DST model embedded within TRNSYS, as they have the same inlet conditions for each borehole. The proposed geothermal borefield models used in this work (Belzile and al., 2016a; 2016b) are needed to simulate the independent boreholes and independent circuit configurations.

4.4 Mitigated loop

A mitigated loop couples solar collectors in series with the geothermal heat pump loop. Figure 4-4 shows a simplified diagram of the system.

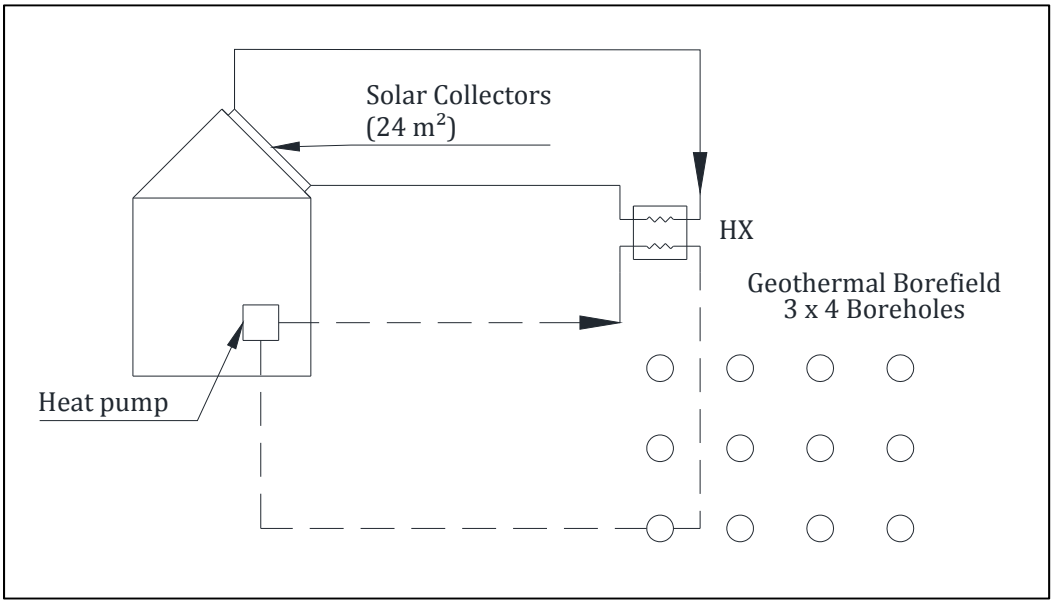

Figure 4-4 Mitigated loop configuration

The 4x3 borefield configuration is used with 300 m boreholes. There are 24 m^2 of solar collector surface on each of the 12 residential buildings. In this configuration, the solar collectors' circuit is coupled to the geothermal heat pump circuit through a heat exchanger (HX in Figure 4-4). The solar collectors circuit is controlled by a differential controller, which operates when the fluid temperature of the solar collector circuit is higher by 10°C with respect to the geothermal heat pump circuit. It stops when this temperature difference is lower than 2°C. Two control strategies were simulated: the "No Sum" strategy where the solar collectors circuit does not operate from May to September and the "All Year" strategy where they provide heat all year long. The results from the first configuration are presented first. Figure 4-5 presents the geothermal borefield outlet fluid temperature of the heat pump circuit for the first and third year.

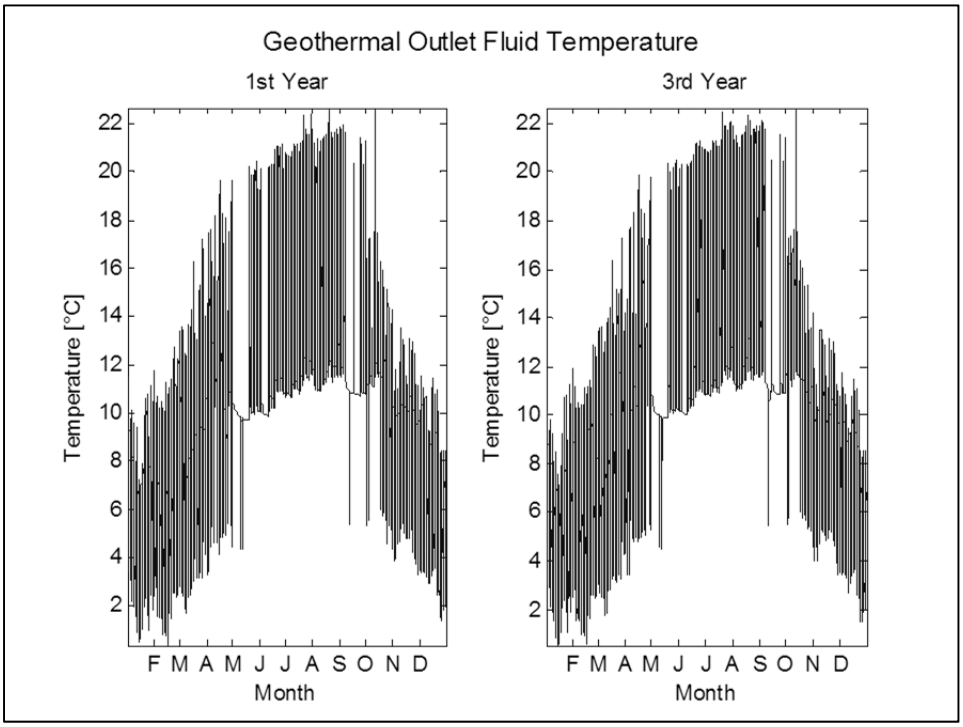

Figure 4-5 Single-loop 3x4 configuration outlet fluid temperature predictions of the geothermal heat pump: No sum strategy; (left) after one year; (right) after 3 years of operation

For the No Sum control strategy, not using the solar collectors during cooling months, the lowest fluid outlet temperature simulated is 0.4°C. This low temperature occurs at the first year and is stable over the years.

The energy balance for each heat pump in the mitigated loop configuration is presented in Figure 4-6. It shows the heating, cooling and net load for the building, the geothermal borefield and the compressor of the heat pump.

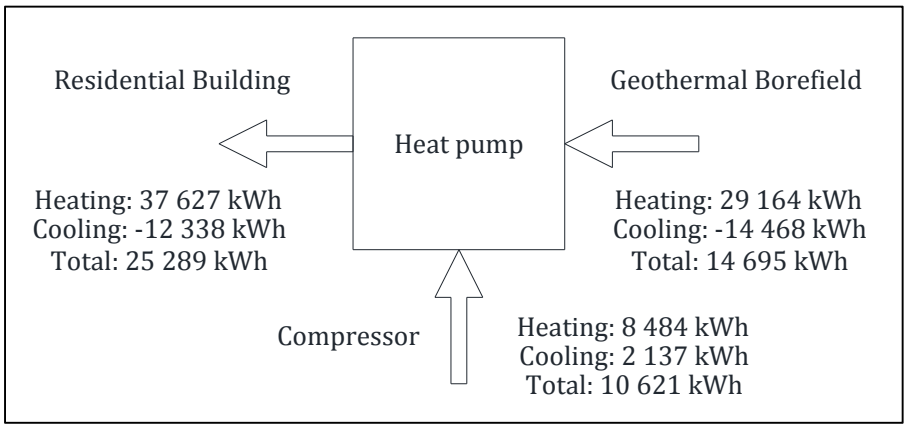

Figure 4-6 Mitigated loop heat pump energy balance

The energy used by the residential heat pump is found to be 10 621 kWh while the difference between heating and cooling for borefield is 14 695 kWh. The energy balance on the heat pump from geothermal borefield and compressor to the residential building gives a 27 kWh difference due to truncation error. The energy balance of the ground is presented in Figure 4-7.

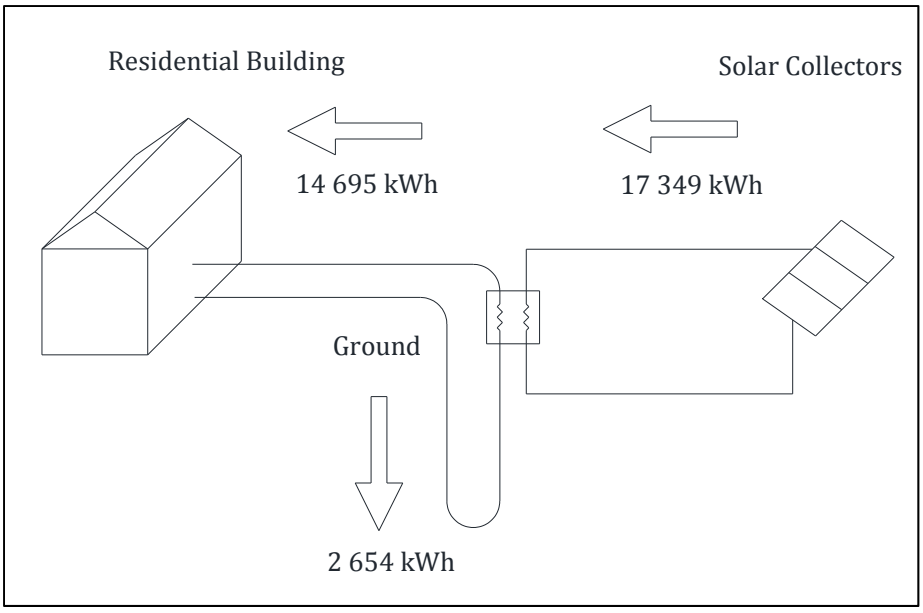

Figure 4-7 Mitigated loop ground energy balance

With the No Sum control strategy, each solar collectors array supplies 17 349 kWh to the circulation loop, the heat pumps extracts 14 695 kWh of heat and 2 654 kWh are stored in the ground. The ground temperature increases to 10.6°C at the end of the third year of simulation. The results for the All Year strategy are provided in section 4.7 where all configurations are compared.

4.5 Independent boreholes

Segregating the inlet conditions of the boreholes in a borefield would be interesting in such a way that the solar collectors could supply heat on a longer period than the instantaneous of a mitigated loop. The compared borefield configurations are one with central heat injection from the 24 m^2 of solar collectors per building and a staggered configuration. The control strategy of the solar collectors loop is to use it all year long. In order to keep fluid temperature to acceptable levels, a total of 24 boreholes were required instead of 12 for the base configuration. In a classical geothermal system, it is well known that boreholes must be spaced at a minimum distance to minimize interferences effects. In the shared borefield, this is less obvious since the smaller distance between the source and sink boreholes can be an advantage when the demands are in phase but an inconvenient when they are out of phase.

For this reason, the distances between boreholes are also a parameter studied in these configurations.

4.5.1 Central configuration

The borefield is a 4x6 configuration and two simulations compare 4.5 m and 6 m between boreholes. The solar collector circuit injects heat at the center of the borefield and the residential heat pumps circuit is located at the outer boreholes. This configuration is shown in Figure 4-8.

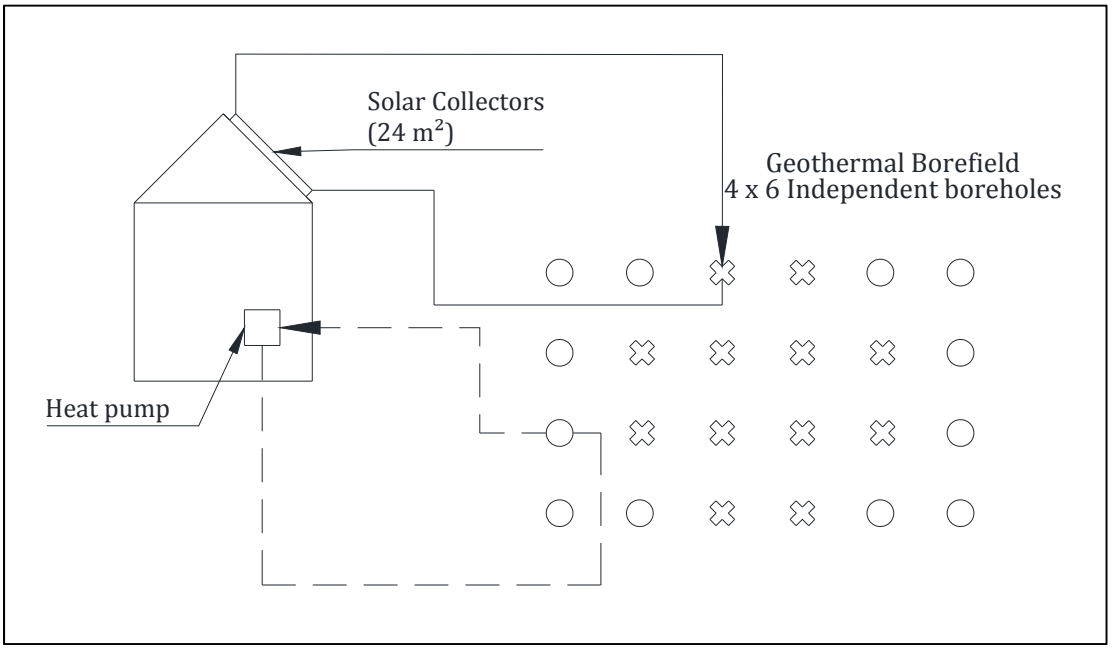

Figure 4-8 Independent boreholes, central configuration

The results from the 4.5 m configuration are presented here, and the 6 m will be presented in the summary tables. Each residential heat pump energy consumption reaches 10 614 kWh over three years of simulation. Each solar collectors array injects 51 781 kWh of energy in the borefield, 29 231 kWh are extracted by each heat pump to heat the building and 14 568 kWh are injected back during cooling, resulting in a heat balance of 37 118 kWh in the borefield.

Coupling the solar collectors circuit at the center of the borefield allowed the storage of a considerable amount of energy. The ground temperature profile at the end of the third year is shown in Figure 4-9.

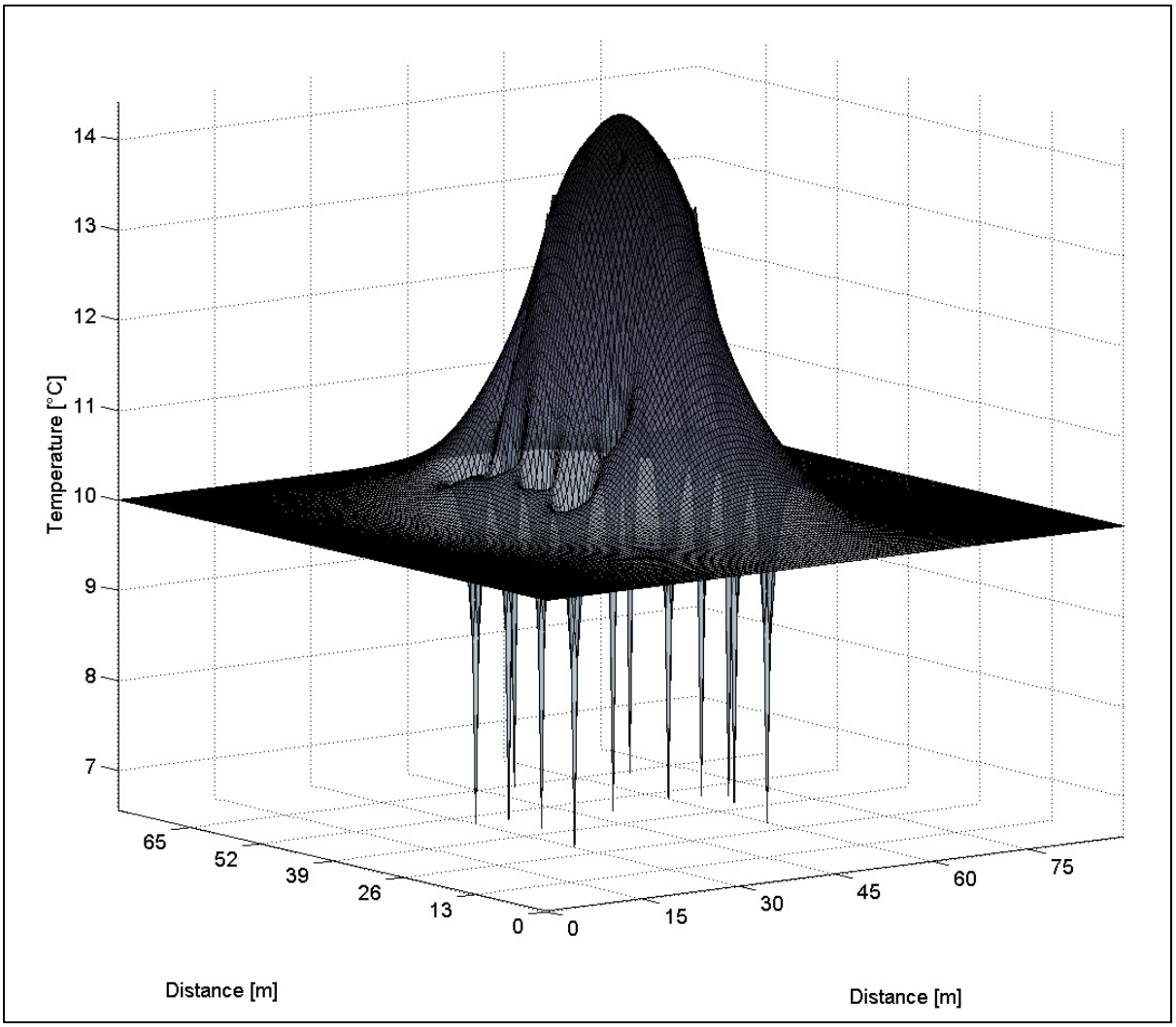

Figure 4-9 Independent Boreholes Central Configuration Ground Temperature Profile

The 12 boreholes configuration of 300 m length resulted in outlet fluid temperature as low as -0.1°C a few hours of the year. The highest outlet fluid temperature is 25.2°C, with an average of 9.9°C the first year and 11.5°C the third. A comparison with the above-mentioned base case involving only with 12 boreholes is provided in section 4.7.

4.5.2 Staggered configuration

A staggered arrangement represented in Figure 4-10 would be of interest so that each borehole circuit is separated by the other in the same borefield. This would increase the interaction effect between the circuits. Three configurations are compared, with distances between boreholes of 3 m, 4.5 m and 6 m. The results from the 3 m configuration are presented here and the others in the next section.

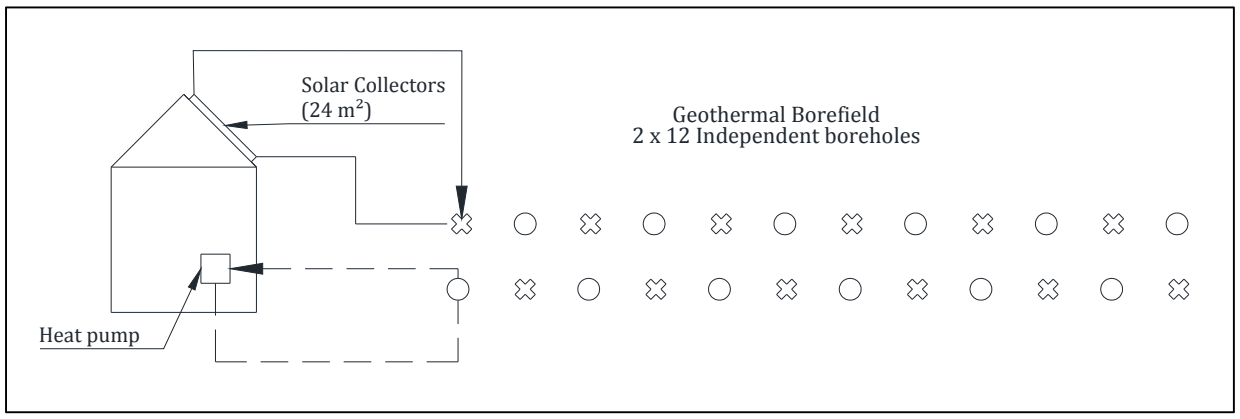

Figure 4-10 Independent boreholes, staggered configuration

The heat pumps energy consumption over three years is 10 617 kWh. The solar collectors inject 56 603 kWh of energy in the borefield, the heat pump extracts 29 229 kWh during heating period and injects 14 582 kWh during cooling period. The heat balance over the borefield is 41 956 kWh injected heat. In this configuration, the maximum temperature is 12.8°C at the center. The lowest outlet fluid temperature is 0.1°C occurring in the first months of the first year and the highest temperature is 25.3°C.

4.6 Independent circuits

Having double U-tubes in each borehole would increase heat transfer rate between two circuits. Again, this would be an advantage when the demands are in phase. It would be suitable for an unbalanced residential application coupled with solar collectors. The simulations done with independent circuits in double U-tubes boreholes consists of the same

single residential heat pump model as in the previous simulations, coupled to 24 m^2 of solar collectors. The number of boreholes is 12 arranged in a 3 x 4 configuration.

4.6.1 Symmetric double U-tubes

In a symmetric case, the legs of each U-tube are equally spaced in the borehole, as shown in Figure 4-11. In a classical borehole, it is well known that it is advantageous to place the tubes as close as possible to the borehole radius, that is as far apart as possible. This configuration was named "Case C" in the work of Remund and Paul (Paul and Remund, 1993) involving a symmetric arrangement of the four legs in the borehole. In the shared borehole configuration, it is not as obvious since part of the heat is transferred to or from the ground and part of it is given by the adjacent circuit. For this reason, two scenarios are analysed: one where the tubes touch the borehole radius (Type C) and one where the tubes all are in contact with each other (Type A).

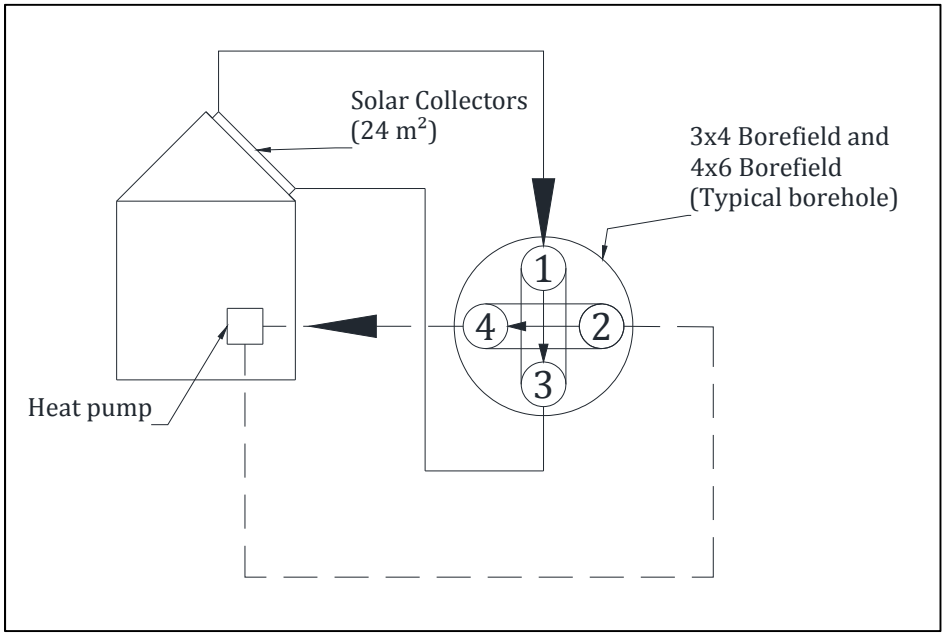

Figure 4-11 Independent circuit, symmetric configuration, Type C

The symmetric 3x4 Type C All Year configuration energy consumption of the residential heat pump is 10 184 kWh and the solar collectors supplies 59 996 kWh to the borefield. The heat pump extracts 29 359 kWh during heating period and injects 14 431 kWh during cooling period. The heat balance over the borefield is 45 068 kWh injected heat.

The temperature rises for the first three years of simulation, driven by the positive energy balance on the ground. The lowest outlet fluid temperature is 4.8°C occurring the first year and the maximal value is 16.7°C occurring the third year during cooling period. The average fluid temperature is 10.7°C the first year and 11.6°C the third year.

4.6.2 Non-symmetric double U-tubes

The non-symmetric configuration of double U-tubes consists in bringing closer the legs of the two U-tubes. The inlet legs are in contact with one another, as well as the outlet legs as shown in Figure 4-12.

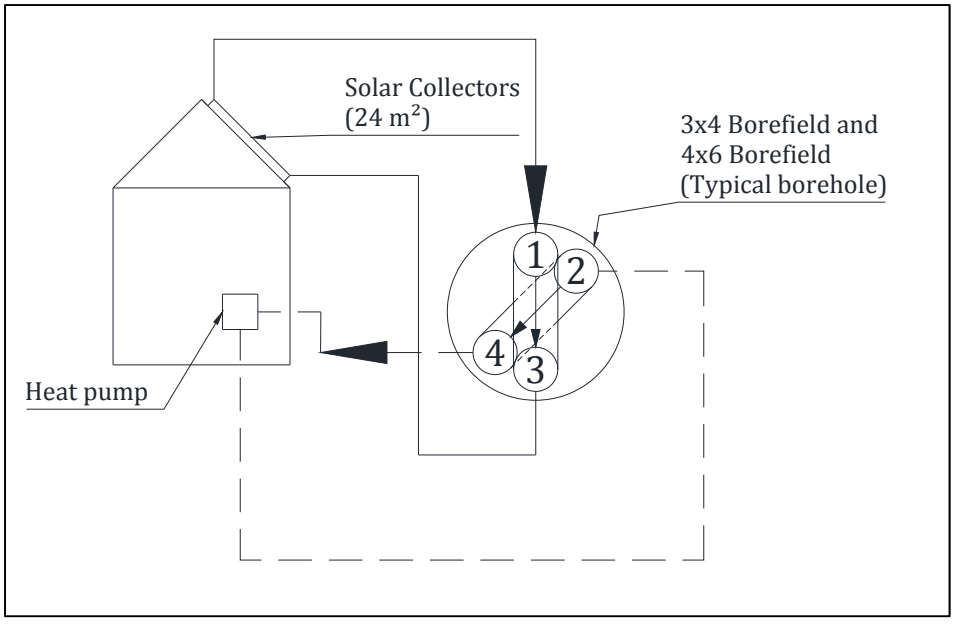

Figure 4-12 Independent circuits, non-symmetric configuration, Type C

In the 3x4 non-symmetric Type C All Year configuration, the heat pump energy consumption is 10 201 kWh and the solar collectors inject 59 808 kWh of heat in the borefield. The heat pump extracts 29 366 kWh during heating period and injects back 14 489 kWh during cooling. The ground maximum temperature at the third year is 11.9°C. The Figure 4-13 presents the outlet fluid temperature from the borefield profile for the heat pump circuit.

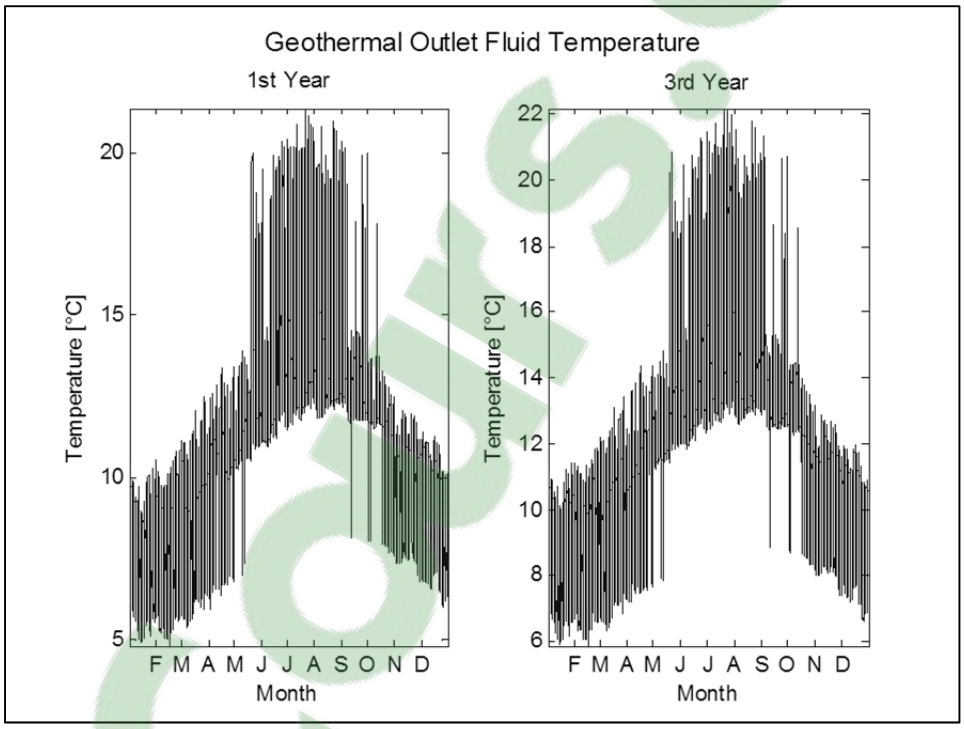

Figure 4-13 Independent circuit non-symmetric configuration heat pump circuit borefield outlet fluid temperature

The fluid temperature profile is higher than the symmetric configuration: 4.8°C minimum temperature in the first year and 22.2°C maximum outlet fluid temperature the third year. The average fluid temperature is 11.2°C the first year and 12.0°C the third.

4.7 Comparison of configurations

The results from all simulations are presented and compared here. The parameters that varied between simulations were:

- 12 and 24 boreholes per borefields;
- Boreholes arrangements in the field for the same number, 2 x 12, 4 x 6.
- Base case, mitigated, independent boreholes and independent circuits configurations;
- The shank spacing types A (legs of the U-tubes in contact with each other) and C (legs of the U-tubes in contact with the borehole wall);
- Control strategies for the solar collectors functioning all year long (All year) and not functioning during summer (No sum).

All of the tabulated results for the figures presented in this section are available in Appendix II.

4.7.1 Ground heat balance

Figure 4-14 summarises the energy balance over the borefield for the 12 boreholes configurations.

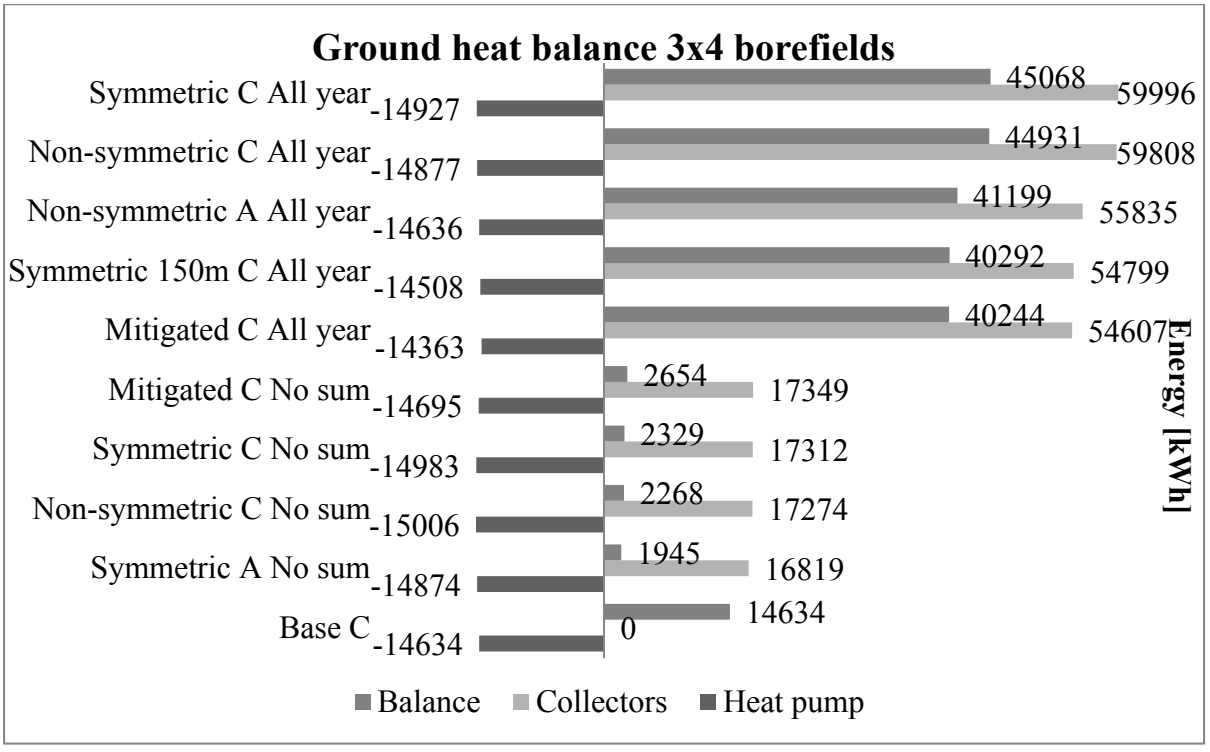

Figure 4-14 Ground heat balance for all simulations involving 3x4 borefields

There is not a huge difference in energy balance of the borefields, but generally speaking, the Type C leg spacing is found to be more advantageous than Type A; the All Year control strategy injected a lot more energy than the No Summer; and the mitigated loop was not far behind the independent circuits configurations. There is a slight variation in energy from the heat pumps, about 1%, which could be due to heat pump performances and simulation parameters.

The Figure 4-15 presents the heat balance of the ground with 24 borehole heat exchangers (BHE) configurations.

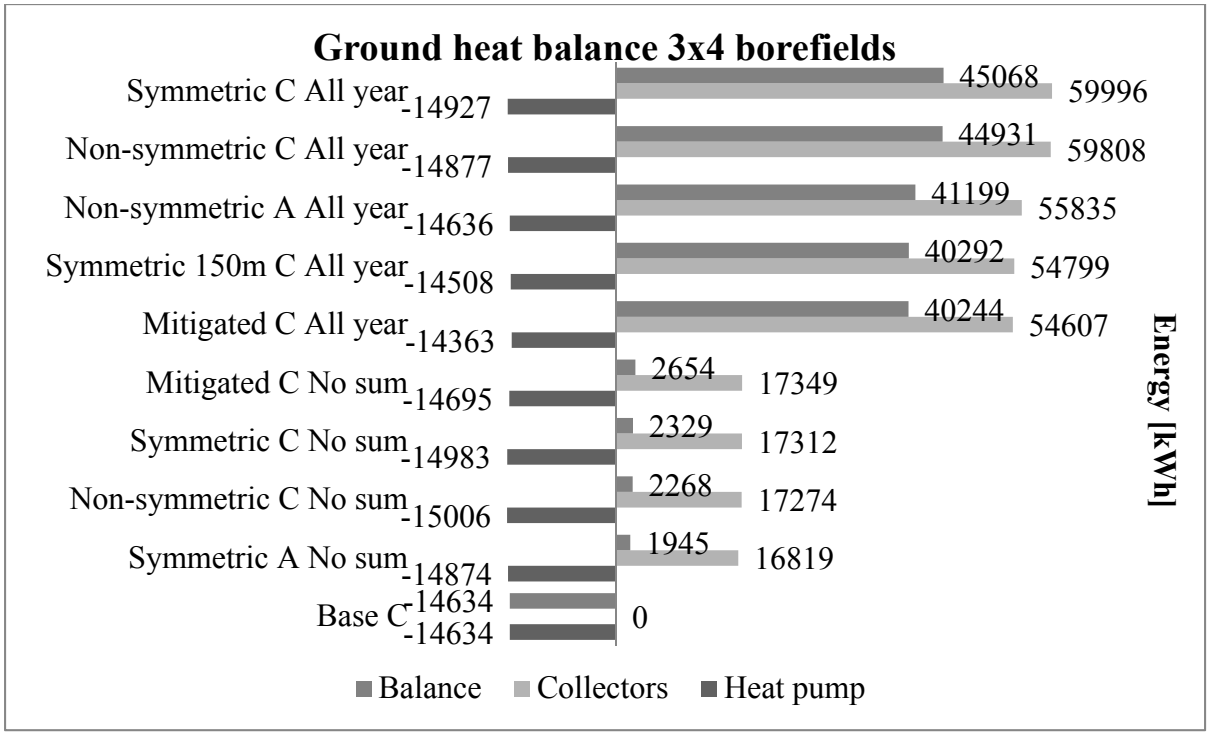

Figure 4-15 Ground heat balance for all simulations involving4x6 borefields

The energy balance is most favorable with the independent circuits configurations. The independent boreholes have a larger energy balance with more space between boreholes, showing the importance of the quantity of ground in geothermal borefields. The ground temperature will have a direct impact on fluid temperatures.

4.7.2 Borefields outlet fluid temperatures

The Table 4-2 shows the results of the simulation of outlet fluid temperatures for selected configurations.

Table 4-2 Geothermal outlet fluid temperature comparison for 16 BHE (heat pump circuit)

BHE	Configurations	Type	Ctrl	min fluid T°	Max fluid T°	Mean fluid T° 1st year	Mean fluid T° 3rd year
3x4	Base	C	-	-0.7	21.7	8.9	8.0
3x4	Mitigated	C	All year	0.4	36.2	13.0	14.9
3x4	Mitigated	C	No sum	0.4	22.7	10.2	10.3
3x4	Non-symmetric	A	All year	2.5	32.9	12.0	12.8
3x4	Non-symmetric	C	All year	4.8	22.2	11.2	12.0
3x4	Non-symmetric	C	No sum	4.8	16.7	10.0	10.0
3x4	Symmetric	A	No sum	2.4	20.2	10.2	10.2
3x4	Symmetric	C	All year	4.8	19.8	10.7	11.6
3x4	Symmetric 150m	C	All year	-0.2	29.0	11.3	12.8
3x4	Symmetric	C	No sum	4.8	16.7	9.9	9.9

The minimum fluid temperature of the 3x4 symmetric All Year Type C is 4.8°C for the first year of operations while the Type A is 2.5°C, showing a potential to reduce the length of the boreholes. Reducing the length of the Type C by half, to 150 m, made the temperature of the first year to fall to a minimum of -0.2°C, rising every year because of the ground heat balance. The highest temperature is found in the non-symmetric AllYear Type A configuration, with 32.9°C and the mitigated loop All Year Type C 36.2°C. The high limit of temperature of the heat pump in cooling mode is 43.3°C, which could be reached in the long run.

The Table 4-3 presents the geothermal borefield outlet fluid temperature for the heat pump circuit, for the 24 BHE configurations

Table 4-3 Geothermal outlet fluid temperature comparison for 24 BHE (heat pump circuit)

BHE	Configurations	Type	Ctrl	min fluid T°	Max fluid T°	Mean fluid T° 1st year	Mean fluid T° 3rd year
4x6	Central 4.5m	C	All year	-0.1	25.2	9.9	11.5
4x6	Central 6m	C	All year	0.1	24.1	9.5	10.7
2x12	Ind staggered 3m	C	All year	0.0	27.0	10.8	12.6
2x12	Ind staggered 4.5m	C	All year	0.1	25.3	10.1	11.6
2x12	Ind staggered 6m	C	All year	0.1	24.1	9.8	10.9
4x6	Non-symmetric	A	All year	6.0	22.1	11.1	11.8
4x6	Non-symmetric	C	All year	7.8	15.9	10.6	11.3

The minimum temperature of the independent borehole configurations is close to the base case, due to the fact that there are 12 boreholes for 12 residential heat pumps. The temperature interference between the heat pump loop boreholes during extraction is more important with smaller distances between boreholes. The independent circuits configurations gave the most stable fluid temperatures, showing that the heat transfer between the loops is more efficient that the independent boreholes.

4.7.3 Heat pumps energy consumption

The energy consumptions of the 3x4 borefields configurations are shown in Figure 4-16.

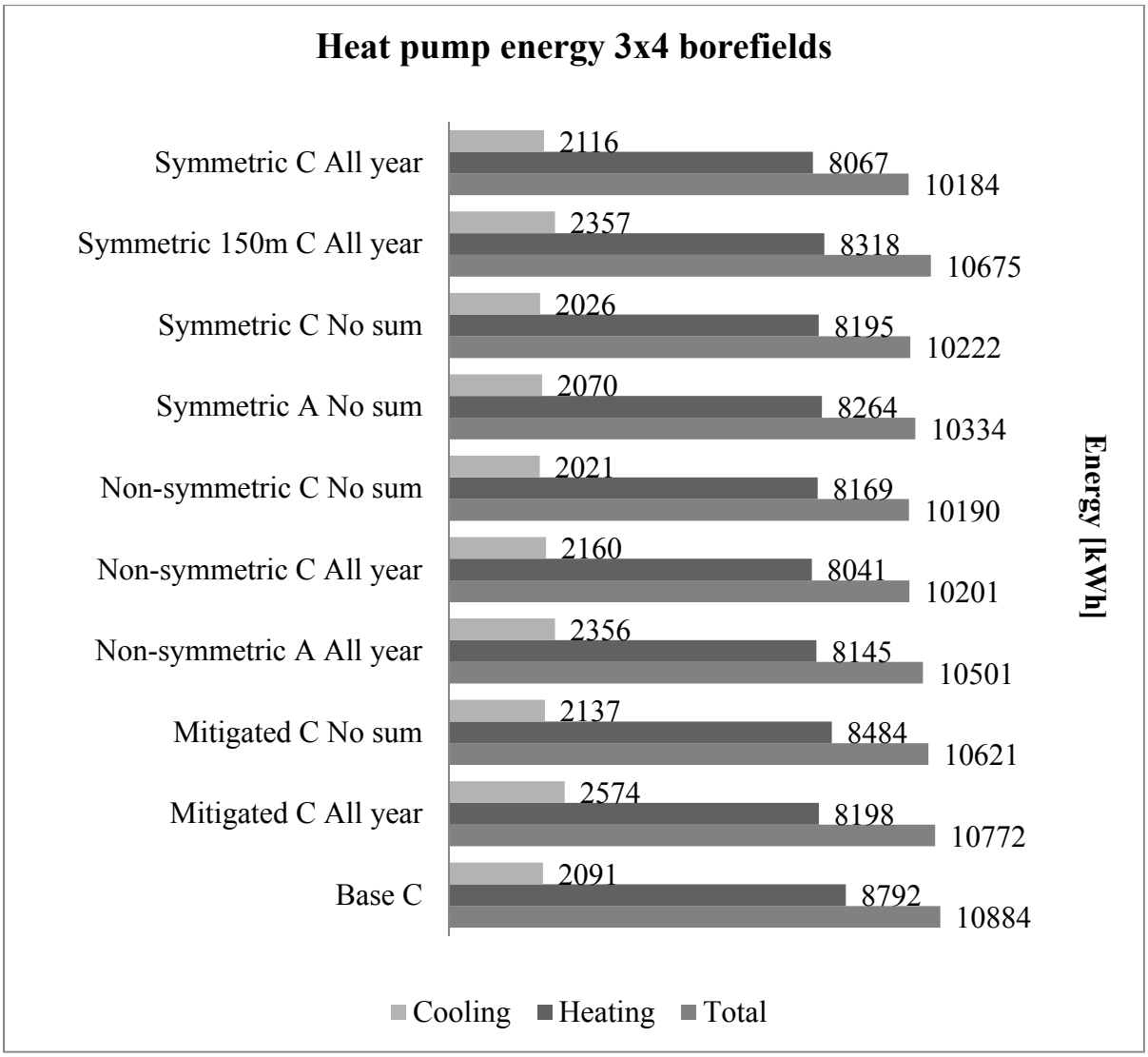

Figure 4-16 Heat pump energy consumption for all simulations involving 3x4 borefields

The mitigated loop allowed a 2.4% of energy savings in the No Sum control strategy over the base case on the three years of simulation. The best results have been with both the symmetric and non-symmetric, Type C All Year configuration, with 6.4% of savings. The Type C has an advantage over the Type A implying that the inlet legs and the outlet legs should be as far as possible from one another. Injecting heat from the solar collectors all year long versus not in the summer did not give much difference in the independent circuits configurations. The gains in heating mode were compensated with the losses in cooling mode.

Figure 4-17 shows the energy consumption of the 24 BHE configurations.

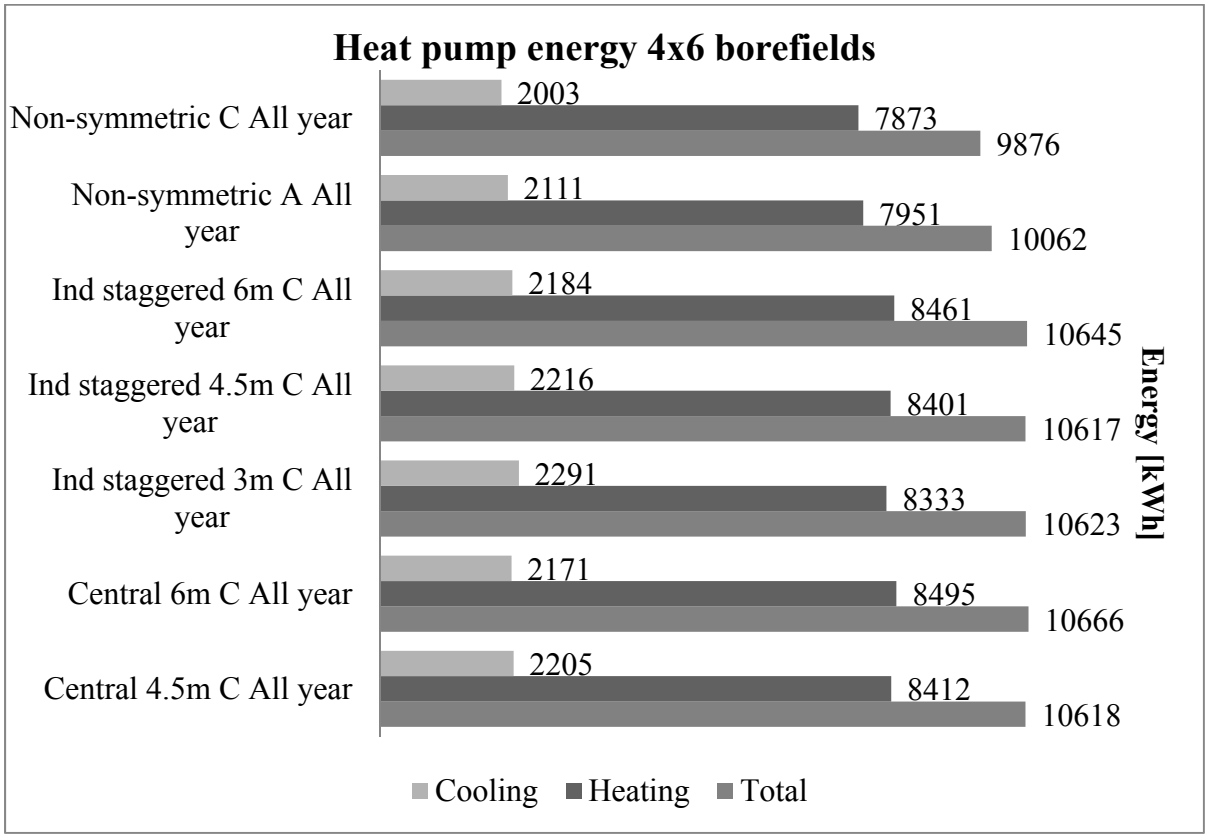

Figure 4-17 Heat pump energy consumption for all simulations involving 4x6 borefields

The independent circuits are clearly advantaged over the independent boreholes configurations. The best results have been found in the staggered arrangement for the independent boreholes. The highest the energy savings are found with closer boreholes. These factors highlight the importance that the heat transfer between the circuits is more important than the amount of energy stored in the ground, at least for the first three years.

In the 3x4 configurations, the lowest energy consumption has been found with the independent circuits with Type C configurations, with 6.1% to 6.4% energy savings. The symmetric vs non-symmetric, as well as all year vs no sum had very low impact on energy consumption. The best independent boreholes configurations are found with Type C also,

with 2.0% to 2.5% savings over base case. In the 24 BHE configurations, the non-symmetric Type C was the most interesting with 9.4% energy savings.

The energy savings were relatively low over the three years of simulation. The best savings of the 3x4 borefields has been obtained with the independent circuits in symmetric configuration with 700 kWh of savings.

The length of the boreholes can be shortened by half in the independent boreholes Type C All Year configurations. The energy savings is still at 1.9% of the base case but the capital cost for the corresponding borefield diminishes.

4.8 Conclusion

Hybrid geothermal heat pump systems can be useful to reduce the size of a geothermal borefield. Coupling residential heat pumps and solar collectors can be done in various configurations. The first configuration studied in this paper is a mitigated loop, where the solar collectors transfer heat to the heat pumps loop through a heat exchanger. The second is independent boreholes in a borefield, where two main configurations are compared: injecting the solar collectors heat in the center of the borefield and a staggered configuration. The third configuration presented involves two independent circuits in each borehole: one with the legs of the U-tubes equally-spaced in the borehole and another where the inlets of the circuits are in contact, as well as the outlets. These systems are compared to a base case where only residential heat pumps are coupled to a geothermal borefield.

Different parameters have been simulated. Two control strategies for the solar collectors loop: one running all year long, while the other stops during summer. Two U-tube legs configurations: Type A and C are compared. Various distances between boreholes are also looked at in the independent boreholes configurations. The best scenario for the 3x4 borefields has been found with the independent circuits configurations Type C U-tubes. The all year control strategy and symmetric vs non-symmetric parameters were found to have

little impact on the results. . The savings ranged from 6.1% to 6.4% with respect to the base configuration. The best performances of the independent boreholes strategy have been obtained with the central configuration with 4.5 m spacing between boreholes: 2.5% less energy was predicted with respect to the base configuration. Generally speaking, predictions allow to state that independent circuits have better performances than the independent boreholes for the parameters specified herein. The main impact of the independent circuits with Type C configurations would be to reduce by half the length of the boreholes, keeping fluid temperatures close to 0°C at the lowest during the first year, but increasing with time.

Even though the independent circuits configuration showed better energy savings over the other configurations, the mitigated loop configuration still requires less material (capital cost) than the others, which would be the most economical option in hybrid geothermal/solar systems only. The independent boreholes configurations required more BHE (hence capital cost) to achieve the performances, which would make them the least interesting solutions. Further study should be carried out on the control strategy of hybrid geothermal systems and in other applications such as waste heat.

CONCLUSION

Geothermal heat pump systems are getting more and more complex and the evaluation of their behavior requires simulation tools to be expanded constantly. Since nearly all available geothermal mathematical models consider only one inlet condition for all of the U-tubes and boreholes of a borefield, in this thesis, a model to simulate geothermal boreholes and borefields where the inlet conditions can be defined independently is presented.

Objectives and methodology

The overall objective of this research was to improve the efficiency of shared and hybrid geothermal systems by segregating heat transfer sources. This involved:

- developing a semi-analytical model that considers independent inlet conditions for each borehole of a borefield;
- and developing a model that considers independent circuits of double U-tubes in each borehole.

The ground model uses a 2D diffusion CVFDM approach coupled to analytical borehole models for the fluid-to-ground heat transfer. A model coupling independent circuits in double U-tubes borehole is also presented.

Summary of results

The ground model used a steady state shape factor to couple the circular borehole to the square control volume of the ground in the source term control volumes. The shape factor influence has been evaluated with Richardson's extrapolation scheme. With a 0.15 m borehole diameter, a 0.35 m control volume had a -0.0033°C difference with the Richardson converged solution and 0.20 m control volumes had converged. A single U-tube fluid-to-ground analytical model is developed based on delta thermal resistances. The proposed analytical single U-tube model coupled to the numerical ground model showed good

agreement with the well-known DST model with constant and variable inlet conditions. A double U-tube model where the angle and distance between the legs, the direction of the flow, mass flowrate and fluid specific heat can be defined independently for each U-tube is also developed.

In a first application, the double U-tube model showed an improvement of 5.5% between the U-tubes in symmetric configuration compared to putting the legs of U-tubes in contact. This improvement can reach 15% in certain configurations.

Detailed hourly simulations coupling residential buildings heat pumps to solar collectors to the same borefield are compared to a classic configuration with only residential heat pumps. The configurations include:

- mitigated loop;
- independent boreholes in a central configuration;
- independent boreholes in a staggered configuration;
- independent circuits in symmetric configuration;
- independent circuits non-symmetric configuration.

Results show that the energy balance on the ground can be largely dependent on the control strategy used with the solar collectors. For the 3x4 borefields, the No Sum control strategy allowed solar gains between 16 819 kWh and 17 349 kWh. The Type C leg spacing had an advantage over Type A. The mitigated loop is the exception, with the No Sum control strategy saving 2.4% energy compared to base case, versus 1.0% for the All Year. For the 24 BHE borefields, the independent circuits had an advantage over the independent boreholes for the solar gains. The central configuration involving 4.5 m spacing between legs gained 13.3% less solar energy than the non-symmetric Type C All Year configuration.

The fluid temperatures were more interesting for the independent circuits than for the independent boreholes and the mitigated loop. For the 300 m boreholes, the minimum fluid temperature was between 2.5°C and 4.8°C, allowing a reduction of boreholes length by half

(150 m) the critical threshold of reach 0°C. The independent boreholes all had minimum fluid temperatures comparable to the base case since 12 boreholes were coupled to the 12 residential heat pumps, as in both cases. The maximum fluid temperature reached 36.2°C and 32.9°C for the mitigated loop with Type C and non-symmetric Type A configurations, respectively, approaching the heat pump upper temperature limit of 43.3°C that could be reached within a few years.

The energy consumption predictions of the heat pumps were the best with independent circuits in Type C configurations, having the symmetric vs non-symmetric and All Year vs No Sum parameters with no important influence. A saving of 6.4% has been found with both symmetric Type C All Year and non-symmetric Type C No Sum 3x4 configurations. As for the 24 BHE configurations, the independent boreholes best result was 2.5% savings for the central 4.5 m configuration. The non-symmetric Type C All Year gave 9.3% savings over base case.

Overall recommendations

In the long run, the All Year control strategy makes the ground temperature increase at a much higher rate than the No Sum counterpart. The later allows near balanced loads, and this should result in more stable heat pumps performances. Indeed, the higher the ground temperature, the better the performances in heating mode, but the cooling mode would then suffer all summer long as demonstrated in the non-symmetric Type C cases.

As a final recommendation for hybrid geothermal configurations such as those investigated herein, independent circuits combined with the No Sum control strategy and Type C leg spacing is be the best solution. This should allow reducing by half the length of the boreholes, thus reducing the initial investment of the system related to the drilling depth and material involved. The independent boreholes configuration was found to provide no advantages over the other ones; the best performances were merely as good as those of the

classic mitigated loop with Type C and No Sum strategy, but it required twice as many boreholes.

Another advantage of the proposed model could be found in applications where the fluid of two systems cannot be mixed but that was not investigated. More potential applications should be investigated, including waste heat recovery and industrial processes. Further work could also be done on borefield configurations and control strategies.

APPENDIX I
INDEPENDENT CIRCUIT MODEL COEFFICIENTS

The dimensionless fluid temperature profiles as a function of borehole depth for variable mass flow rates in both legs are presented in this appendix for the configuration 1-3, 2-4 with different thermal capacitances.

$$\gamma^2 = \frac{X+Y}{2} \quad , \eta^2 = \frac{X-Y}{2}$$

$$X = (a^2 - c^2)(\alpha^2 + 1) + 2\alpha(b^2 - d^2)$$

$$Y = \sqrt{((a^2 - c^2)(\alpha^2 + 1) + 2\alpha(b^2 - d^2))^2 - 4\alpha^2((a^2 - b^2)^2 + (c^2 - d^2)^2 - 2(a^2 + b^2)(c^2 + d^2) + 8abcd)}$$

The values of the G coefficients are given by:

$$h_1 = a^2 + b^2 + c^2 - d^2$$

$$h_2 = a^2 + b^2 - c^2 + d^2$$

$$h_3 = a^2 - b^2 + c^2 + d^2$$

$$h_4 = -a^2 + b^2 + c^2 + d^2$$

$$f_1 = a + c - b - d$$

$$G12 = (1-\theta_b)\left(\gamma^2 + \alpha^2\left(c^2 - a^2\right) + \alpha\left(d^2 - b^2\right)\right) - \theta_b\left(\alpha(b-d)(a+c) + (a-c)(b+d)\right) + (cd - ab)(1+\alpha)$$

$$G12' = 0 \quad , \quad G12'' = (bc - ad)(\alpha - 1)$$

$$G13 = \alpha^2\left(-a\,h_4 + 2bcd\right) + \alpha\left(b\,h_3 - 2acd\right) + \gamma^2\left(b - a - e\right) + f_1 e\alpha\left(\alpha(a-c) - (b-d)\right)$$

$$G13' = -c\gamma^2 + \alpha^2(c\,h_2 - 2abd) \quad , \quad G13'' = -d\gamma^2 + \alpha(d\,h_1 - 2abc)$$

$$G14 = -(1-\theta_b)\left(\eta^2 + \alpha^2\left(c^2 - a^2\right) + \alpha\left(d^2 - b^2\right)\right) + \theta_b\left(\alpha(b-d)(a+c) + (a-c)(b+d)\right) - (cd - ab)(1+\alpha)$$

$$G14' = 0 \quad , \quad G14'' = (bc - ad)(1 - \alpha)$$

$$G15 = \alpha^2 (a\,h_4 - 2bcd) - \alpha(b\,h_3 - 2acd) - \eta^2 (b - a - e) - f_1 e\alpha\big(\alpha(a-c) - (b-d)\big)$$

$$G15' = c\eta^2 - \alpha^2 (c h_2 - 2abd) \quad , \qquad G15'' = d\eta^2 - \alpha(d h_1 - 2abc)$$

$$G22 = -(1+\theta_b)\gamma^2 + \left(a^2 - c^2\right) + \alpha^2 (ab - cd) + \alpha\left(ab - cd + b^2 - d^2\right) + \theta_b \left(a^2 - c^2 - \alpha^2 (a-c)(b+d) - \alpha f_1 (b-d)\right)$$

$$G22' = \alpha\big(bc - ad\big)\big(1-\alpha\big) \quad , \qquad G22'' = 0$$

$$G23 = -\alpha^2 (b\,h_3 - 2acd) + \alpha(a\,h_4 - 2bcd) - \alpha\gamma^2 (b - a + e) - f_1 e\,\alpha\big(\alpha(b-d) - (a-c)\big)$$

$$G23' = -\alpha d\gamma^2 + \alpha^2 (d\,h_1 - 2abc) \quad , \qquad G23'' = -\alpha c\gamma^2 + \alpha(c\,h_2 - 2abd)$$

$$G24 = (1+\theta_b)\eta^2 - (a^2 - c^2) - \alpha^2 (ab - cd) - \alpha(ab - cd + b^2 - d^2) - \theta_b \left(a^2 - c^2 - \alpha^2 (a-c)(b+d) - \alpha f_1 (b-d)\right)$$

$$G24' = \alpha\big(bc - ad\big)\big(\alpha - 1\big) \quad , \qquad G24'' = 0$$

$$G25 = \alpha^2 (b\,h_3 - 2acd) - \alpha(a\,h_4 - 2bcd) + \alpha\eta^2 (b - a + e) + f_1 e\,\alpha\big(\alpha(b-d) - (a-c)\big)$$

$$G25' = \alpha\, d\eta^2 - \alpha^2 (d\,h_1 - 2abc) \quad , \qquad G25'' = \alpha c\eta^2 - \alpha(c\,h_2 - 2abd)$$

$$G32 = -\theta_b \gamma^2 + (1-\alpha)(cb - ad) + \theta_b \left(\alpha^2 (a^2 - c^2) - (a-c)(b+d) - \alpha f_1 (b-d)\right)$$

$$G32' = \gamma^2 - \alpha^2 (a^2 - c^2) - \alpha(b^2 - d^2) \quad , \qquad G32'' = (1+\alpha)(a\,b - c\,d)$$

$$G33 = -\alpha^2 (c\,h_2 - 2abd) + \alpha(d\,h_1 - 2abc) + \gamma^2 (c - d + e) - f_1 e\,\alpha\big(\alpha(a-c) - (b-d)\big)$$

$$G33' = a\,\gamma^2 + \alpha^2 (a\,h_4 - 2bcd) \quad , \qquad G33'' = b\,\gamma^2 + \alpha(b\,h_3 - 2acd)$$

$$G34 = \theta_b \eta^2 - (1-\alpha)(cb - ad) - \theta_b \left(\alpha^2 (a^2 - c^2) - (a-c)(b+d) - \alpha f_1 (b-d)\right)$$

$$G34' = -\eta^2 + \alpha^2 (a^2 - c^2) + \alpha(b^2 - d^2) \quad , \qquad G34''' = -(1+\alpha)(a\,b - c\,d)$$

$$G35 = \alpha^2 (c\,h_2 - 2abd) - \alpha(d\,h_1 - 2abc) - \eta^2 (c - d + e) + f_1 e\,\alpha\big(\alpha(a-c) - (b-d)\big)$$

$$G35' = -a\eta^2 - \alpha^2 (a\,h_4 - 2bcd) \quad , \qquad G35'' = -b\eta^2 - \alpha(b\,h_3 - 2acd)$$

$$G42 = -\theta_b \gamma^2 + \alpha(1-\alpha)(cb - ad) + \theta_b \left((a^2 - c^2) - \alpha^2 (a-c)(b+d) - \alpha f_1 (b-d)\right)$$

$$G42' = \alpha(\alpha+1)\,(a\,b - c\,d) \quad , \qquad G42'' = \gamma^2 - (a^2 - c^2) - \alpha(b^2 - d^2)$$

$$G43 = -\alpha^2 (d\,h_1 - 2abc) + \alpha(c\,h_2 - 2abd) - \alpha\gamma^2 (c - d - e) + f_1 e\,\alpha\big(\alpha(b-d) - (a-c)\big)$$

$$G43' = \alpha b\,\gamma^2 + \alpha^2 (b\,h_3 - 2acd) \quad , \quad G43'' = \alpha a\,\gamma^2 + \alpha (a\,h_4 - 2bcd)$$

$$G44 = \theta_b \eta^2 - \alpha(1-\alpha)(cb - ad) - \theta_b \left((a^2 - c^2) - \alpha^2 (a-c)(b+d) - \alpha f_1 (b-d)\right)$$

$$G44' = -\alpha(\alpha+1)\,(a\,b - c\,d) \quad , \quad G44'' = -\eta^2 + (a^2 - c^2) + \alpha(b^2 - d^2)$$

$$G45 = \alpha^2 (d\,h_1 - 2abc) - \alpha (c\,h_2 - 2abd) + \alpha \eta^2 (c - d - e) - f_1 e \alpha \left(\alpha (b-d) - (a-c)\right)$$

$$G45' = -\alpha b \eta^2 - \alpha^2 (b\,h_3 - 2acd) \quad , \quad G45'' = -\alpha a \eta^2 - \alpha (a\,h_4 - 2bcd)$$

$$\theta_3(0) = \frac{A_{22} C_1 - A_{12} C_2}{\Delta} \quad , \quad \theta_4(0) = \frac{A_{22} C_1 - A_{12} C_2}{\Delta}$$

$$\Delta = A_{11} A_{22} - A_{12} A_{21}$$

$$A_{11} = (G_{12}' - G_{32}')\cosh(\gamma) + (G_{13}' - G_{33}')\frac{\sinh(\gamma)}{\gamma} + (G_{14}' - G_{34}')\cosh(\eta) + (G_{15}' - G_{35}')\frac{\sinh(\eta)}{\eta}$$

$$A_{12} = (G_{12}'' - G_{32}'')\cosh(\gamma) + (G_{13}'' - G_{33}'')\frac{\sinh(\gamma)}{\gamma} + (G_{14}'' - G_{34}'')\cosh(\eta) + (G_{15}'' - G_{35}'')\frac{\sinh(\eta)}{\eta}$$

$$A_{21} = (G_{22}' - G_{42}')\cosh(\gamma) + (G_{23}' - G_{43}')\frac{\sinh(\gamma)}{\gamma} + (G_{24}' - G_{44}')\cosh(\eta) + (G_{25}' - G_{45}')\frac{\sinh(\eta)}{\eta}$$

$$A_{22} = (G_{22}'' - G_{42}'')\cosh(\gamma) + (G_{23}'' - G_{43}'')\frac{\sinh(\gamma)}{\gamma} + (G_{24}'' - G_{44}'')\cosh(\eta) + (G_{25}'' - G_{45}'')\frac{\sinh(\eta)}{\eta}$$

$$C_1 = -\left[(G_{12} - G_{32})\cosh(\gamma) + (G_{13} - G_{33})\frac{\sinh(\gamma)}{\gamma} + (G_{14} - G_{34})\cosh(\eta) + (G_{15} - G_{35})\frac{\sinh(\eta)}{\eta}\right]$$

$$C_2 = -\left[(G_{22} - G_{42})\cosh(\gamma) + (G_{23} - G_{43})\frac{\sinh(\gamma)}{\gamma} + (G_{24} - G_{44})\cosh(\eta) + (G_{25} - G_{45})\frac{\sinh(\eta)}{\eta}\right]$$

APPENDIX II

RESIDENTIAL/SOLAR APPLICATIONS RESULTS

The heat balances of the heat pumps in heating mode are:

Heating

BHE	Configurations	Type	Ctrl	Heat to air	Heat to water	Compressor	Balance
3x4	Base	C	-	37813	-29042	8792	-21
3x4	Mitigated	C	All year	37541	-29362	8198	-78
3x4	Mitigated	C	No sum	37627	-29164	8484	-20
3x4	Non-symmetric	A	All year	37473	-29348	8145	-19
3x4	Non-symmetric	C	All year	37388	-29366	8041	-19
3x4	Non-symmetric	C	No sum	37450	-29300	8169	-19
3x4	Symmetric	A	No sum	37506	-29262	8264	-20
3x4	Symmetric	C	No sum	37461	-29285	8195	-19
3x4	Symmetric 150m	C	All year	37572	-29274	8318	-20
3x4	Symmetric	C	All year	37407	-29359	8067	-19

Heating

BHE	Configurations	Type	Ctrl	Heat to air	Heat to water	Compressor	Balance
4x6	Central 4.5m	C	All year	37623	-29231	8412	-20
4x6	Central 6m	C	All year	37652	-29177	8495	-20
2x12	Ind staggered 3m	C	All year	37583	-29270	8333	-20
2x12	Ind staggered 4.5m	C	All year	37610	-29229	8401	-20
2x12	Ind staggered 6m	C	All year	37625	-29184	8461	-20
4x6	Non-symmetric	A	All year	37334	-29401	7951	-19
4x6	Non-symmetric	C	All year	37325	-29471	7873	-18

The heat balances of the heat pumps in cooling mode are:

Cooling

BHE	Configurations	Type	Ctrl	Heat to air	Heat to water	Compressor	Balance
3x4	Base	C	-	-12323	14408	2091	7
3x4	Mitigated	C	All year	-12432	14999	2574	28
3x4	Mitigated	C	No sum	-12338	14468	2137	7
3x4	Non-symmetric	A	All year	-12362	14711	2356	7
3x4	Non-symmetric	C	All year	-12335	14489	2160	7
3x4	Non-symmetric	C	No sum	-12280	14294	2021	7
3x4	Symmetric	A	No sum	-12324	14388	2070	7
3x4	Symmetric	C	No sum	-12283	14303	2026	7
3x4	Symmetric 150m	C	All year	-12416	14766	2357	7
3x4	Symmetric	C	All year	-12321	14431	2116	7

Cooling

BHE	Configurations	Type	Ctrl	Heat to air	Heat to water	Compressor	Balance
4x6	Central 4.5m	C	All year	-12369	14568	2205	7
4x6	Central 6m	C	All year	-12367	14532	2171	7
2x12	Ind staggered 3m	C	All year	-12407	14690	2291	7
2x12	Ind staggered 4.5m	C	All year	-12373	14582	2216	7
2x12	Ind staggered 6m	C	All year	-12367	14544	2184	7
4x6	Non-symmetric	A	All year	-12308	14412	2111	7
4x6	Non-symmetric	C	All year	-12252	14248	2003	7

The total heat balances of the heat pumps are:

BHE	Configurations	Type	Ctrl	Total Heat to air	Heat to water	Compressor	Balance
3x4	Base	C	-	25490	-14634	10884	-15
3x4	Mitigated	C	All year	25109	-14363	10772	-49
3x4	Mitigated	C	No sum	25289	-14695	10621	-14
3x4	Non-symmetric	A	All year	25111	-14636	10501	-12
3x4	Non-symmetric	C	All year	25052	-14877	10201	-12
3x4	Non-symmetric	C	No sum	25170	-15006	10190	-13
3x4	Symmetric	A	No sum	25182	-14874	10334	-13
3x4	Symmetric	C	No sum	25179	-14983	10222	-13
3x4	Symmetric 150m	C	All year	25156	-14508	10675	-13
3x4	Symmetric	C	All year	25086	-14927	10184	-12

BHE	Configurations	Type	Ctrl	Total Heat to air	Heat to water	Compressor	Balance
4x6	Central 4.5m	C	All year	25254	-14663	10618	-13
4x6	Central 6m	C	All year	25285	-14645	10666	-14
2x12	Ind staggered 3m	C	All year	25176	-14580	10623	-13
2x12	Ind staggered 4.5m	C	All year	25237	-14647	10617	-13
2x12	Ind staggered 6m	C	All year	25258	-14640	10645	-13
4x6	Non-symmetric	A	All year	25026	-14989	10062	-12
4x6	Non-symmetric	C	All year	25073	-15222	9876	-12

The ground heat balances of the configurations are:

Ground

BHE	Configurations	Type	Ctrl	Heat pump	Collectors	Balance
3x4	Base	C	-	-14634	0	-14634
3x4	Mitigated	C	All year	-14363	54607	40244
3x4	Mitigated	C	No sum	-14695	17349	2654
3x4	Non-symmetric	A	All year	-14636	55835	41199
3x4	Non-symmetric	C	All year	-14877	59808	44931
3x4	Non-symmetric	C	No sum	-15006	17274	2268
3x4	Symmetric	A	No sum	-14874	16819	1945
3x4	Symmetric	C	No sum	-14983	17312	2329
3x4	Symmetric 150m	C	All year	-14508	54799	40292
3x4	Symmetric	C	All year	-14927	59996	45068

Ground

BHE	Configurations	Type	Ctrl	Heat pump	Collectors	Balance
4x6	Central 4.5m	C	All year	-14663	51781	37118
4x6	Central 6m	C	All year	-14645	54146	39500
2x12	Ind staggered 3m	C	All year	-14580	54634	40054
2x12	Ind staggered 4.5m	C	All year	-14647	56603	41956
2x12	Ind staggered 6m	C	All year	-14640	57467	42827
4x6	Non-symmetric	A	All year	-14989	58528	43539
4x6	Non-symmetric	C	All year	-15222	59709	44486

The fluid temperatures of the configurations are:

BHE	Configurations	Type	Ctrl	min fluid T°	Max fluid T°	Mean fluid T° 1st year	Mean fluid T° 3rd year
3x4	Base	C	-	-0.7	21.7	8.9	8.0
3x4	Mitigated	C	All year	0.4	36.2	13.0	14.9
3x4	Mitigated	C	No sum	0.4	22.7	10.2	10.3
3x4	Non-symmetric	A	All year	2.5	32.9	12.0	12.8
3x4	Non-symmetric	C	All year	4.8	22.2	11.2	12.0
3x4	Non-symmetric	C	No sum	4.8	16.7	10.0	10.0
3x4	Symmetric	A	No sum	2.4	20.2	10.2	10.2
3x4	Symmetric	C	All year	4.8	19.8	10.7	11.6
3x4	Symmetric 150m	C	All year	-0.2	29.0	11.3	12.8
3x4	Symmetric	C	No sum	4.8	16.7	9.9	9.9

BHE	Configurations	Type	Ctrl	min fluid T°	Max fluid T°	Mean fluid T° 1st year	Mean fluid T° 3rd year
4x6	Central 4.5m	C	All year	-0.1	25.2	9.9	11.5
4x6	Central 6m	C	All year	0.1	24.1	9.5	10.7
2x12	Ind staggered 3m	C	All year	0.0	27.0	10.8	12.6
2x12	Ind staggered 4.5m	C	All year	0.1	25.3	10.1	11.6
2x12	Ind staggered 6m	C	All year	0.1	24.1	9.8	10.9
4x6	Non-symmetric	A	All year	6.0	22.1	11.1	11.8
4x6	Non-symmetric	C	All year	7.8	15.9	10.6	11.3

The energy consumptions of the heat pumps are:

BHE	Configurations	Type	Ctrl	Energy HP	Savings	%
3x4	Base	C	-	10884	-	0.0%
3x4	Mitigated	C	All year	10771	113	1.0%
3x4	Mitigated	C	No sum	10621	263	2.4%
3x4	Non-symmetric	A	All year	10501	383	3.5%
3x4	Non-symmetric	C	All year	10201	683	6.3%
3x4	Non-symmetric	C	No sum	10190	694	6.4%
3x4	Symmetric	A	No sum	10334	550	5.1%
3x4	Symmetric	C	All year	10184	700	6.4%
3x4	Symmetric 150m	C	All year	10675	209	1.9%
3x4	Symmetric	C	No sum	10222	662	6.1%

BHE	Configurations	Type	Ctrl	Energy HP	Savings	%
4x6	Central 4.5m	C	All year	10614	270	2.5%
4x6	Central 6m	C	All year	10670	214	2.0%
2x12	Ind staggered 3m	C	All year	10622	262	2.4%
2x12	Ind staggered 4.5m	C	All year	10619	265	2.4%
2x12	Ind staggered 6m	C	All year	10651	233	2.1%
4x6	Non-symmetric	A	All year	10066	818	7.5%
4x6	Non-symmetric	C	All year	9877	1007	9.3%

LIST OF REFERENCES

Al-Khoury, R. 2011. « A Spectral Model for Shallow Geothermal Systems ». *International Journal of Numerical Methods for Heat & Fluid Flow,* vol. 22, n° 1, p. 4-4.

ANSI/ARI/ASHRAE/ISO. 2005. « Water-source Heat Pumps—Testing and Rating for Performance—Part 1: Water-to-Air and Brine-to-Air Heat Pumps ».

ASHRAE. 2007. « HVAC Applications ». *American Society of Heating, Refrigerating, and Air Conditioning Engineers, Inc. Atlanta, GA*.

ASHRAE. 2008. *ASHRAE handbook : heating, ventilating, and air-conditioning systems and equipment*. Atlanta, Ga.: ASHRAE.

Badache, Messaoud, Parham Eslami-Nejad, Mohamed Ouzzane, Zine Aidoun et Louis Lamarche. 2016. « A new modeling approach for improved ground temperature profile determination ». *Renewable Energy,* vol. 85, p. 436-444.

Bauer, D., W. Heidemann, H. Müller-Steinhagen et HJG Diersch. 2009. « Modelling and simulation of groundwater influence on borehole thermal energy stores ». In.

Bauer, D., W. Heidemann, H. Müller-Steinhagen et H.J.G. Diersch. 2011. « Thermal resistance and capacity models for borehole heat exchangers ». *International Journal of Energy Research,* vol. 35, n° 4, p. 312-320.

Bell, A.A. 2007. *HVAC equations, data, and rules of thumb*. McGraw-Hill.

Belzile, Patrick, Louis Lamarche et Daniel R Rousse. 2016a. « Geothermal heat exchange in boreholes with independent sources ». *Applied Thermal Engineering*.

Belzile, Patrick, Louis Lamarche et Daniel R Rousse. 2016b. « Semi-analytical model for geothermal borefields with independent inlet conditions ». *Geothermics,* vol. 60, p. 144-155.

Bennet, Johan, Johan Claesson et Göran Hellström. 1987. *Multipole method to compute the conductive heat flows to and between pipes in a composite cylinder*. Department of Building Technology and [Department of] Mathematical Physics, Lund Institute of Technology.

Bernier, M.A., P. Pinel, R. Labib et R. Paillot. 2004. « A multiple load aggregation algorithm for annual hourly simulations of GCHP systems ». *Hvac&R Research,* vol. 10, n° 4, p. 471-487.

Bernier, Michel A. 2006. « Closed-loop ground-coupled heat pump systems ». *Ashrae Journal,* vol. 48, n° 9, p. 12-25.

Bernier, Michel A, Antoine Chahla et Patrice Pinel. 2008. « Long-Term Ground-Temperature Changes in Geo-Exchange Systems ». *ASHRAE Transactions,* vol. 114, n° 2.

Blomberg, T., J. Claesson, P. Eskilson, G. Hellström et B. Sanner. 2008. *Earth Energy Designer*. < http://www.buildingphysics.com/index-filer/Page1099.htm >.

Carslaw, HS, et JC Jaeger. 1959. « Conduction of Heat in Solids (paperback,) ».

Chapuis, S. 2008. « Étude préliminaire sur le stockage solaire saisonnier par puits géothermiques ». In., p. 14-23.

Chiasson, A.D. 1999. « Advances in modeling of ground-source heat pump systems ». Oklahoma State University.

Chiasson, A.D., et C. Yavuzturk. 2003. « Assessment of the viability of hybrid geothermal heat pump systems with solar thermal collectors ». *ASHRAE transactions,* vol. 109, n° 2, p. 487-500.

Chiasson, AD, C Yavuzturk et WJ Talbert. 2004. « Design of school building HVAC retrofit with hybrid geothermal heat-pump system ». *Journal of architectural engineering,* vol. 10, n° 3, p. 103-111.

Cimmino, Massimo, et Michel Bernier. 2014. « A semi-analytical method to generate g-functions for geothermal bore fields ». *International Journal of Heat and Mass Transfer,* vol. 70, p. 641-650.

Claesson, J., et P. Eskilson. 1988. « Conductive heat extraction to a deep borehole: Thermal Analyses and Dimensioning Rules ». *Energy,* vol. 13, n° 6, p. 509-527.

Claesson, J., et G. Hellström. 2011. « Multipole method to calculate borehole thermal resistances in a borehole heat exchanger ». *Hvac&R Research,* vol. 17, n° 6, p. 895-911.

Claesson, J., et S. Javed. 2011. « An Analytical Method to Calculate Borehole Fluid Temperatures for Time-scales from Minutes to Decades ». *ASHRAE Transactions.,* vol. 117, p. 279-288.

Curtis, R, J Lund, B Sanner, L Rybach et G Hellström. 2005. « Ground source heat pumps–geothermal energy for anyone, anywhere: current worldwide activity ». In *Proceedings World Geothermal Congress, Antalya, Turkey*. p. 24-29.

De Carli, M., M. Tonon, A. Zarrella et R. Zecchin. 2010. « A computational capacity resistance model (CaRM) for vertical ground-coupled heat exchangers ». *Renewable Energy,* vol. 35, n° 7, p. 1537-1550.

Dinçer, Ibrahim, et Marc Rosen. 2011. *Thermal energy storage : systems and applications*. Hoboken, N.J.: Wiley.

EnerLogic, et James J. Hirsch & Associates. 2009. *DOE2*. < http://doe2.com/ >.

Eskilson, P. 1987. *Thermal analysis of heat extraction boreholes*. Department of Mathematical Physics, University of Lund.

Eskilson, Per, et Johan Claesson. 1988. « Simulation model for thermally interacting heat extraction boreholes ». *Numerical Heat Transfer,* vol. 13, n° 2, p. 149-165.

Eslami-Nejad, P., et M. Bernier. 2011a. « Heat Transfer in Double U-Tube Boreholes With Two Independent Circuits ». *Journal of Heat Transfer,* vol. 133, p. 082801.

Eslami-Nejad, Parham, et Michel Bernier. 2011b. « Coupling of geothermal heat pumps with thermal solar collectors using double U-tube boreholes with two independent circuits ». *Applied Thermal Engineering,* vol. 31, n° 14, p. 3066-3077.

Florides, G., et S. Kalogirou. 2007. « Ground heat exchangers--A review of systems, models and applications ». *Renewable Energy,* vol. 32, n° 15, p. 2461-2478.

Fossa, M. 2011. « The temperature penalty approach to the design of borehole heat exchangers for heat pump applications ». *Energy and Buildings*.

Gentry, J.E., J.D. Spitler, D.E. Fisher et X. Xu. 2006. « Simulation of hybrid ground source heat pump systems and experimental validation ». In. Citeseer.

Girard, Aymeric, Eulalia Jadraque Gago, Tariq Muneer et Gustavo Caceres. 2015. « Higher ground source heat pump COP in a residential building through the use of solar thermal collectors ». *Renewable Energy,* vol. 80, p. 26-39.

Goldstein, Barry, Gerardo Hiriart, Ruggero Bertani, Christopher Bromley, Luis Gutiérrez-Negrín, Ernst Huenges, Hirofumi Muraoka, Arni Ragnarsson, Jefferson Tester et Vladimir Zui. 2011. « Geothermal Energy ». In *IPCC Special Report on Renewable Energy Sources and Climate Change Mitigation*, sous la dir. de Edenhofer, Ottmar, Rafael Pichs-Madruga, Youba Sokona, Kristin Seyboth, Patrick Matschoss, Susanne Kadner, Timm Zwickel, Patrick Eickemeier, Gerrit Hansen, Steffen Schlömer et Christoph von Stechow. Cambridge, United Kingdom and New York, NY, USA: Cambridge University Press.

Hackel, S., et A. Pertzborn. 2011a. « Effective Design and Operation of Hybrid Ground-Source Heat Pumps; Three Case Studies ». *Energy and Buildings*.

Hackel, Scott, et Amanda Pertzborn. 2011b. « Effective design and operation of hybrid ground-source heat pumps: Three case studies ». *Energy and Buildings,* vol. 43, n° 12, p. 3497-3504.

Hackel, Scott, et Amanda Pertzborn. 2011c. *Hybrid Ground-Source Heat Pump Installations: Experiences, Improvements, and Tools*. Energy Center of Wisconsin.

He, M., S. Rees et L. Shao. 2009. « Simulation of a domestic ground source heat pump system using a transient numerical borehole heat exchanger model ». In.

Hellström, G. 1989. « Duct ground heat storage model, Manual for Computer Code ». *Department of Mathematical Physics, University of Lund, Sweden*.

Hellström, G. 1991. *Ground heat storage: thermal analyses of duct storage systems*. vol. 1. University of Lund. Department of Mathematical Physics.

Hellström, G., et B. Sanner. 2001. « PC-programs and modeling for borehole heat exchanger design ». *Proc. IGD 2001 Bad Urach, Supplement*.

Hellström, G., B. Sanner, M. Klugescheid, T. Gonka et S. Mårtensson. 1997. « Experiences with the borehole heat exchanger software EED ». *Proc. MEGASTOCK,* vol. 97, p. 247-252.

Hern, S.A. 2004. « Design of an experimental facility for hybrid ground source heat pump systems ». Oklahoma State University.

Hwang, S., R. Ooka et Y. Nam. 2010. « Evaluation of estimation method of ground properties for the ground source heat pump system ». *Renewable Energy,* vol. 35, n° 9, p. 2123-2130.

Incropera, F.P., et D.P. DeWitt. 2007. *Fundamentals of heat and mass transfer*. John Wiley.

Ingersoll, L.R. 1954. *Heat conduction: with engineering, geological, and other applications*. University of Wisconsin Press.

Ingersoll, LR, et HJ Plass. 1948. « Theory of the ground pipe heat source for the heat pump ». *ASHVE transactions,* vol. 47, p. 339-348.

Kavanaugh, S.P. 1985. « Simulation and experimental verification of vertical ground-coupled heat pump systems ». Medium: X; Size: Pages: 192 p.

Kavanaugh, S.P. 2010. *Ground Source Heat Pump System Designer.* < http://www.geokiss.com/software/Ver50Inst2-20.pdf >.

Kavanaugh, Stephen P., Kevin D. Rafferty, Refrigerating American Society of Heating et Engineers Air-Conditioning. 1997. *Ground-source heat pumps : design of geothermal systems for commercial and institutional buildings*. Atlanta: American Society of Heating, Refrigerating and Air-Conditioning Engineers.

Kim, Wonseok, Jongmin Choi et Honghyun Cho. 2013. « Performance analysis of hybrid solar-geothermal CO2 heat pump system for residential heating ». *Renewable Energy,* vol. 50, n° 0, p. 596-604.

Koohi-Fayegh, S., et M. A. Rosen. 2014. « An analytical approach to evaluating the effect of thermal interaction of geothermal heat exchangers on ground heat pump efficiency ». *Energy Conversion and Management,* vol. 78, n° 0, p. 184-192.

Koohi-Fayegh, S., et M.A. Rosen. 2012. « Examination of thermal interaction of multiple vertical ground heat exchangers ». *Applied Energy*.

Kummert, Michaël, et Michel Bernier. 2008. « Sub-hourly simulation of residential ground coupled heat pump systems ». *Building Services Engineering Research and Technology,* vol. 29, n° 1, p. 27-44.

Kusuda, T., P.R. Achenbach et United States. Dept. of the Army. Office of Civil Defense. 1965. *Earth temperature and thermal diffusivity at selected stations in the United States*. National Bureau of Standards.

Lamarche, L. 2009. « A fast algorithm for the hourly simulations of ground-source heat pumps using arbitrary response factors ». *Renewable Energy,* vol. 34, n° 10, p. 2252-2258.

Lamarche, L., et B. Beauchamp. 2007a. « A new contribution to the finite line-source model for geothermal boreholes ». *Energy and Buildings,* vol. 39, n° 2, p. 188-198.

Lamarche, L., et B. Beauchamp. 2007b. « New solutions for the short-time analysis of geothermal vertical boreholes ». *International Journal of Heat and Mass Transfer,* vol. 50, n° 7-8, p. 1408-1419.

Lamarche, L., S. Kajl et B. Beauchamp. 2010. « A review of methods to evaluate borehole thermal resistances in geothermal heat-pump systems ». *Geothermics,* vol. 39, n° 2, p. 187-200.

Lamarche, Louis. 2013. « Short-term behavior of classical analytic solutions for the design of ground-source heat pumps ». *Renewable Energy,* vol. 57, p. 171-180.

Lazzarotto, Alberto. 2014. « A network-based methodology for the simulation of borehole heat storage systems ». *Renewable energy,* vol. 62, p. 265-275.

Lee, CK, et HN Lam. 2007. « Effects of groundwater flow direction on performance of ground heat exchanger borefield in geothermal heat pump systems using 3-D finite difference method ». In., p. 337-341.

Li, Z., et M. Zheng. 2009. « Development of a numerical model for the simulation of vertical U-tube ground heat exchangers ». *Applied Thermal Engineering,* vol. 29, n° 5-6, p. 920-924.

Lubis, L.I., M. Kanoglu, I. Dincer et M.A. Rosen. 2011. « Thermodynamic analysis of a hybrid geothermal heat pump system ». *Geothermics*.

Man, Y., H. Yang, N. Diao, J. Liu et Z. Fang. 2010. « A new model and analytical solutions for borehole and pile ground heat exchangers ». *International Journal of Heat and Mass Transfer,* vol. 53, n° 13, p. 2593-2601.

Marcotte, D., et P. Pasquier. 2008. « On the estimation of thermal resistance in borehole thermal conductivity test ». *Renewable Energy,* vol. 33, n° 11, p. 2407-2415.

Marcotte, D., P. Pasquier, F. Sheriff et M. Bernier. 2010. « The importance of axial effects for borehole design of geothermal heat-pump systems ». *Renewable Energy,* vol. 35, n° 4, p. 763-770.

Mihalakakou, G., M. Santamouris, JO Lewis et DN Asimakopoulos. 1997. « On the application of the energy balance equation to predict ground temperature profiles ». *Solar Energy,* vol. 60, n° 3-4, p. 181-190.

Miyara, A. 2011. « Thermal performance investigation of several types of vertical ground heat exchangers with different operation mode ». *Applied Thermal Engineering*.

Molina-Giraldo, N., P. Blum, K. Zhu, P. Bayer et Z. Fang. 2011. « A moving finite line source model to simulate borehole heat exchangers with groundwater advection ». *International Journal of Thermal Sciences*.

Morrison, A. 2000. « GS2000 Software TM ». In.

Nathenson, Manuel, et Marianne Guffanti. 1988. « Geothermal Gradients in the Conterminous United States ». *J. Geophys. Res.,* vol. 93, n° B6, p. 6437-6450.

Niibori, Y., Y. Iwata, S. Ichinose et G. Fukaya. 2005. « Design of the BHP system considering the heat transport of groundwater flow ». In.

Nordell, Bo, et Anna-Karin Ahlström. 2007. « Freezing problems in borehole heat exchangers ». In *Thermal Energy Storage for Sustainable Energy Consumption*. p. 193-203. Springer.

Pahud, D. 1999. « PILESIM-LASEN ». *Simulation Tool for Heating/Cooling Systems with Heat Exchanger Piles or Borehole Heat Exchangers. User Manual. Swiss Federal Office of Energy, Switzerland*.

Pahud, D., A. Fromentin et JC Hadorn. 1996. « The duct ground heat storage model (DST) for TRNSYS used for the simulation of heat exchanger piles ». *DGC-LASEN, Lausanne*.

Pahud, Daniel. 2002. « Geothermal energy and heat storage ». 133 p. < http://www.isaac.supsi.ch/isaac/pubblicazioni/Geotermia%20-%20Pompe%20di%20calore/Lecture%20notes/%282002%29%20Geothermal%20energy%20and%20heat%20storage%20.%20Lecture%20notes/a-notes%20de%20cours%20-%20complet.pdf >.

Pasquier, Philippe, et Denis Marcotte. 2012. « Short-term simulation of ground heat exchanger with an improved TRCM ». *Renewable Energy,* vol. 46, p. 92-99.

Patankar, S.V. 1980. *Numerical heat transfer and fluid flow*. Hemisphere Pub. Corp.

Paul, N.D. 1996. *The effect of grout thermal conductivity on vertical geothermal heat exchanger design and performance*. Mechanical Engineering Dept., South Dakota State University.

Paul, ND, et CP Remund. 1993. « A Nationally Acceptable Grouting Manual for GSHP Boreholes ». *Final Report, EPRI Project RP3881-1. Palo Alto, CA: Electric Power Research Institute. Remund, CP, and JT Lund*, p. 95-106.

Philippe, M., M. Bernier et D. Marchio. 2009. « Validity ranges of three analytical solutions to heat transfer in the vicinity of single boreholes ». *Geothermics,* vol. 38, n^{o} 4, p. 407-413.

Remund, C.P. 1999. *Borehole thermal resistance: Laboratory and field studies*. Medium: X; Size: page(s) 439-445 p.

Rottmayer, S.P. 1997. « Simulation of ground coupled vertical U-tube heat exchangers ». UNIVERSITY OF WISCONSIN.

Ruan, W., et W.T. Horton. 2010. « Literature Review on the Calculation of Vertical Ground Heat Exchangers for Geothermal Heat Pump Systems ».

Rybach, L. 2001. « Design and performance of borehole heat exchanger/heat pump systems ». *Proc. European Summer School of Geothermal Energy Applications, Oradea/Romania (CD-ROM)*.

Sharqawy, M.H.E. 2008. *Modeling of heat transfer in a vertical ground heat exchanger*. King Fahd University of Petroleum Minerals .King Fahd University of Petroleum and Minerals (Saudi Arabia).

Shonder, J.A., V. Baxter, J. Thornton et P. Hughes. 1999. *A new comparison of vertical ground heat exchanger design methods for residential applications*. Medium: X; Size: page(s) 1179-1188 p.

Shonder, John A, et Patrick J Hughes. 1998. *Increasing confidence in geothermal heat pump design methods*. Richard Stockton College of New Jersey.

Signorelli, S., T. Kohl et L. Rybach. 2005. « Sustainability of production from borehole heat exchanger fields ». In.

Simeb. 2011. « Simeb - Simulation énergétique de bâtiments ». < http://simeb.ca/ >.

Sutton, M.G., D.W. Nutter et R.J. Couvillion. 2003. « A ground resistance for vertical bore heat exchangers with groundwater flow ». *Journal of energy resources technology,* vol. 125, p. 183.

Thermal Dynamics Inc. 2012. *Ground Loop Design.* < http://www.groundloopdesign.com >.

Toshkov, ET. 2013. « Build-up of hybrid installation with ground source heat pump and solar collectors ». *Thermo techniques,* vol. 4, n° 2, p. 24-27.

Toshkov, ET, AG Georgiev et RK Popov. 2014. « Measuring system of a hybrid installation with ground source heat pump and solar collectors ». *Годишник на ТУ София, филиал Пловдив" Journal of Fundamental Sciences and Applications",* vol. 20.

Trillat-Berdal, Valentin, Bernard Souyri et Gilbert Achard. 2007. « Coupling of geothermal heat pumps with thermal solar collectors ». *Applied Thermal Engineering,* vol. 27, n° 10, p. 1750-1755.

TRNSYS. 2011a. « TRNSYS ». < http://www.trnsys.com/ >.

TRNSYS. 2011b. « TRNSYS Simulation Studio ».

Wang, H., C. Qi, H. Du et J. Gu. 2009. « Thermal performance of borehole heat exchanger under groundwater flow: A case study from Baoding ». *Energy and Buildings,* vol. 41, n° 12, p. 1368-1373.

Wetter, M., et A. Huber. 1997. « Vertical borehole heat exchanger EWS Model ». *TRNSYS type,* vol. 451.

Yang, H., P. Cui et Z. Fang. 2010. « Vertical-borehole ground-coupled heat pumps: A review of models and systems ». *Applied Energy,* vol. 87, n° 1, p. 16-27.

Yavuzturk, C., et J. D. Spitler. 2000. « Comparative Study of Operating and Control Strategies for Hybrid Ground-Source Heat Pump Systems Using a Short Time Step Simulation Model ». *ASHRAE transactions,* vol. 106, n° 2, p. 192-209.

Yavuzturk, C., et J.D. Spitler. 1999. « A short time step response factor model for vertical ground loop heat exchangers ». *ASHRAE transactions,* vol. 105, n° 2, p. 475-485.

Young, Thomas Ray. 2004. « Development, verification, and design analysis of the borehole fluid thermal mass model for approximating short term borehole thermal ». Oklahoma State University.

Zarrella, A., M. Scarpa et M. De Carli. 2011. « Short time step analysis of vertical ground-coupled heat exchangers: The approach of CaRM ». *Renewable Energy*.

Zeng, H., N. Diao et Z. Fang. 2003. « Heat transfer analysis of boreholes in vertical ground heat exchangers ». *International Journal of Heat and Mass Transfer,* vol. 46, n° 23, p. 4467-4481.

Zeng, HY, NR Diao et ZH Fang. 2002. « A finite line-source model for boreholes in geothermal heat exchangers ». *Heat Transfer—Asian Research,* vol. 31, n° 7, p. 558-567.